IDENTIFYING TOPOGRAPHIC CONTROLS OF TERRESTRIAL VEGETATION USING REMOTE SENSING DATA IN A SEMIARID MOUNTAIN WATERSHED, IDAHO, USA

by

Ricci Loughridge

A thesis

submitted in partial fulfillment

of the requirements for the degree of

Master of Science in Hydrologic Sciences

Boise State University

December 2014

© 2014

Ricci Loughridge

ALL RIGHTS RESERVED

BOISE STATE UNIVERSITY GRADUATE COLLEGE

DEFENSE COMMITTEE AND FINAL READING APPROVALS

of the thesis submitted by

Ricci Loughridge

Thesis Title: Identifying Topographic Controls of Terrestrial Vegetation Using Remote Sensing Data in a Semiarid Mountain Watershed, Idaho, USA

Date of Final Oral Examination: 06 December 2013

The following individuals read and discussed the thesis submitted by student Ricci Loughridge, and they evaluated her presentation and response to questions during the final oral examination. They found that the student passed the final oral examination.

Alejandro N. Flores, Ph.D.	Chair, Supervisory Committee
Shawn Benner, Ph.D.	Member, Supervisory Committee
Jennifer Pierce, Ph.D.	Member, Supervisory Committee
Mark Seyfried, Ph.D.	Member, Supervisory Committee

The final reading approval of the thesis was granted by Alejandro N. Flores, Ph.D., Chair of the Supervisory Committee. The thesis was approved for the Graduate College by John R. Pelton, Ph.D., Dean of the Graduate College.

ACKNOWLEDGEMENTS

I would like to give special appreciation to my lead advisor Dr. Alejandro Flores for the tremendous support, patience, and guidance throughout this extensive research process. With his support and encouragement, he has allowed me to grow as a research scientist with great understanding of the hard work and diligence it takes to become successful. I can't thank him enough for being my inspiration and exemplar. In addition to Dr. Flores's great help, I would also like to thank my committee members—Dr. Shawn Benner, Dr. Mark Seyfried, and Dr. Jennifer Pierce—for their ongoing advice and brilliant suggestions, which have ultimately made this document have better direction and cohesion. Also, I would like to thank Dr. Nancy Glenn and her expert knowledge of remote sensing applications in the field and data processing. Other important folks without whom my research would not have been possible are the hard working technicians that endured blood, sweat, and tears to collect these data; thank you, Paige LaPorte, Phill Hummer, and Remy Brooks. Special thanks go to my colleagues within the Boise State Geoscience Department and my close friend Kelsey Dillon, who allowed me to exchange experimental methods and ideologies, supported me during writing, and motivated me to keep striving to reach my goals. Also, I would like to express my gratefulness for the funding contributed by the National Aeronautics and Space Administration (NASA) and the Jet Propulsion Lab (JPL), without which this research would not have been possible.

ABSTRACT

Global climate change is a significant research focus area in contemporary Earth science. Changes in climatic patterns have already resulted in shifting energy flows with associated changes in hydrologic and ecologic systems. More specifically, changes in vegetation distribution and abundance are one of the most visible and potentially significant effects of a changing climatic regime. However, to monitor and predict future changes in vegetation, the initial conditions must be well characterized. This thesis examines the distribution of vegetation in a semiarid mountain watershed in three important ways: (1) quantifying the factors affecting the distribution of broad classes of vegetation at the hillslope scale (e.g., 30-100 m), (2) quantifying factors affecting the organization of vegetation at sub-hillslope scales, and (3) quantifying the factors influencing the distribution of vegetation water content. The first of these themes is aimed at producing a hillslope-scale classification map of 4 broad classes (sagebrush steppe, Douglas fir, ponderosa pine, and deciduous/riparian) of vegetation within Dry Creek Experimental Watershed (DCEW) at the 30 m spatial resolution using remote sensing and geospatial data, field data, and 2 supervised learning classifiers known as artificial neural network (ANN) and classification and regression tree (CART). We investigated possible drivers of vegetation distribution by partitioning 11 topographic and remote sensing inputs into the ANN and CART models. Results show that the ANN had better overall accuracy (82.3%) than the CART (77.22%); however, it is less informative

of the input variables used to classify due to the complex nature of the ANN architecture. Therefore, the CART model was used to determine that 5 of the 11 predictors were significant drivers of vegetation distribution.

At the sub-hillslope scale, we quantified the percent cover of specific biotic and abiotic cover types (grass, forb, shrub, bare ground, and etc.) contained within the sagebrush-steppe class: the diameter at breast height (DBH), frequency, and density for the conifer classes; and percent composition and width of the "green line" of riparian reaches. We also investigated influences of topographic effects on abundance within the sagebrush steppe, and Douglas fir and ponderosa pine ecosystems. Preliminary results of sagebrush steppe indicate percent cover of bare ground was 47.89% ± 3.29%, grass was 17.716% ± 4.6%, forb was 13.03% ± 2.3%, and shrub was 16.0% ± 4.09%. Moreover, there was a significant ($p = 0.05$) association between grass cover and topographic aspect, with North slopes having a grass cover of 14.58% ± 7.33% and South slopes with 11.67 % ± 6.0 % at the 95% confidence level ($P = 0.05$). The average DBH for mature Douglas fir and ponderosa pine was 84.6 cm ± 19.4 and 82.4 cm ± 24.2, respectively. Frequency and density of Douglas fir (> 1.4 m in height) was 100% and 17.57 per 100 m pixel while ponderosa pine was 57.14% and 8.77 per pixel. The most prevalent trends in riparian vegetation suggest that willow and water birch decrease in percent composition with elevation gain, while mountain maple increase in percent composition. Also, the breadth of the "green line" decreases with gaining elevation.

Finally, the National Aeronautics and Space Administration (NASA) has been using microwave passive and active remote sensing to develop algorithms to retrieve global soil moisture. However, there are issues with the above ground vegetation over

laying the soil in which leaf water content attenuates the signal through the leaves and increases sensitivity to moisture below the top centimeter of the soil surface (Njoku & Li 1999). Therefore, we investigated spatial and temporal changes in the vegetation water content (VWC) of grass/forb life form and the relative vegetation water content (RVWC) of shrubs within the sagebrush steppe ecosystem for NASA's model development in the Soil Moisture Active Passive (SMAP). Our data suggest that to define this value, calculations are spatially and temporally dependent, and to determine the VWC across DCEW, further data acquisition and processing must be completed.

TABLE OF CONTENTS

LIST OF TABLES

LIST OF FIGURES

LIST OF PICTURES

1. INTRODUCTION TO VEGETATION

Global climate change is currently an overwhelming concern in today's scientific community. According to the 2007 Intergovernmental Panel on Climate Change (IPCC) Fourth Assessment Report, temperatures are expected to rise as a result of increased concentrations of greenhouse gases in the atmosphere associated with anthropogenic emissions. Even if greenhouse emissions suddenly stopped, the increase in global mean temperatures would not cease given the slow equilibration of atmospheric composition via the ocean. Some of the specific consequences hypothesized to occur are increasing variability and intensity in heavy precipitation, floods, droughts, heat waves, wildfires, and tropical storms (IPCC 2007). More specifically, northern and upland ecosystems are expected to experience increased runoff and earlier spring peak discharge. In addition, increased evapotranspiration from vegetation caused by higher temperatures may cause local desertification through a decrease in water availability, despite the projected global increase in precipitation. Alterations in climatic patterns have already resulted in shifting energy flows with associated changes in hydrologic and ecologic systems. For example, rising ocean temperatures have already contributed in global shifts in the ranges and abundance of algae, zooplankton, and fish migrations. In fact, one study projects 15-37% of land plants and animals are expected to become extinct by 2050 as a result of climate change (Wagner 2008). Ultimately, the loss of biodiversity will likely be caused by a

shift in physical characteristics of the landscape and shrinking ecosystems disabling mobility and longevity of plants and animals (Wagner 2008).

Availability of water and temperature regimes are two of the major determinants of the predictability of ecologic and hydrologic processes. Water and temperature both influence the biogeochemical pathways that shape ecosystems, transfer energy, and impact biomass. For example, vegetation can modify microclimate by the interception and partitioning of solar energy into different components of the energy balance in a way that can reduce temperature extremes. Vegetation supports snow accumulation, decreases surface wind speeds, and even promotes cloud production (Hiemstra *et al.* 2002; Freedman *et al.* 2001). Moreover, vegetation affects the water balance through evapotranspiration, which changes local soil moisture, thereby modulating runoff, infiltration, groundwater recharge, and water storage within the biomass (Dingman 2002).

Improved understanding of the role of vegetation in controlling local water, energy, and biogeochemical cycles is needed to support prediction and mitigation of global climate change. Understanding the drivers to which these biogeochemical feedbacks are propagated is important for modeling future vegetative conditions and the associated environmental response (Nolin 2012; Kallarackal & Roby 2012; Way & Oren 2010; Johnstone *et al*. 2010). Thus, vegetation classification and mapping on regional scales has been implemented in order to gain understanding of the underlying climatic, topographic, and lithologic variables that control vegetative land cover (Benediktsson & Sveinsson 1997; Heermann & Khazenie 1992). Other applications for which mapping and monitoring vegetation is important include fire risk assessment, wildlife habitat

assessment, land management planning, recreation, forest health, and watershed protection. In order to predict regional vegetation trends, it is necessary to develop efficient techniques to survey and catalog terrestrial vegetation parameters in a way that captures the larger variability in ecosystems, as well as the associated climatic and topographic variables, and anthropogenic disturbance (e.g., logging and agriculture practices) that influence vegetation growth and abundance. Therefore, vegetation classification, mapping, and long-term monitoring efforts have become imperative topics within the environmental research community. These efforts are critically important to improve ecological and hydrological modeling and to better understand the response of terrestrial ecosystems to local geomorphological and hydrological change, as well as how these ecosystems influence global hydrologic cycle, carbon cycle, and energy budgets.

The purpose of this thesis is to provide a moderately fine resolution map of vegetation communities within a local watershed located in the southwestern part of Idaho, USA, in addition to providing specific vegetation growth characteristics and their response to topographic and atmospheric processes with respect to time. The responses of vegetation to topographic drivers such as aspect, elevation, and potential solar radiation or seasonal variability are not well understood within the reaches of this watershed and other adjacent ecosystems in southwestern Idaho. As part of future studies, these maps will provide a baseline inventory of specific communities of plants (ecosystems), their distribution, and abundance, which can be used for long-term monitoring studies where vegetation is expected to spatially change with global climate change. Furthermore, measurement of specific vegetation growth patterns such as plant water content or dry

biomass weight over the course of the growing season within this watershed can be used for a multitude of future dynamic energy transfer studies of the science community.

1.1 Thesis Partitioning

This thesis has been divided into three distinct but overlapping parts that concern vegetation distribution and abundance that begins with mapping broad vegetation classes and ends with fine-scale vegetation characteristics for the purpose of understanding topographic effects and quantifying vegetative life forms for long-term monitoring in response to climatic changes. All parts pertain to the same study area known as Dry Creek Experimental Watershed, which is described in detail in the following chapter. Following the site description, part one discusses the classification of four broad-scale vegetation classes (sagebrush steppe, Douglas fir, ponderosa pine, and riparian) at 30 m resolution using two different supervised learning classification techniques. This section includes an overview of methods, presentation of results, and a discussion of classifier performance and vegetation trends associated with topographic controls and visible/near-infrared remote sensing imagery. The second part of this thesis presents a more detailed analysis of major vegetation life forms within the sagebrush steppe, conifer, and riparian ecosystems at a spatial 30 m and 100 m scale, consistent with the resolution of the remote sensing data used throughout the study. The final section describes a methodology and some results for the determination of vegetation water content (VWC) collected within the sagebrush steppe ecosystem. VWC is an important land vegetation parameter that varies in space and time in a way that reflects the dynamics of terrestrial vegetation, but also impacts the ability to remotely sense soil moisture in the microwave region of the electromagnetic spectrum. This final part is aimed at developing mechanisms to

independently estimate VWC in order to improve estimates of soil moisture from microwave measurements associated with NASA's forthcoming Soil Moisture Active Passive (SMAP) mission (Entekhabi *et al*. 2010).

2. STUDY AREA AND SITE DESCRIPTION

The Dry Creek Experimental Watershed (DCEW) covers approximately 27 km^2, and is located 16 km northeast of Boise, Idaho in a region known as the lower Boise foothills (McNamara *et al*. 2005). This perennial stream watershed is intensely studied and maintained by Boise State University (BSU), and includes 5 weather stations, 8 soil moisture sites, 1 eddy covariance tower, several snow lysimeters, and 7 stream gaging stations. Data are collected in real-time and can be downloaded at http://icewater.boisestate.edu/boisefront/realtimedata.htm. Elevation in DCEW ranges from 1000 to 2100 m above sea level trending northeast of the watershed. Figure 1 shows an aerial map of DCEW.

According to calculations derived in ArcMap 10.1, slopes range from 0 to 69 degrees with the steepest slopes on north aspects. Average daily potential solar radiation ranges from 654 to 4946 $kWh/m^2/d$ where radiance is greatest on south-facing aspects. This region of Idaho, including southeastern Oregon, has a Mediterranean climate where the summers are dry and hot and the winters are wet and cold (Smith *et al*. 2011). Precipitation in this region is most abundant during October through May, when the area receives approximately 90% of the total precipitation in the form of rain and snow, while the remaining 10% precipitation occurs in June through September (Daniel Tappa, personal communication, February 1, 2013).

DCEW is located in the Idaho Batholith, which is composed mostly of granodiorite approximately 80 million years in age. Dominate minerals from the decomposition of granite include quartz, plagioclase/potassium feldspars, and micas (Hyman *et al.* 1998). The major soil types are Argixerolls, Haploxerolls, and Haplocambids (Harkness 1997), which are well-drained and typically have gravely loam textures (USDA 1997; Smith *et al.* 2011). In complex terrain, characteristics such as soil moisture, texture, and depth coincide with vegetation and solar energy. In the case of DCEW, the north-facing aspect at high elevations are generally less than 2 m deep and tend to be thicker. As a result, north-facing hillslopes are associated with the highest water holding capacity, while south aspects are thinner and drain easily (Geroy *et al.* 2011; Kunkel *et al.* 2011; Tesfa *et al.* 2009).

Vegetation at low elevations and on most south-facing slopes is dominated by the diverse vegetation community known as the sagebrush steppe ecosystem (Picture 2). More specifically, this community is comprised of shrubs such as sagebrush (*Artimesia sp*.), rabbitbrush (*Chrysothamnus sp*.), and bitterbrush (*Purshia sp.*); native grasses such as three-awn (*Artistida sp.*), and Thurber's needlegrass (*Stipa thurberiana*); and invasive grasses known as cheatgrass (*Bromus tectorum*) and medusa head (*Taeniatherum caput-medusae*). Some common forbs are arrowleaf balsamroot (*Balsamorhiza sagittata*), skeleton weed (*Chondrilla sp.*), lupine (*Lupinus argentous*), buckwheat (*Eriogonum spp*.), and yarrow (*Achillea millefolium*). The decline of sagebrush steppe ecosystems has resulted in many studies evaluating the effects of woody encroachment, invasive grass, and forb species, which are correlated with fire regimes and rangeland management practices (Miller & Rose 1999; Taylor 2003; Nelson & Pierce 2010).

At high elevations, Dry Creek vegetation are characterized by mixtures of conifers such as ponderosa pine (*Pinus ponderosa*) and Douglas fir (*Psuedosuga menziesii).* Ponderosa pine typically grows on south-facing slopes in Idaho (Graham & Jain 2005), and are characterized as having three needles, though they can also have 2 needles per fascicle, and have yellow-orange pealing bark resembling puzzle pieces. They are also known for withstanding frequent low severity wildfires and growing in clumps due to frequent heterogeneous fires that isolate ponderosa stands and exterminate other fire intolerant species (Graham & Jain 2005) (Picture 3). Ponderosa contain the mass of their root system in the top 60 cm of the soil mantle. However, where shallow soils overlie fractured bedrock, they can have a deep taproot that extends 12 m into fissures of bedrock (Burns & Honkala 1990). In addition, ponderosa generally grow in dry areas and are able to withstand drought conditions due to a higher allocation of sapwood to heartwood, which enable them to store more water and thrive in dry climates (Stout & Sala 2003).

Douglas fir is not a true fir (i.e., not *Abies* sp.), generally grows on north-facing slopes, and is characterized as having leaves that are flat, blunt, and on a twisted petiole (Picture 4). Root systems may develop a taproot but in shallow soils often express plate-like systems where lateral growth occurs in a downslope orientation (Burns & Honkala 1990). They are fire tolerant but are generally found in areas where fires are less frequent. As a result, Douglas fir will often supplant ecosystems that have been fire-suppressed, which subsequently has been found to change the structure and function of soil chemistry (Graham & Jain 2005).

In addition, DCEW contains deciduous trees such as chokecheery (*Prunis virginiana*), rocky mountain maple (*Acer glabrum*), and water birch (*Betula occidentalis*), which are primarily found in areas where slope angles are low and water accumulation is most frequent. These species are typically aggressive colonizers, disturbance tolerant, and associated with ponderosa and Douglas fir understory (Graham & Jain 2005). Another deciduous shrub known as snowbrush (*Ceanothus sp.*) is an evergreen and is commonly found at high elevations and where solar radiation is highest.

Empirically, south-facing slopes in the sagebrush steppe ecosystem have lower densities of shrubs with a high proportion of rhizomatous grasses and invasive forbs such as skeleton weed and medusa head intermittently growing in the interstitial spaces between shrubs. Although these grasses and forbs grow in large numbers, their small size leave a large proportion of exposed bare ground. North-facing slopes tend to have high densities of shrubs and thick bunchgrasses with fewer patches of exposed bare ground. DCEW is primarily managed by the United States Forest Service (USFS) but has some areas managed by the state of Idaho or the Bureau of Land Management (BLM) (Figure 2). According to USFS management history, DCEW has not been logged in the last 100 years (Ray Eklund, personal communication, March 21, 2013); however, there have been personal observations of logging on suspected private land as recent as the last 2 years. Furthermore, there is no known spatial image history reported for DCEW, but processed Landsat scenes for the years 1993 to 1995 suggest there was logging in upper DCEW and that a fire occurred in the lower south-facing slopes in 1996 (Mike Poulos, personal communication, May 19, 2014). In addition, DCEW agricultural practices consist of annual browsing and grazing by sheep and cattle, which primarily consume forbs and

grasses. This practice frequently disrupts soil adhesion properties, creating local slope instability and sedimentation of stream discharge (Brady & Weil 2004; Lefrançois *et al.* 2007).

3. ARTIFICIAL NEURAL NETWORK AND CLASSIFICATION TREE

This chapter of the thesis discusses vegetation mapping at the 30 m spatial scale using two types of classifiers that determine four broad classes of the primary ecosystems with in the study area, DCEW. In addition, the accuracy and resulting maps produced are discussed with the implications of topographic controls of specific vegetation distribution and abundance.

There are many ways in which scientists classify vegetation. Most common practices are by means of Artificial Neural Networks (ANNs), classification and regression trees (CART), and statistical classifiers. Commonly, these methods use supervised learning, which uses input parameters derived from remotely sensed data and ancillary field data to classify a predetermined output of vegetation type or class. The use of remotely sensed data is ubiquitous in terrestrial ecology and many data are available across a wide range of spatial resolutions, temporal revisit, and wavelength. For the purpose of this study, 30 m resolution Landsat 5 TM was downloaded free of cost. There are limitations when using remote sensing data to classify vegetation when the resolution of the data is coarser than the intrinsic variability in vegetation properties and cover. Primary problems associated with this problem of “coarse resolution” are mixed pixels containing two or more vegetative classes. This leads to a bias in reflectance values that yields uncertain spectral differences between classes.

The lower foothills of Boise, Idaho are located approximately 16 km north of downtown Boise and are not well classified using the combination of ancillary field data and remotely sensed data. The focus of this section is to define broad classifications of four vegetation groups: sagebrush-steppe ecosystem, ponderosa pine, Douglas fir, and riparian/deciduous trees across DCEW. The two types of classifiers used in this study are ANN and CART. Both procedures are formulated to include 11 input variables derived from digital elevation models (DEMs), which represent topographic variability within DCEW, and Landsat 5 Thematic Mapper (TM) remotely sensed data, which are used to represent directly observable characteristics of the vegetation in the visible and near infrared wavelengths. Through a series of data denial experiments in which classifications are developed using only remotely sensed inputs, only topographic inputs, and a combination of topographic and remote sensing inputs, we are able to better understand topographic controls on the distribution of vegetation in this semiarid ecosystem. Improved understanding of topographic controls on vegetation distribution will ultimately lead to enhanced understanding of the role of hydroclimatology on the organization of terrestrial ecosystems in future studies.

3.1.1 Artificial Neural Networks

Artificial neural networks are known for their increased accuracy given a low sample size with no *a priori* knowledge of assumptions or normal distributions (Rumelhart et al., 1986). The ability to produce high classification accuracy with non-linear complex patterns while generalizing in noisy environments has resulted in ANNs being used in large parts of the scientific community, especially remote sensing (Kavzoglu 2009; Mas & Flores 2008). Furthermore, the multilayer perceptron (MLP)

with the back propagation learning algorithm to generate ANNs is particularly common due to the ability to produce successful classification with minimal error (Heermann & Khazenie 1992).

The MLP network has three divisions of data. The first division, known as the training set, is used to compute the iterative gradient descent and to update weights and biases. This procedure is effective at minimizing the overall training mean square error or performance between the desired and actual outputs. The second set of data used is the validation set, which is monitored during training to avoid over-fitting the data. During the initial phase of training, the validation error and training set errors usually decrease but with continued iterations will eventually increase, otherwise known as over fitting. Once the increase occurs, or if there is not a change in error after a predetermined number of iterations, the network saves the weights and biases at the minimum validation error. The third division of data is the testing set, which is independent of all training and validation. This is used to compare different models. Usually, the data for each division is divided into 70, 15, and 15 percent for training, validation, and testing, respectively.

The general architecture of the MLP is divided into three parts: the input layer, hidden layer, and output layer (Figure 5). The input layer and output (target) layer nodes are connected to the hidden layer but are not connected directly to one another.

There are two stages of training used in a MLP network. For the first stage, the input layer of spectral bands and topography data used to train the model are propagated forward through the hidden layer using a tan-sigmoid transfer function to estimate the output layer. The output layer is the predetermined class associated with the given inputs collected from field data. In the second stage, backprogation is used to calculate

derivatives of performance with respect to the weight and bias of each input. More specifically for the hidden layer, weights are randomly initialized to each of the hidden nodes and used for computation in the following equation:

$$dX = mc*dXprev + lr*mc*dperf/dX \quad \textit{(Equation 1)}$$

Where mc is the momentum constant, dXprev is the previous change to the weight or bias, lr is the learning rate, and dperf is the previous change in performance. Therefore, the weights associated with the nodes are adjusted until the total summed mean squared error over all training patterns reaches a predetermined threshold, usually 0. This process is iterated through training as long as the derivative of a node's transfer function can be calculated (Paolo & Schowengerdt 1995; Kavzoglu 2009). Learning rates and momentums are generally set arbitrarily using the trial and error method. As a result, convergence can be slow and consequently produce less than optimal results (Yu & Lui 2002). To avoid this process and to speed up convergence, the use of adaptive learning and momentum rate algorithms adjusts the learning and momentum rate at each connected weight during the training phase (Paolo & Schowengerdt 1995; Heermann & Khazenie 1992; Yu & Lui 2002).

Finally, a measure of accuracy is calculated by constructing confusion matrices or tables that contain information on how many predicted classes match the actual class. As a result, overall user and producer accuracies can be calculated to determine errors in classification or misclassification (Congalton & Green 2009). User accuracy is a measure of how well the map would perform in the field and producer accuracy is a measure of how well the model actually classified each class correctly (Figure 6). In addition, the kappa statistic can be used as another measure of accuracy, which takes into account the

random chance of correct classification and can be used for comparisons of multiple model accuracies (Congalton & Green 2009)

Although ANNs are well known for their incredible accuracy in classification, it is difficult to disentangle the process it uses to classify a given output (Qui & Jenson 2004). This is known as the "black box" where the meaning in most cases is hidden in the weights of the hidden layer. This makes it nearly impossible to interpret due to their complex nature (Olden & Jackson 2002; Qui & Jenson 2004).

3.1.2 Classification Trees

Other classifiers such as the classification and regression tree (CART) can be useful for interpreting the primary drivers during the classification process. CART classifiers have a binary tree structure proposed in detail by Breiman *et al.* (1984), which establishes a branching tree from the root through iterative operations until it reaches terminal leafs associated with a specified class. This classifier also does not require parametric distribution of inputs, which allows it to be used with no *a priori* knowledge (Breiman *et al.* 1984). More specifically, the tree must establish structure by dividing the root node from input variables in which the measure of the impurity between two subclasses is minimized. In other words, the tree splits into two pure classes where the purest node contains only one class and an impure node contains mixed classes. Then, the tree grows by successive divisions of nodes using the same measure of the impurity until there is no significant decrease and consequently becomes the terminal leafs or classification output. Once the tree is established through training, necessary pruning for large datasets may be necessary for optimal classification (Moisen 2008; Martinez &

Martinez 2001). Finally, binary rules are created from the tree and are used to predict classifications of new samples.

One common method for testing the accuracy of the CART model is *k*-fold cross validation, which takes the original data set and subsets the data in approximately equal samples or *k* subsamples. Generally, there are 10 subsamples or *k*-folds. This means the model is trained with *k*-1 subsamples and tested with the remaining set *k* times. Then the mean square error produced from the predicted and actual classification for each k-fold test set is averaged to determine accuracy. The advantage of this method is that all data is incorporated in the training set *k* times and is tested once (Martinez & Martinez 2001). In addition, confusion matrices can also be calculated from the tree determining the overall classification accuracy, user and producer accuracy, and misclassification errors.

3.2 Classification Materials and Methods

3.2.1 Field Sampling

Field sampling was conducted in the spring and summer of 2011 and 2012. Sample sites where chosen randomly using ArcMap GIS 10.1 software toolbox. The quantity of samples was chosen in 2011 to fit the distribution of North, East, South, and West aspects within DCEW. However, for the 2012 season, samples were restricted to north-facing slopes due to a deficient data set from the 2011 season. This deficiency resulted from difficult accessibility given high degree of slope, dense vegetation, and proximity to roads.

In total, 79 field sites were visited (Figure 3). Classes chosen for this study were based on detectability, spectral discernibility, and measurability using processed satellite imagery on two dates with maximum difference in green reflectance in the visible and the

near infrared parts of the electromagnetic spectrum. For example, deciduous species should have converse greenness between the peak growing season, known as “green up,” and summer senescence enabling better detection of their distribution, while coniferous species that keep their needles year round will remain some degree of green year round. However, deciduous evergreen species are technically deciduous in classification but retain most of their green leaves year round are expected to bias model classification results and must be taken into consideration. Furthermore, deciduous vegetation located near perennial streams and springs have water availability throughout all seasons that can have notable differences of greenness and water retention compared to adjacent dry vegetation with ephemeral water availability. Understory shrubs were not measured since satellite detection is limited by over-story canopies. Hence, the four broad classes of vegetation chosen were sagebrush steppe, ponderosa, Douglas fir, and deciduous.

For the sagebrush steppe class, data collected represented presence or absence in a 30 m plot. For conifer sites, frequency of specific tree species and diameter at breast height (DBH) were measured for each tree in two 30 m plots oriented at vertical angles. For the riparian class, presence or absence of riparian/deciduous vegetation was recorded by walking a 50 m transect along streambeds.

3.2.2 Preprocessing Data

To determine which input variables could be a driver in the distribution of vegetation, boxplots of common variables used in remote sensing and vegetation studies were created for each vegetation class of interest using GIS DEM data, and were processed using Matlab Release 2012b. Figure 7 represents distributions of remote sensing data for August and June 2011 and Figure 8 represents topographic controls.

For remotely sensed data, Row 40 and Path 31 of Landsat 5 TM data was downloaded from the United States Geological Survey Earth Explorer (USGS EE) website for the dates June 25, 2010 and August 25, 2011. These days were chosen based on relatively cloudless conditions overlying DCEW and the maximum difference in vegetation vigor. Pixel size for Landsat 5 is 30 m resolution and 1 downloaded image is 31,110 km^2. This study is focused on the area in which field data was collected, thus an area of approximately 69 km^2 or a 276 by 276 pixel matrix was subsampled from the Landsat image overlying DCEW and its surrounding area for analysis.

For remote sensing features, raw digital numbers in spectral bands 2, 3, and 4 with wavelengths of 0.52 to 0.60, 0.63 to 0.69, and 0.76 to 0.90 µm, respectively were converted to top of atmosphere (TOA) reflectance using the Landsat Ecosystem Disturbance Adaptive Processing System (LEDAP) described by Masek *et al*. (2006). This method takes into account cloud and atmospheric conditions for the day of interest that could potentially bias true reflectance values. Bands 2 and 3 are in the visible part of the electromagnetic spectrum where band 2 is known as the green band and band 3 is the red band. Band 4 is in the near infrared (NIR) zone of the spectrum and is usually a measure of water or healthy green vegetation when reflectance values are high. This is a result from water being an excellent absorber of NIR wavelengths.

Also, the calculated Normalized Difference Vegetation Index (NDVI) described in the article by Butterfield and Malmström (2009) was included as remotely sensed inputs. NDVI is a measure of greenness in which the peak growing season “green up” and the peak senescence season should have a maximum difference of NDVI values for deciduous and annual vegetation.

Topographic features used were slope (degrees), elevation (m), and potential solar radiance ($Wh/m^2/yr$). Initially, these features were calculated from a 1 m Light Detection and Ranging (LIDaR) DEM collected in 2009 by the Idaho LIDaR Consortium using the ArcMap GIS 10.1 toolbox software and used for training inputs. However, before training inputs were extracted from GIS, the DEM was aggregated into thirty 1 m cells to obtain an average value for slope, elevation, and potential solar radiance of a 30 m pixel. For data assimilation, the 30 m spatial resolution DEM used was the Shuttle Radar Topography Mission (SRTM), and was obtained from the Endeavor shuttle mission conducted by NASA in 2000 (Farr *et al*. 2007). Features from both DEMs were the same at each of the samples sites, so equivalency was assumed.

Most outputs of classification were determined in the field sampling procedure by the presence or absence of the class of interest. However, for conifers where there is a mixture of tree species, diameter at breast height (DBH) and frequency were used to determine the dominant tree class for the sample site with respect to a satellite's vantage point. The assumption made here is that areas with low frequency relative to the other tree species, but with high DBH, correlates to a higher canopy cover, and is therefore the dominate tree class of that given pixel.

Using Matlab Release 2012b, we imported 11 geo-referenced 276x276 matrices representing TOA reflectance and NDVI for both dates and the topographic controls derived from the SRTM DEM for DCEW and the surrounding area. These 11 matrices were stacked into a data cube and used for data assimilation to predict vegetation classes in DCEW using both classifying models (ANN and CART).

3.2.3 Training and Data Assimilation

To determine dominant drivers that influence the distribution of vegetation communities, both classifiers were trained, tested, and assimilated in Matlab Release 2012b with 3 features of topography, 8 features of remotely sensed data, and finally the combination of all 11 features containing topography and remotely sensed data. As for the ANN, samples were randomly subdivided into 60, 20, and 20 percent or 47, 16, and 16 samples used for training, validation, and testing, respectively. The specific MLP used was the gradient descent with adaptive momentum and learning rate backpropogation. There were 12 hidden layers selected, the momentum was set to 0.9, and the learning rate was set to 0.1. To stop training and consequently over-fitting, the minimal error was set to 0 and the maximum iterations with no change in error was set to 6.

An error, or confusion matrix, was constructed to show the number of pixels that were correctly and incorrectly classified for each model run. Overall accuracy, user accuracy, and producer accuracy was computed, in addition to the kappa statistic and Z-score. As for the classification tree, the same inputs were used to train the model and the cross validation error rate was calculated using 10 k-folding method described in Moisen (2008). In addition, confusion matrices were computed that include the overall accuracy, and user and producer accuracies. To compare models, the kappa statistic and z-score were computed, and a comparison was made for each division of inputs to determine if there were significant differences in model performance.

Once classifiers were trained, both models were forced through DCEW and the surrounding region using the data cube, which contained 11 matrices derived from the SRTM DEM and the LEPAD TOA reflectance from the dates of June 25, 2011 and

August 25, 2011. This yielded a spatial map of the predicted vegetation classes throughout the DCEW area.

3.3 Classification Results

3.3.1 Model Accuracy

Confusion matrices of the MLP ANN with gradient descent momentum and learning rate adaptation are listed in Table 1. The overall accuracy for remote sensing inputs is 75.9%, for topographic inputs is 74.7%, and for all inputs combined is 82.3%. As for the CART, one confusion matrix was made for each division of inputs by the summation of 10 confusion matrices created using the 10-kfold cross validation, which are provided in Table 2. For the same three data-denial experiments, the overall accuracies are 68.35%, 70.89%, and 77.22%, respectively. The kappa statistic and z-score were calculated for all models where kappa values of 0.41 to 0.60 are in moderate agreement and 0.61 to 0.80 are in good agreement (Landis & Koch 1977) (Table 3). All models are in good agreement for both the ANN and CART, excluding the spectral inputs of CART, which is in moderate agreement. The z-score for all models are well over 3 standard deviations which suggest the models are classifying correctly regardless of random chance. In addition, a pairwise comparison of the ANNs vs. CARTs performance for each division of inputs was calculated in which classification using only topographic inputs are significantly different between the models (P value < 0.03) (Table 4). The ANN producer's accuracy, which indicates the percent of correctly classified pixels, better classified the sagebrush-steppe and the ponderosa ecosystems given only spectral and all combined inputs. However, given topographic inputs, the CART model classified the sagebrush-steppe and the ponderosa ecosystems better and the ANN classified

Douglas fir more accurately. Furthermore, the CART model's performance was markedly better when classifying riparian/deciduous vegetation.

3.3.2 Classification Maps and Comparison of ANN and CART

The maps produced for each division of data using both classifiers are shown in Figure 9 through Figure 14. The map with the highest accuracy was produced using all 11 inputs using the ANN MLP (Figure 9). A comparison of the number of pixels and percent classified as sagebrush steppe, ponderosa, Douglas fir, and riparian/deciduous for the ANN and CART are provided in Table 6 and Table 7.

The ANN classified sagebrush steppe as 36%, 68%, and 58%; ponderosa as 8%, 14%, and 8%; Douglas fir as 25%, 17%, and 23%; and riparian/deciduous as 31%, <1%, and 11% (spectral, topographic, and both spectral and topographic), for DCEW and the surrounding area. As for the CART, sagebrush steppe was 23%, 55%, and 40%; ponderosa was 1%, 4%, and 15%; Douglas fir was 37%, 39%, and 15%; and riparian/deciduous was 38%, 2%, and 31%.

3.3.3 CART Tree Splitting

The tree produced using 8 remote sensing inputs determined 4 of the 8 inputs for classification were important in classification: the green and NIR band for August, the June NIR band, and the June calculated NDVI (Figure 15). The greatest measure of impurity, the root node, is the August green band where pixels with reflectance less than 0.06 are classified as a conifer (ponderosa or Douglas fir) and values that are greater than or equal to 0.06 are either sagebrush steppe or riparian/deciduous. More specifically, 62% of sagebrush pixels have August NIR reflectance less than 0.27. However, where sagebrush pixels have August NIR greater than or equal to 0.27, they also have June NIR

reflectance greater than or equal to 0.21. Riparian/deciduous pixels have August NIR reflectance greater than 0.27 but less than 0.21 NIR in June. Ponderosa pixels have NIR greater than or equal to 0.23 in August and June NDVI greater than or equal to 0.68. Conversely, 74% of Douglas fir pixels have August NIR less than 0.23, but where pixels have greater NIR in August they also have June NDVI values less than 0.68.

For topographic inputs, all inputs were used for classification. The tree obtained in this model is shown in Figure 16 in which elevation has the greatest measure of impurity. Generally, sagebrush-steppe and riparian/deciduous pixels were classified in areas where elevation is less than 1563 m. However, pixels with the greatest elevation and potential solar radiance were classified as sagebrush steppe or ponderosa, but areas with lower values of potential solar radiance and high elevation are classified as Douglas fir.

Finally, with all inputs used for the model, the August green band is still the greatest measure of impurity. Figure 17 displays the model using 5 of the 11 inputs for classification. Pixels with lower potential solar and slope values are classified as riparian/deciduous. Douglas fir and ponderosa pixels have slope angles greater than 21 degrees. However, Douglas fir has NIR in June less than 0.32. Ponderosa pixels have higher NIR in June than Douglas fir but also have potential solar radiation greater than or equal to 1.35E6 $Wh/m^2/yr$, and elevation greater than or equal to 1996 m. Lastly, sagebrush-steppe pixels have low slope angles of less than 18 degrees, potential solar radiance of greater than or equal to 1.35E6, but can also have large degree slopes.

3.4. Classification Discussion

3.4.1 Model Comparison

As expected, the overall accuracy of the ANN approach in classifying the four vegetation groups used in this study is higher in every simulation compared to CART. Both the ANN and CART models perform well at classification given only remote sensing data but gained nearly 8% accuracy with all inputs included into the models. By comparing the producer's accuracy of the ANN and CART, it appears the CART may classify riparian/deciduous areas better than the ANN, but underestimate sagebrush steppe and Douglas fir. Conversely, the ANN generally performs better at classifying ponderosa and sagebrush steppe. These discrepancies between the two classifiers may be a result of small sample sizes of the ponderosa (n = 10) and riparian/deciduous (n = 10) classes and/or the division of training and test sets. Perhaps the ANN randomly selected too few samples for these classes, and consequently not enough were used to train the model. Unfortunately, the ANN does not allow us to make inferences as to which inputs are used for the detection of each class. To better understand the possible drivers of vegetation distribution, we must interpret the CART model to infer the likely influences.

3.4.2 Vegetation Analysis

Spectral wavelengths enable us to make inferences of specific vegetation vigor and water storage during the 'green up' and senesced months. In recall, healthy vegetation is given by high reflectance values in the green and NIR bands, in addition to calculated NDVI. More specifically, the NIR band is used as a measure of water content within vegetation tissue, so when reflectance is high during drought conditions we can assume the plant is acquiring groundwater sources through a deep taproot, a nearby

perineal water source, or has advantageous physiological characteristics that enable it to store water in dry climates. For example, given only remote sensing inputs into the CART model, pixels assigned as sagebrush steppe have high August green band reflectance, low August NIR and high June NIR. This is expected since August is the driest and hottest month of the summer, while June follows a month of high snowmelt and precipitation with consequential healthy vigor vegetation. We can infer that the plants in the sagebrush ecosystem generally have shallow root systems and derive their water in the form of surface runoff and/or have low potential of water storage for the month of August. However, we are not able to make this same seasonal implication with riparian/deciduous trees since the NDVI values are low during the June season although stream discharge is high. This may correspond to the specific date at which the Landsat scene was captured and did not represent the peak growth or green up potential from underdeveloped leaves in the month of June.

As for the conifers, ponderosa pine has high reflectance in the August NIR bands and June NDVI, which suggests water availability year round. This is likely a result of root physiology in which a long tap root may have access to groundwater and the higher sapwood to heartwood ratio expressed in ponderosa pines. Douglas fir has low August NIR reflectance, which suggests they may not have accessibility to groundwater during the drought season and their root systems are shallow, using only surface runoff or shallow subsurface flow. When considering the topographic inputs to the CART model, we can empirically make an observation of the role of elevation in vegetation distribution simply by observation of conifer trees at the apex of the mountain and rarely any near the base. However, the CART is able to detect that high potential solar radiance, large degree

slopes, and high elevations are the major drivers of the distribution of ponderosa pixels, and where potential solar radiance is low but has high elevation there is Douglas fir present. Furthermore, sagebrush steppe is located in areas with low elevation and low slope angles but can also be found in areas that have very high elevation, slope, and solar radiation. This extreme difference may be a result of sagebrush steppe biomass preference to areas with well drained soils and high solar radiation. It also important to note deciduous evergreens within the watershed are also located in these areas too. It is important to note that both the ANN and CART models did poorly at detecting the riparian/deciduous class given only Landsat inputs. However, topography inputs to the CART model are using low slope and low elevation to detect the riparian/deciduous class. Furthermore, given only topographic inputs into the CART model, ponderosa pixels were poorly detected; however, when all inputs into the CART model are assimilated, the resulting map shows all representative classes.

Both the ANN and CART models were similar in classification. However, from empirical observation in the field, the ANNs resulting map appears to classify these four classes better than the CART. The drivers in which classification was made seems reasonable since the CART model was able to detect the subtle spectral differences in water content between the two species of conifers given their different root physiology, in addition to detecting riparian and deciduous trees given small sample size and low percent of area relative to the entire watershed.

With all 11 inputs used in the ANN, a broad class regional scale vegetation map in 30 m resolution is provided. This map can be used for future hydrological modeling within DCEW in which specific vegetation types are known and consequently the fate

and transport of water through the watershed can be explored at a finer scale. In addition, other possible outcomes produced from this map may help determine above ground carbon storage or vegetation water content given additional remote sensing data and ancillary field data. The next chapters of this thesis will discuss the methods, preliminary results, and possibilities of future hydrologic modeling given the resulting ANN map.

4. VEGETATION MEASUREMENT OF THREE ECOTONES WITHIN DRY CREEK EXPERIMENTAL WATERSHED

4.1 Introduction to Vegetation Measurement

For the majority of this thesis, vegetation has been expressed at 30 m spatial resolution for the purpose of producing maps of four broad classes on a regional scale with the intentions of determining vegetation parameters in local hydrologic models. In heterogeneous landscapes, such as sagebrush-steppe ecosystems, there is a mixture of species within 30 m and even 1 m resolutions that cannot be detected via remote sensing applications. Furthermore, remote sensing techniques often do not detect quantities or size of specific species or individuals. For example, in a forested ecosystem, one pixel determined to be a particular vegetation class could imply the pixel has just one very large tree, multiple medium trees, or many small trees. This lack of information could play an important role in understanding ecosystem function and vegetation success rates. Therefore, as a result of vegetation sizes, spatial variabilities, and difficulties of measuring unique spectral signatures on a microscale, this chapter is dedicated to the *in situ* measurement and quantification of specific life forms within the four broad classes derived from the prior chapter.

Scientists often need specific vegetative cover data to detect temporal shifts in vegetation community and parameterize ecological succession or state and transition models. Ecological succession is defined as the directional change in ecosystem structure

and function resulting from biotically driven changes in resource supply (Chappin III *et al.* 2011). This term is a topic of considerable debate amongst many ecologists since a stable "climax community" is assumed to be the end member of many vegetation types converging into one community characteristic that is a product of the regional climate. Although this idea is logically simple, it is often not observed in nature (Golley 1977). Eugene Odum's paper in 1969 states that succession should be understood as resulting from differential growth, differential survival, and perhaps dispersal of species adapted to grow at different points of stress gradients. The weakness with this model is most apparent in semiarid ecosystems as a result of irregular climatic and anthropogenic events easily influencing grazing practices and vegetation change (Westoby *et al.* 1989). Today, the state and transition models are widely accepted to represent plant community dynamics in which there are alternative stable states and non-linear changes in the function of the system. Simply put, there are always two directions (states) that are governed by events (transitions) that may or may not result in the crossing of non-reversible thresholds of plant community and function (Havstad & Herrick 2003).

In order to build sufficiently fine-grained data to support ecological state and transition models, it is important to measure and monitor long- and short-term changes in vegetation. These data are also critically important to facilitate improved understanding of biogeochemical cycling, wildlife habitat assessment, fuel load management, and desertification. By measuring fine-resolution distributions of vegetation, ecohydrologists can understand and quantify relationships between the hydrologic cycle and ecological processes and function (Havstad & Herrick 2003). For example, increases in bare ground, the interstitial spaces between shrubs, play important roles in the flows of energy,

sediment, carbon, and water throughout the landscape. For these reasons, the measurement and quantification of vegetation on a microscale are vital for understanding the consequences of a changing climatic regime.

Important measurements of vegetation community structure that exert controls on hydrologic and geomorphic processes include percent plant cover, frequency, density, relative density, and composition. Cover measurement examines plant and soil surface characteristics and gives an indication of runoff and erosional patterns on a fine scale by the quantification of vertical projection of plants or plant parts onto the ground when viewed from above (Bonham 1989). In addition, frequency is one of the most common measurements used by ecologist today since it requires little time to collect. This is a measurement of species in a given sample unit in which the presence or absence of a plant is reported as a percentage. Measurements such as cover and composition are also frequently needed to indicate a change in species population over time. Another useful measurement used as an indicator of vegetation change is density (Havstad & Herrick 2003), where individual plants are counted and recorded as the number of individuals per unit area. This is often less important for bunchgrasses and forbs since individual plants are difficult to distinguish from one another (Bonham 1989). Relative density, usually recorded as a percentage, is a measure of density given all species in a sample unit. Composition of vegetation is a list of plant species that occur in a particular sampling unit. Additionally, composition of riparian vegetation surveys can be used to indicate patterns of frequency and severity of disturbances (Tabacchi *et al.* 1998).

It is important to note that there are variations in vegetation among time intervals dependent on growing season, grazing periods, prior tree harvest, and even periodic

infestation of insects and disease (Bonham 1989). Thus, these variations should be considered when designing the sampling protocol to detect spatial and temporal changes, in addition to the proper size and shape of the sampling unit used for differing vegetation types.

In this chapter of the thesis, we examine the specific vegetation community distribution and abundance of three ecotones within DCEW: the sagebrush-steppe, conifer, and riparian ecosystems. Data collection for each ecotone was conducted at the same sampling location at which the samples in the previous chapter were sampled (Figure 3). The purpose of this vegetation analysis is to provide an inventory database of vegetation within DCEW with expectations of detecting temporal shifts in ecosystem function and process over future long-term monitoring goals, as well as distinguishing possible topographic controls of specific vegetation habitat within each ecosystem. Lastly, these data will then be available to parameterize specific vegetation characteristics that affect energy transfer dynamics through landscapes using ecohydrologic models.

4.2. Vegetation Analysis Materials and Methods

4.2.1 Sagebrush-Steppe Ecosystem

For sagebrush steppe, measurements of bare ground, grass, forbs, shrubs, detritus, and rock were recorded to determine percent cover, in addition to shrub frequency for a 30 m^2 pixel or macro-plot. The sampling unit used was a 1 x 2 m micro-plot or quadrat oriented length-wise down slope. To determine the minimum number of micro-plots needed to capture a representative sample, we began by randomly sampling 50 micro-plots within a macro-plot. Then, we plotted the number of micro-plots against the standard deviation for each life form measurement to depict the minimum number of

sample units necessary for one macro-plot (Figure 17). The number of micro-plots chosen for the sagebrush-steppe ecosystem was 20 and the number of macro-plots sampled was 40. Macro-plots used in this study were selected at random using the random generator in ArcMap 10. To assign locations of micro-plots, we started at the center of the macro-plot and used random paces and azimuths, where 1 pace is 2 footsteps, is not to exceed the boundary of the macro-plot, and micro-plots were not to overlap. For each micro-plot, there were 3 transects within a quadrat oriented downslope (600 cm total) for the quantification of percent ground cover using the continuous line intercept method described in Bonham's 1989 book "Measurements for Terrestrial Vegetation" (Picture 4). For each transect, the distance of each functional group was measured and recorded on a continuous line. In addition, frequency of shrubs was determined using the total number of micro-plots within the 30 m^2 macro-plot.

4.2.2 Conifer Ecosystem

The sampling unit used was a 100 m^2 macro-plot where two 30 m^2 micro-plots oriented in vertical angles were used for data collection to determine the average vegetation values. Density and frequency of mature and juvenile Douglas fir and ponderosa pine species in each micro-plot were recorded. There were a total of 28 macro-plots sampled. In addition, we measured the DBH (1.4 m) of each individual tree that was $\geq$ 1.4 m and counted individuals that were not at DBH. Individuals not at DBH were recorded as juveniles. Finally, using a convex spherical densiometer, we measured the percent canopy cover for each micro-plot at 4 points oriented 5 m away from the corners and towards the center of the micro-plot. Then, we calculated the overall canopy cover by taking the proportion of 24 points (1 measurement for each cardinal direction at each

corner of both micro-plots) that intercepted canopy while holding the densiometer level and approximately 1.4 m from the ground.

4.2.3 Riparian Ecosystem

We used the USDAs Forest Service General Technical Report RMRS-GTR-47 2000 protocol to determine the percent composition of species through the main channel of Dry Creek (Winward 2000). There were a total of 10 linear transects over the course of approximately 10 km and 500 m elevation change. The protocol uses a 50 m linear transect stretched from upstream to downstream, and for every pace along the stream the tree species nearest to the pace foot on the left and right of the stream were recorded and tallied. The total composition for the reach of the stream is calculated using the following equation.

$$\frac{\text{Total steps of each species (both sides)}}{\text{Total steps taken (both sides)}} = \text{Percent composition} \qquad \textit{Equation 2}$$

In addition, three cross-sectional transects at 0, 25, and 50 m markers on the stream transect were used to measure the riparian vegetation breadth by recording the distance of the “green line” to the end of riparian vegetation community starting from the center of the stream. Green line is the vegetation that most often occurs below the stream’s bankfull edge (Winward 2000). Lastly, we took measurements of canopy cover using a densiometer 10 m from both sides of the bank’s edge and at the green line along the cross-sectional transects.

4.3. Vegetation Analysis Results

4.3.1 Sagebrush Results

For the sagebrush-steppe ecotone, percent cover of bare ground was 47.89 ± 3.29, grass was 17.72 ± 4.6, forb was 13.03 ± 2.30, shrub was 16.0 ± 4.09, detritus was 4.16 ± 1.38, and rock was 1.21 ± 0.84 at the 95% confidence interval (Table 8). The frequency of shrubs found for the total 810 micro-plots contained within DCEW was 56%.

As for topographic controls, grass was the only measurement that significantly varied with regard to North, East, South, and West aspects. North slopes were 14.58 ± 7.33 and South slopes were 11.67 ± 6.0 at the 95% confidence level (P = 0.05) (Table 9). Boxplots of each measurements distribution with respect to aspect are provided in Figure 18 to 21. There were trends in elevation in which shrubs increase in percent cover with increasing elevation while grass decreases with elevation (Figure 22). However, there were no noticeable trends in forb cover or bare ground with elevation and no trends of any cover as a function of slope (Figure 23).

4.3.2 Conifer Results

The overall average DBH for mature Douglas fir and ponderosa pine was 83.92 cm ± 19.37 and 73.94 cm ± 20.83, respectively. The frequency and density or number of individuals of mature Douglas fir was 100% and 17.57 per micro-plotsor 58.57 per macro-plot while ponderosa pine was 57.14% and 8.77 per micro-plot or 29.23 per macro-plot.

The distribution of the DBHs of mature Douglas fir and ponderosa pine with respect to aspect is provided in Figure 24, where Douglas fir has a tighter distribution across all aspects and the largest diameters on the North (111.0 cm) and East (126.6 cm)

facing slopes. Ponderosa pine had largest diameters on North and East aspects; however, there were only 3 individuals on the North aspect out of the 4 macro-plots sampled. Table 10 indicates frequency of mature Douglas fir was 100% for nearly all aspects excluding the East, while ponderosa pine was present about 50% of the time excluding the South aspect where it was more frequent. The greatest density of mature Douglas fir was on the North aspect (approximately 30 per 30 m^2), whereas ponderosa pines were in greater numbers on the South and West (approximately 11 per 30 m^2) facing slopes. Moreover, the relative densities of Douglas fir on all aspects are greater than ponderosa pine and substantially greater on the North and East aspects. Results show Douglas fir and ponderosa pine juveniles, or individuals not tall enough to measure at DBH, were present on nearly all aspects. There was no presence of ponderosa pine juveniles on the North aspect but their greatest relative density was on South-facing slopes (Table 10). In addition, Figure 25 and Figure 26 are histograms of the density of mature Douglas fir with respect to aspect where 30.5 individuals per micro-plot were on North slopes and approximately 15 individuals were on all other aspects. Ponderosa pine had roughly 11 individuals per 30 m^2 micro-plot on South and West slopes, 6.7 on East slopes, and was nearly absent from the North aspect. Density of juveniles (< 1.4 m) on North and West slopes was nearly zero for both Douglas fir and ponderosa pine while the greatest density for both conifer species were on East and South aspects (Figure 26).

For percent canopy cover, trends in slope, and elevation each point was assigned a dominant conifer class (either Douglas fir or ponderosa pine) using the method discussed in Chapter 3. In review, these classes were not chosen simply based on number of individuals but also the size of DBH for the determination of the dominant conifer

species with respect to a remote sensing vantage point. Overall, both plots of dominant Douglas fir or ponderosa pine had a 90% closed canopy cover with ± 3.05 and ± 1.08 (α =0.05), correspondingly (Table 11). Moreover, percent canopy cover for the dominant Douglas fir sampling points on North-facing slopes was 90% (± 8.3), East-facing slopes was 88.68% (± 12.8), South-facing slopes was 89.7% (± 7.1), and West-facing slopes was 91.70% (± 3.5). There were no points on the North-facing slopes dominated by ponderosa, however East-facing slopes was 88.34% (± 0.8), South-facing slopes was 88.2% (± 2.0), and West-facing slopes was 92.00% (± 4.1) (Table 12). Trends in degree slope and dominant conifer class indicate ponderosa pine decreases in abundance with increased slope angles but is most abundant at the highest elevations of 1700 m or greater. Douglas fir macro-plots are most abundant at 20-29 degree slope and 1500-1699 m elevation (Figure 27 and Figure 28).

4.3.3 Riparian Results

There were 10 transects measured on Dry Creek, and given a moderately low sample size, we were able to detect subtle trends in deciduous and coniferous riparian vegetation growing along the banks. The most prevalent trends discovered were willow and water birch decreases as elevation increases, while mountain maple increases (Figure 29). There was also an increase in total conifer species at the edge of the bank as elevation increases. Moreover, the breadth of the green line across the creek decreases as elevation increases. The lowest elevation of the creek reaches lengths of 31.4 m across and the highest elevation measures 9.4 m across (Figure 30).

Canopy cover for over-story 10 m from the edge of the bank was 87.3% (± 4.7%) and at the green line was 93.3% (± 2.2%). There were no significant trends or correlation

with elevation and percent canopy cover. A species list of the stream's bank vegetation is provided in Table 13.

4.4 Vegetation Discussion

4.4.1 Sagebrush-Steppe Ecotone

For the sagebrush-steppe ecotone, bare ground covers approximately 45-50% of the landscape. This measurement has significant hydrologic implications as a result of runoff, infiltration, groundwater recharge, and evaporation, in addition to biogeochemical cycles through which energy are transferred back and forth between systems. Empirically, it appears there may have been a significant difference in the percent of bare ground with respect to North- and South-facing slopes; however, our study found that the only significant difference between these two aspects was the percent cover of grass. We propose that the measurement of forb cover may have biased true bare ground exposer on the South aspect as a result of the plant physiology of the dominant forb species. In general, forbs on the North-facing slopes were robust, such as arrowleaf balsamroot or lupine, while the South aspect was dominated by a noxious and invasive forb known as skeleton weed, which has very long thin branching stems, lacks leaves, and can reach heights up to 40 cm. When these long skinny plant parts parallelly intersect the transect, it can imply the skeleton weed is larger than it truly is, which reduces the exposure of actual bare ground. It seems very reasonable that grass on the North- and South-facing slopes significantly differed since it was visually obvious there were greater densities of bunch grasses on the North aspect compared to the South aspect. Unfortunately, the specific quantity of bunch grasses proved difficult to measure as a result of life history strategies of grasses. The distinction between individual plants, proliferating through

roots (rhizomatous) or through seed head production, often resembled small bunches that were not as full-bodied. Hence, the density of bunch grasses could not be recorded but was lumped into the broader life form group: grass.

Results proved shrub cover increased with elevation while grass cover decreased. When looking at shrub cover as a function of aspect, there was no significant difference in the average cover but the distribution on South-facing slopes was much wider than other aspects. This may be a result of a true larger variance or because there was much larger sample size on the South aspect. Lastly, there were no slope trends for any major life form within the sagebrush-steppe ecosystem. Possible reasons for this might be a result of present sagebrush-steppe species generally having shallow roots systems, which make it adept to grow on any incline or soil type while maintaining reproductive success.

4.4.2 Conifer Comparison

Conifer results indicate that the dominant species is Douglas fir and can be found throughout DCEW 100% of the time, while ponderosa pine is found nearly 50% in our samples.

Douglas fir is especially abundant on the North aspect and has nearly double the number of individuals per 100 m^2 macro-plot compared to other aspects containing its species. There were only three ponderosa pines located in our plots on the North aspect, one of which was the largest ponderosa (DBH 185 cm) sampled in the watershed. Unfortunately, the logging history of DCEW is not well documented and we must consider this isolated ponderosa may have been left behind from early logging efforts. Moreover, the Douglas fir present on this aspect were some of the largest within DCEW and had similar DBHs of 111 cm, which we postulate are likely close in age. Not

surprising, this heavily populated area of Douglas fir has nearly 0 juveniles of any conifer growing within the stand. Presumably, this is a result of a closed canopy from relatively large trees blocking sunlight from the forest floor during the brief hours this aspect can obtain sunlight. Unfortunately, closed canopy data collected for this study were approximately 90% for every aspect, representing no difference in open/closed canopy for sunlight to travel. The East aspect also has some of the largest Douglas fir trees but make up about 70% of the population compared to ponderosa pine. Ponderosa had nearly a uniform size across all aspects. Interestingly, this aspect has a majority of ponderosa pine juveniles growing at a ratio of approximately 13:1 per micro-plot. We can predict over long-term monitoring this aspect might be supplanted by ponderosa pine. For the South and West aspect, the density of mature Douglas fir and ponderosa trees remain the same with a proportion approximately 60/40 percent, respectively. Unlike the East aspect, the West aspect is dominated by Douglas fir juveniles (approximately 85%), which would give us reason to believe in future studies the West aspect might be even more abundant in Douglas fir.

As mentioned before, macro-plots dominated by Douglas fir are located on North-facing slopes, occur in areas with slope angles $\geq$ 20 degrees, and elevations of 1500 - 1699 m. Ponderosa pine are seldom found on slope angles greater than 30 degrees but are found at the highest elevations (1700-1999) within in the watershed. This may be a result of most South-facing hillsides on the North end of the watershed having lower degree slope angles than the hillsides on the North aspect. We could assume based on soil and water properties as a function of solar radiation that this might explain the distribution of both conifer species. In review, ponderosa pines are known to have a deep tap root that

can acquire water from great depths as oppose to Douglas fir, which have shallow and lateral root systems. The North aspect generally has thicker and more aggregate soils than the South aspect, which enable better establishment of Douglas fir roots. In addition, ponderosa pine have greater sapwood to heartwood ratios, enabling them to retain water for longer periods of time than Douglas fir, making it drought tolerant on the South aspect where there is higher solar radiance.

4.4.3 Riparian

Riparian vegetation measurements were limited due to time and research priority and analysis must be given with caution from the subsequent small sample size. There were general trends with regard to specific vegetation species and elevation in which mountain maple prefer higher elevations and species like water birch and willow prefer lower elevation. Also, as expected, the reach of the stream closest to the headwaters of DCEW had the smallest green line breadth. These results were expected due to the nature of stream channel down cutting from higher slope gradients expressed at higher elevations in a mountainous terrain. This sharp gradient consequently restricts the establishment of riparian vegetation communities on steep channel banks, disabling large breadths of green line.

4.5 Conclusion

The purpose of this part of the study was to quantify the major vegetation life forms and abiotic cover of DCEW with interests in establishing a baseline data set for long-term vegetation monitoring under a changing climatic regime, in addition to comparing vegetative quantities with respect to slope, elevation, and aspect to make inferences of possible drivers in vegetation distribution and abundance. There were a

total of 79 macro-plots sampled to measure vegetation within DCEW, which took many hours and resources to obtain. Nonetheless, the major findings of the distribution and abundance of the biotic and abiotic cover within the sagebrush-steppe ecosystem will be useful data for future inputs to ecohydrological models. Although fine-scale vegetation measurements are sometimes difficult and tedious to collect, they are essential in understanding changing ecosystems in effort to predict future processes and feedbacks. Our conifer analysis already suggests there is shifting change in species of ponderosa pine saplings occurring in some Douglas fir dominated landscapes. Whether those data can give us information about the toggle between multiple states of the state and transition model or if crossing over a nonreversible threshold will occur is to be determined in future work. Additionally, our results of this chapter corroborate our findings in the prior chapter's discussion of CART model tree splitting. Although frequency data of the broad classes were the target inputs to the CART, we now know with more certainty that the model did not chose these measures of impurity by chance or necessarily small sample size. Finally, with our efforts in identifying vegetation in the riparian zone of DCEW and the subsequent species list produced, we have provided a useful tool for prospective research to better understanding specific species and hydrological interaction through the hyporheic zone that influence lateral water flow patterns and stream discharge in this basin. Although our efforts were abundant, more samples for conifer and riparian ecosystems would have benefitted computational certainties. Furthermore, by using our methods in other geographic and complex landscapes of Northwest U.S., we will further our progression of understanding vegetation growth in complex terrains under a changing climatic system. With communal

efforts across the semiarid mountainous watersheds of the U.S., predictions of changing biogeochemical and energy flows are possible to predict and could influence energies in mitigation and preparation on a large scale.

The final chapter of this thesis discusses specific water content and plant vigor of the sagebrush-steppe ecosystem in efforts to support the SMAP mission funding by NASA. As well as gaining information for remote sensing research, these data are another useful tool in providing information about the micro-climate produced by living vegetation via photosynthetic properties and land atmospheric interactions. These implications will also affect outcomes of the state and transition model and future vegetation growth pattern predictions.

5. VEGETATION WATER CONTENT

5.1 Introduction to Vegetation Water Content

The land surface and atmospheric interface is one of the most important influences in regional weather and global climate. Moisture with in the soil surface drives vapor pressure gradients and consequently temperature and vegetation characteristics (Delworth & Manobe 1989). Many studies measure soil moisture within the first few centimeters of the surface to determine feedbacks within the biogeochemical cycle, in addition to the application of modeling weather forecasts, droughts, land cover changes, and floods (Brubaker & Entekhabi 1996). The final chapter of this thesis focuses on the water content contained within the vegetation of the sagebrush ecosystem and the resulting dry biomass per unit area in efforts to provide a usable dataset in the complex terrain of DCEW.

The National Aeronautics and Space Administration (NASA) have been using microwave passive and active remote sensing to develop algorithms to retrieve global soil moisture. However, there are issues with the above ground vegetation over laying the soil in which leaf water content attenuates the frequency of the signal through the leaves and increases sensitivity to moisture below the top centimeter of the soil surface (Njoku & Li 1999). Therefore, vegetation water content (VWC) is an important parameter for NASA's model development in the Soil Moisture Active Passive (SMAP) mission. There are limited global VWC datasets wherein NASA is giving great effort and funding for the

growth of accurate data under varying topographic and vegetative regions with the aim to perfect soil moister retrieval algorithms.

Typically, VWC is calculated as the ratio of fresh weight (from the field) to dry weight (after oven drying) (Wu *et al*. 2009). It is usually expressed in weight per unit area when a known unit of measurement is used such as 1 m^2 quadrat.

$$VWC = (FW - DM) / (FW + DM) \qquad \textit{Equation 3}$$

Furthermore, spectral analysis has become more often used as a method to detect vegetation water characteristics. Since the 1980s remote sensing technologies have advanced significantly, which has enabled easy transport of hand held equipment in the field with high spatial resolution. Spectral curves produced by vegetation is a function of leaf internal structure, biochemical constituents such as pigments, water, nitrogen, cellulose, and lignin that scatter and absorb spectral signatures (Seelig *et al*. 2008; Govender *et al.* 2009) (Figure 27). Other factors that are most influential at the plant leaf or canopy level are species, site, age or maturity of plants and foliage, nutrients, leaf orientation, background, and geometrical arrangement of the object or scene, sensor, and ground (Govender *et al.* 2009). Furthermore, spectral data at the leaf level contain the least amount of variability since vegetation cover can be highly heterogeneous at low resolutions, which introduces uncertainties as a result of mixed pixel variability (Jiang *et al.* 2006).

Other than soil moisture remote sensing applications, VWC is used in studies to estimate produce yields, fire susceptibility, and the assessment of drought conditions. These data are also used in rangeland studies where the resultant of VWC measurements

known as dry matter (DM) or dry biomass is used to calculate above ground carbon storage and livestock forage supply (Hirata *et al.* 2005; Martinez Carrotero *et al.* 2007).

The purpose of this study is to examine temporal shifts of VWC with respect to elevation and aspect at 5 sites in a sagebrush-steppe ecosystem for the purpose of soil moisture retrieval in the semiarid mountainous watershed known as DCEW. We propose with further remote sensing data, ancillary field data, vegetation maps, and an accurate VWC dataset the total above ground biomass and carbon storage can be used to answer prominent rangeland questions. Additionally, the VWC dataset can be used for future hydrologic modeling to detect and predict changes in plant water storage and consequently biogeochemical fluxes.

5.2 Study Site

As mentioned before, the study area of our research is within DCEW, however the specific sites at which data was collected were chosen by a former researcher (Smith *et al.* 2011), who installed soil moisture probes at varying depths on opposing aspects but at nearly equal elevations nearby weather stations maintained throughout the watershed. There are a total of 5 locations within the sagebrush-steppe ecosystem (Figure 33). The sites with the lowest elevation of 1130 m are known as Lower South (LS) and Lower North (LN), which have slopes of 28 and 31 degrees, respectively. The Mid-Lower South (MLS) and Mid-Lower North (MLN) sites are found approximately midway through the watershed, which is 1292 m above sea level and have slopes of 20 and 28 degrees, correspondingly. Finally, the Mid-High South (MHS) has the greatest elevation (1457 m) of the 5 sites with a 27 degree slope. The opposing North aspect was not sampled for this part of the study as a result of the dense conifer ecosystem, which did not contain

sagebrush-steppe vegetation. Vegetation at each location is comprised of typical sagebrush-steppe species of grasses, forbs, and shrubs. Further detail of distribution and abundance is discussed in Chapter 4. For the purpose of this study, grasses and forbs were combined during sampling while individual species of shrubs were not. Antelope bitterbrush (*Purshia tridentate*) is found at 3 of the 5 sampling locations (Picture 5). It has moderate to very deep roots and typically grows 1 to 2 m in height. Flowering begins in late spring to early summer and is heavily utilized in early spring by wildlife (USDA 2014). Rabbitbrush (*Ericameria, sp.*) is located at 4 of the 5 locations (Picture 6). This genus is often deep rooted and typically flowers in mid to late August. Lastly, there are a variety of sagebrush species mixed in the sagebrush-steppe ecosystem. Each species has a preferred elevation and soil type but Wyoming big sage (*Artemisia tridentata*) is more commonly found in DCEW. Their root systems are complex with a deep tap root and shallow diffuse roots near the surface that create "hydraulic lift," which enable deep soil moisture to be brought to the surface via the tap root during the day and is released into the soil at night (USDA 2014) (Picture 7).

5.3 VWC Materials and Methods

5.3.1 Field Collection

To determine VWC within the grass/forb life form, we clipped 3 samples of above ground biomass to the soil surface using a 0.25 m^2 plot (Picture 8). Vegetation was bagged and transported to the lab within 2 hours of collection to be processed immediately or stored in the freezer for future processing. In addition, we clipped branches containing leaves and woody stems of the shrub species identified at each site to obtain the relative vegetation water content (RVWC). To further investigate the water

content contained within the leaves throughout the spring and summer, we identified and permanently marked 3 specimens of each available species of shrub and 3 samples of grass/forb at each site. Then, using a FieldSpec ® Hand Held Spectroradiometer (HH2), we collected spectra from 325 to 1075 nm wavelengths at each marked location of grass/forb and shrub species on a weekly basis. However, there were atmospheric limitations while collecting and consequently missing data due to precipitation events occurring in the spring. Calibration of the instrument was done every 10 minutes using a white reflectance panel to account for atmospheric changes such as cloud cover, humidity, and temperature changes during the collection period. Also, the instrument was optimized concomitantly to account for signal-to-noise ratio. For each marked location, 5 spectra were collected, resulting in 15 spectra per vegetation type.

5.3.2 Data Processing

To measure VWC, all vegetation was weighed and oven dried at 75 C for 24 hours and re-weighed. VWC and dry matter for the grass/forb mixture was recorded as g/m^2 and for shrub vegetation types RVWC was recoded as the ratio of wet mass to total mass. Spectra were converted from raw digital numbers to reflectance using ViewSpec Pro ™ software.

5.4 VWC Results

5.4.1 Lower South and Lower North

The vegetation water content and dry biomass of the grass/forb life form at Lower South (LS) location is listed in Figure 34. There were 15 samples collected over the time frame of March 25, 2012 to August 27, 2013. VWC began at 1200 g/m^2 and declined to 656 g/m^2 while the DM began at 1584 g/m^2 and declined to 784 g/m^2. There was only

one species of shrub, bitterbrush, located at this site and results show in mid-June there was a maximum peak of approximately 33% RVWC (Figure 35). The VWC for Lower North (LN) was collected over the course of 16 days, which also began on March 25, 2013. For the grass/forb life form, VWC began at 2640 g/m^2 and declined to 768 g/m^2 while DM began at 1568 g/m^2 and declined to 720 g/m^2 (Figure 36). Overall, the average VWC for this site was 1241 g/m^2 (± 315 g/m^2) and appears to have a declining linear trend over time. Sagebrush and rabbitbrush were the only species present where the RVWC indicate sagebrush reached a maximum water content of approximately 39% in early July and rabbitbrush was approximately 35% in late July (Figure 37 and Figure 38).

5.4.2 Mid-Lower North and Mid-Lower South

There were 12 days sampled at the Mid-Lower North (MLN) and Mid-Lower South (MLS) sites. For MLS, VWC for grass/forb samples began at 1280 g/m^2, peaked at 2320 g/m^2 on May 28, 2012, and declined to 316 g/m^2. DM steadily declined from 832 g/m^2 to 137 g/m^2 over the entire sampling period (Figure 39). The shrub species located at MLS were bitterbrush and rabbitbrush and the RVWC for both shrubs follow a bell curve with peak water contents of approximately 36% around June 20, 2012 for bitterbrush and June 28, 2012 for rabbitbrush (Figure 40 and Figure 41). As for MLN, the VWC for grass/forb samples also followed a bell shape curve, where the start and end of the season were approximately 1500 g/m^2 and peaked to 4000 g/m^2 on June 8, 2012, while DM generally remained constant (1082 g/m2, ± 190 g/m^2) (Figure 42). Shrubs located at MLN were bitterbrush, rabbitbrush, and sagebrush. Bitterbrush at this location did not have a peak RVWC but remained relatively constant at approximately 45% throughout the sampling season (Figure 43). Rabbitbrush had a peak RVWC of about

40% on July 19, 2012 and sagebrush had a peak of about 35% around June 14, 2012 (Figure 44 and Figure 45).

5.4.3 Mid-High South

The Mid-High South (MHS) location was only sampled for 7 days. This location was the most difficult to access due to snow drifts on the road and hiking distance from the other sites. Furthermore, during the month of May, there was a high amount of precipitation at this elevation, which prevented frequent sampling. Thus, there was no data collected from April 28, 2012 to June 13, 2012. VWC and DM for the grass/forb life form at this location appear to decrease throughout the sampling season, which began at 1104 g/m^2 and ended at 50 g/m^2 (Figure 46). The shrubs located at this site were rabbitbrush and sagebrush, which had a peak RVWC of 41% on June 28, 2012 and 42% on June 20, 2012, respectively (Figure 47 and Figure 48).

5.5 VWC Discussion

5.5.1 Grass and Forbs

For each location sampled, there are varying slopes and elevations gradients that consequently had different periods of peak vegetation water content and dry biomass. In addition, we can assume the South aspect has greater actual solar radiation compared to the North aspect and therefore had differential stress gradients allowing dissimilar growing periods from one another. Also, by combing the category of grasses and forbs, variance was introduced as a function of the specific forb size (i.e., balsam arrowroot, lupine, etc.) contained in the quadrat and the time of season at which forbs were vigorous and flowering.

For the LS and LN sites, the time at which the highest water content was observed was at the beginning of the sample period and slowly decreased as the summer progressively got warmer and dryer. We believe that if we had begun sampling sooner in the season, instead of a linear decreasing trend over time, there would have been a polynomial trend capturing the increased retention and later release of VWC. Also, DM should have increased with the growing season and remained relatively constant or slightly decreasing throughout senescence as a function of slow decomposition and erosion rates.

For the Mid-Lower South (MLS) and Mid-Lower North (MLN) sites, the elevation was higher, and thus the growing season started later in the season compared to lower elevations. However, for MLS, the peak VWC was in May and had a less obvious polynomial trend when compared to MLN. Had sampling began sooner in the season for MLS, we likely would have been able to capture more of the increasing trend in VWC and DM, leading up to its peak in late May. For MLN, the peak came in early June and our data present a good indication of the changing VWC and DM over time.

For the Mid-High Site (MHS), the trend of VWC and DM are less clear due to the low sample size. We presume, had there been less inclement weather and better accessibility, sampling could have continued during the dates of April 28 to June 13, 2012, and the peak would have been captured during that time.

5.5.2 Shrubs

Each shrub species has different strategies to adapt in a semiarid mountainous terrain and therefore responds differently under climatic constraints. Generally, during the peak “green up” season, all shrubs maintain about 40% of their mass as water and the

remaining as dry biomass. However, antelope bitterbrush had the least flux of water content throughout the season regardless of elevation. Perhaps, their deep tap root system may have helped acquire deep soil water at times of drought more efficiently and/or their leaf morphology enabled better retention of water via the waxy leaf surface or more frequent stomata closures. Rabbitbrush and sagebrush follow the expected bell curve, which demonstrated that as the season provided more water, plant water storage in the leaves and stems increased, and conversely as water became a limiting resource as the summer progressed, the plant stored less water.

5.6 Conclusion

Overall, the purpose of this part of the study was to retrieve Vegetation Water Content per unit area for DCEW with intentions of extrapolating in similar sagebrush-steppe ecosystems across the semiarid mountainous terrain of the U.S. Unfortunately, after field collection, the 3 clipped samples of grass/forb and shrubs were combined into one bin during the oven drying process and consequently no error bars could be obtained. Also, the examination of spectra using the HH2 hand-held spectroradiameter collected for the 5 sites were not reviewed or further processed as a result of the time it would take to carefully analyze and correlate VWC with reflectance and NDVI. Perhaps, with intense spectral analysis, a strong correlation would have been discovered, which would have great usefulness in using only satellite remote sensing tools and less field collection to derive VWC estimations at large resolutions. Regardless of these mistakes, our data suggest that to define this value, calculations are spatially and temporally dependent. Although time and space is a factor to consider, a value can be reached with the addition of more data acquisition and processing. Using the broad-scale classification map,

discussed in Chapter 3 for each ecotone (sagebrush steppe, conifer, and riparian/deciduous), each classification can be analyzed further to determine the estimated VWC at a given time for DCEW. For example, for the sagebrush-steppe ecosystem, the percent cover data derived in Chapter 3 would allow the calculation of VWC of grasses and forbs combined, and by using an allometric equation and percent shrub cover, the entire ecosystem could be quantified. However, for the conifer and riparian/deciduous ecosystems, a bit more data acquisition and processing are needed. First, height data such as LiDAR for DCEW would be needed to estimate the total volume of trees, and with the addition of our density measurements and other allometric equations, VWC could be estimated. Then, using the map from Chapter 3, the sum of VWC for sage steppe and other ecosystems could be extrapolated across DCEW.

5.7 Final Discussion

Important results of this thesis document have provided data and information that will enable prospective researchers to develop studies to further investigate the drivers and major roles of biogeochemical pathways within the Dry Creek Experimental Watershed and adjacent ecosystems contained inside the semiarid Northwest U.S. A review of some of the important findings in this research is the production of an accurate 30 m resolution map (using an ANN) of the primary ecosystems in the intensely monitored and maintained watershed managed by Boise State University. Furthermore, implications using the CART model suggested the classification process used by the ANN indicate topographic inputs were a driver of classification and thus the distribution of specific classes is likely a function of elevation, slope, and aspect. Also, detailed vegetation quantification of the sagebrush steppe's major biotic and abiotic cover, in

addition to the quantification of the two central conifer species in the conifer ecosystem, were calculated. Statistical analyses of the topographic factors within the sagebrush-steppe ecosystem indicate the percent cover of grass was significantly higher on North-facing slopes than South-facing slopes. Also, nearly 50% of this ecosystem was exposed bare ground and with gaining elevation shrub cover increases while grass decreases. Furthermore, Douglas fir is the dominant conifer species within the watershed and is substantially more abundant and largest on the North aspect. This species prefers habitats where there is an incline of 20 degrees or more and an elevation range of 1500–1699 m. On the other hand, ponderosa pine is located in areas of 30 degree inclines or less but can also be located at the highest elevation in DCEW. Generally, these conditions are found on the South aspect. We believe the major driver of distribution and abundance of these two species is a function of solar radiation and its effects on the soil water characteristics via biogeochemical influences and specific root system structures. Moreover, when making predictions of future state and transitions a larger proportion of juveniles or immature Douglas fir is found growing on the West aspect of mixed stands while ponderosa pine juveniles appear to be dominating the East aspect. Future long-term monitoring via in situ measurement will be necessary in corroborating these predictions.

Although are efforts in vegetation water content data collection were vast, our sampling procedures were less than desirable. We can say with confidence that VWC and RVWC are greatly affected with elevation and time. However, the specific dates at which peak VWC and RVWC, and DM are to be used with caution as a result of our sample processing in addition to changing annual variability. We hope future works of others might encompass the copious amounts of spectra collected and the acquisition of the

necessary data and allometric equations necessary to provide DCEW with an estimated VWC of the multiple classes of vegetation contained within this complex terrain.

REFERENCES

Benediktsson, J. A., & Sveinsson, J. R. (1997). Feature extraction for multisource data classification with artificial neural networks. *International Journal of Remote Sensing, 18*(4), 727-740.

Bonham, C. D. (1989). *Measurement for terrestrial vegetation.* New York: Wiley.

Breiman, L., Friedman, J. H., Olshen, R. A., & Stone, C. J. (1984). *Classification and regression trees.* Washington, DC: Chapman & Hall/CRC Press.

Brady, N. C., Weil, R. R., & Brady, N. C. (2004). Elements of the nature and properties of soils. Upper Saddle River, N.J: Prentice Hall.

Brubaker, K. L. & Entekhabi, D. (1996). Analysis of feedback mechanisms in land-atmosphere iteraction. *Water Resources Research, 32*(5), 1343-1357.

Burns, R. M., & Honkala, B. H. (1990). *Silvics of North America* (Vol. 1). Washington, DC: United States Department of Agriculture.

Butterfield, H. S., & Malmström, C. M. (2009). The effects of phenology on indirect measures of aboveground biomass in annual grasses. *International Journal of Remote Sensing, 30*(12), 3133-3146.

Chappin III, F. S., Matson, P. A., & Vitousek, P. M. (2011). *Principles of terrestrial ecosystem ecology.* New York: Springer.

Congalton, R. G., & Green, K. (2009). *Assessing the accuracy of remotely sensed data: principles and practices.* Boca Raton, FL: CRC Press/Taylor & Francis.

Delworth, T., & Manabe, S. (1989). The influence of soil wetness on near-surface atmospheric variability. *Journal of Climate, 2*(12), 1447-1462.

Dingman, S. L. (2002). *Physical hydrology.* Upper Saddle River, NJ: Prentice Hall.

Entekhabi, D., Njoku, E. G., O'Neill, P. E., Kellogg, K. H., Crow, W. T., Edelstein, W. N., Entin, J. K., Goodman, S. D., Jackson, T. J., Johnson, J., Kimball, J., Piepmeier, J. R., Koster, R. D., Martin, N., McDonald, K. C., Moghaddam, M., Moran, S., Reichle, R., Shi, J. C., Spencer, M. W., Thurman, S. W., Tsang, L., & Van Zyl, J. (2010). The soil moisture active passive (SMAP) mission. *Proceedings of the IEEE, 98*(5), 704-716.

Farr, T. G., et al. (2007), The Shuttle Radar Topography Mission, Rev. Geophys., 45, RG2004, doi:10.1029/2005RG000183.

Freedman, J. M., Fitzjarrald, D. R., Moore, K. E., & Sakai, R. K. (2001). Boundary layer clouds and vegetation–atmosphere feedbacks. *Journal of Climate, 14*(2), 180-197.

Geroy, I. J., Gribb, M. M., Marshall, H. P., Chandler, D. G., Benner, S. G., & McNamara, J. P. (2011). Aspect influences on soil water rentention and storage. *Hydrological Processes, 25*(25), 3836-3842.

Golley, F. B. (1977). *Ecological succession.* Stroudsburg, PA: Dowden, Hutchinson & Ross.

Govender, M., Dye, P.J., Weiersbye, I. M., Witkowski, E. T. F., & Ahmed, F. (2009). Review of commonly used remote sensing and ground-based technologies to measure plant water stress. *Water SA, 35*(5), 741-752.

Graham, R. T., & Jain, T. B. (2005). *Ponderosa pine ecosystems.* General Technical Report, Department of Agriculture, Forest Service, US, Klamath Falls, OR.

Harkness, A. L. (1997). *Soil survey of Boise Front project, Idaho: interim and supplemental report.* Boise, Idaho: Natural Resources Conservation Service.

Havstad, K. M., & Herrick, J. E. (2003). Long-term ecological monitoring. *Arid Land Research and Management, 17*(4), 389-400.

Heermann, P. D. & Khazenie, N. (1992). Classification of multispectral remote sensing data using a back-propogating neural network. *Geoscience and Remote Sensing, IEEE Transactions, 30*(1), 81-88.

Hiemstra, C. A., Liston, G. E., & Reiners, W. A. (2002). Snow redistribution by wind and interactions with vegetation at upper treeline in the Medicine Bow Mountains, Wyoming, USA. *Arctic, Antarctic, and Alpine Research*, *34*(3), 262-273.

Hirata, M., Koga, N., Shinjo, H., Fujita, H., Gintzburger, G., Ishida, J., & Miyazaki, A. (2005). Measurement of above-ground plant biomass, forage availability, and grazing impact by combining satellite image processing and field survey in a dry area of north-eastern Syria. *Grass and Forage Science, 60*(1), 25-33.

Hyman, M. E., Johnson, C. E., Bailey, S. W., Hornbeck, J. W., & April, R. H. (1998). Chemical weathering and cation loss in a base-poor watershed. *Geological Society of America Bulletin, 110*(1), 85-95.

Jiang, Z., Huete, A. R., Chen, J., Chen, Y., Li, J., Yan, G., & Zhang, X. (2006). Analysis of NDVI and scaled difference vegetation index retrievals of vegetation fraction. *Remote Sensing of Environment, 101*(3), 366-378.

IPCC (2007). Climate Change 2007: The Physical Science Basis. Contribution of Working Group I to the Fourth Assessment Report of the Intergovernmental Panel on Climate Change [Solomon, S., D. Qin, M. Manning, Z. Chen, M. Marquis, K.B. Averyt, M.Tignor and H.L. Miller (eds.)]. Cambridge University Press, Cambridge, United Kingdom and New York, NY, USA.

Johnstone, J. F., Chapin III, F. S., Hollingsworth, T. N., Mack, M. C., Romanovsky, V. & Turetsky, M. (2010). Fire, climate change, and forest resilience in interior Alaska. *Canadian Journal of Forest Research, 40*(7), 1302-1312.

Kallarackal, J., & Roby, T. J. (2012). Response of trees to elevated carbon dioxide and climate change. *Biodiversity and Conservation, 21*(5), 1327-1342.

Kavzoglu, T. (2009). Increasing the accuracy of neural network classification using refined training data. *Environmental Modeling & Software, 24*(7), 850-858.

Kavzoglu, T., & Mather, P. M. (2003). The use of backpropgating artificial neural networks in land cover classification. *Internal Journal of Remote Sensing, 24*(23), 4907-4938.

Kunkel, M. L, Flores, A. N., Smith, T. J., McNamara, J. P., & Benner, S. G. (2011). A simplified approach for estimating soil carbon and nitrogen stocks in semi-arid complex terrain. *Geoderma, 165*(1), 1-11.

Landis, J. R., & Koch, G. G. (1977). The measurement of observer agreement for categorical data. *Biometrics*, *33*(1), 159-174.

Lefrançois, J., Grimaldi, C., Gascuel-Odoux, C., & Gilliet, N. (2007). Suspended sediment and discharge relationships to identify bank degredation as a main sediment source on small agriculture catchments. *Hydrological Processes, 21*(21), 2923-2933.

Martinez Carretero, E., Dalmasso, A., & Trione, S. (2007). Carbon storage in *Larrea divaricata* and *L. cuneifolia* (Zygophyllaceae) in drylands of central-western Argentina. *Arid Land Research and Management, 21*(4), 273-285.

Martinez, W. L., & Martinez, A. R. (2001). *Computational statistics handbook with MATLAB.* Boca Raton, FL: CRC Press.

Mas, J. F., & Flores, J. J. (2008). The application of artificial neural networks to the analysis of remotely sensed data. *International Journal of Remote Sensing, 29*(3), 617-663.

Masek, J. G., Vermote, E. F., Saleous, N. E., Wolfe, R., Hall, F. G., Huemmrich, K. F., Gao, F., Kutler, J., & Lim, T.-K. (2006). A Landsat surface reflectance dataset for North America, 1990-2000. *Geoscience and Remote Sensing Letters, IEEE, 3*(1), 68-72.

McNamara, J. P., Chandler, D., Seyfried, M., & Achet, S. (2005). Soil moisture states, lateral flow, and streamflow generation in a semi-arid, snowmelt-driven catchment. *Hydrological Processes, 19*(20), 4023-4038.

Miller, R. F., & Rose, J. A. (1999). Fire history and western juniper encroachment in sagebrush steppe. *Journal of Range Management, 52*(6), 550-559.

Moisen, G. G. 2008. Classification and regression trees. In: Jørgensen, Sven Erik; Fath, Brian D. (Editor-in-Chief). Encyclopedia of Ecology, volume 1. Oxford, U.K.: Elsevier. p. 582-588.

Nelson, N. A., & Pierce, J. (2010). Late-Holocene relationships among fire, climate and vegetation in a forest-sagebrush ecotone of southwestern Idaho, USA. *The Holocene, 20*(8), 1179-1194.

Njoku, E. G., & Li, L. (1999). Retrieval of land surface parameters using passive microwave measurements at 6-18 GHz. *Geoscience and Remote Sensing, IEEE Transactions, 37*(1), 79-93.

Nolin, A. W. (2012). Perpectives on climate change, mountain hydrology, and water resources in the Oregon Cascades, USA. *Mountain Research and Development, 32*(S1), S35-S46.

Odum, E. P. (1969). The strategy of ecosystem development. Sustainability: Sustainability, 164, 58.

Olden, J. D., & Jackson, D. A. (2002). Illuminating the "black box": a randomization approach for understanding variable contributions in artifical neural networks. *Ecological Modelling, 154*(1-2), 135-150.

Paola, J. D., & Schowengerdt, R. A. (1995). A detailed comparison of backpropogation neural network and maximum-likelihood classifiers for urban land use classification. *Geoscience of Remote Sensing, IEEE Transactions, 33*(4), 981-996.

Qui, F., & Jensen, J. R. (2004). Opening the black box of neural networks for remote sensing image classification. *International Journal of Remote Sensing, 25*(9), 1749-1768.

Rumelhart, D. E.; Hinton, G. E.; Williams, R. J. (1986). Learning representations by back-propagating errors. *Nature 323*(6088), 533–536. doi:10.1038/323533a0

Seelig, H.-D., Hoehn, A., Stodieck, L. S., Klaus, D. M., Adams III, W. W., & Emery, W. J. (2008). The assessment of leaf water content using leaf reflectance ratios in the visible, near-, and short-wave-infrared. *International Journal of Remote Sensing, 29*(13), 3701-3713.

Smith, T. J., McNamara, J. P., Flores, A. N., Gribb, M. M., Aishlin, P. S., & Benner, S. G. (2011). Smal soil storage capacity limits benefit of winter snowpack to upland vegetation. *Hydrological Processes, 25*(25), 3858-3865.

Stout, D. L., & Sala, A. (2003). Xylem vulnerability to cavitation in *Psuedotsuga menziesii* and *Pinus ponderosa* from contrasting habitats. *Tree Physiology, 23*(1), 43-50.

Tabacchi, E., Correll, D. L., Hauer, R., Pinay, G., Planty-Tabacchi, A. M., & Wissmar, R. C. (1998). Development, maintenance and role of riparian vegetation in the river landscape. *Freshwater Biology, 40*(3), 497-516.

Taylor, C. A. (2003). Rangeland monitoring and fire: wildifires and prescribed burning, nutrient cycling, and plant succession. *Arid Land Research and Management, 17*(4), 429-438.

Tesfa, T. K., Tarboton, D. G., Chandler, D. G., & McNamara, J. P. (2009). Modeling soil depth from topographic and land cover attributes. *Water Resources Research, 45*(10).

United States Department of Agriculture, Soil Conservation Service. 1997. Soil survey of Boise Front Project, Idaho.

USDA. (2014, August 20). *The PLANTS Database.* Retrieved August 2014, 2014, from USDA, NRCS: http://plants.usda.gov

Wagner, V. (2008). *Endangered Species.* Detriot: Greenhaven Press.

Way, D. A., & Oren, R. (2010). Differential responses to changes in growth temperature between trees from different functional groups and biomes: a review and synthesis of data. *Tree Physiology, 30*(6), 669-688.

Westoby, M., Walker, B., & Noy-Meir, I. (1989). Opportunistic management for rangelands not at equilibrium. *Journal of Range Management, 42*(4), 266-274.

Wu, C., Niu, Z., Tang, Q., & Huang, W. (2009). Predicting vegetation water content in wheat using normalized difference water indices derived from ground measurments. *Journal of Plant Research, 122*(3), 317-326.

Yu, C. C., & Lui, B.-D. (2002). A backpropogation algorithm with adaptive learning rate and momentum coefficient. *Neural Networks, 2002, IJCNN'02. Proceedings of the 2002 International Joint Conference, 2*, 1218-1223.

APPENDIX A

Tables

Tables

Table 1. Confusion matrices of ANN representing spectral features, topographic features, and both spectral and topographic features combined. Bold numbers are correctly classified pixels where surrounding numbers are misclassifications. Asterisked values in bold are the overall accuracies.

Spectral Features

	Sage	Pond	DF	Rip/Dec	
Sage	**39**	2	1	5	
Pond	1	**7**	4	2	
DF	0	1	**14**	3	
Rip/Dec	0	0	0	**0**	
					***75.9**

Topographic Features

	Sage	Pond	DF	Rip/Dec	
Sage	**36**	5	2	4	
Pond	1	**2**	1	0	
DF	2	3	**16**	1	
Rip/Dec	1	0	0	**5**	
					***74.7**

Spectral and Topographic Features

	Sage	Pond	DF	Rip/Dec	
Sage	**39**	3	2	4	
Pond	1	**6**	1	0	
DF	0	1	**16**	2	
Rip/Dec	0	0	0	**4**	
					***82.3**

Table 2. Confusion matrices of CART representing spectral features, topographic features, and both spectral and topographic features combined. Bold numbers are correctly classified pixels where surrounding numbers are misclassifications. Asterisked values in bold are the overall percent accuracies

Spectral Features

	Sage	Pond	DF	Rip/Dec	
Sage	**33**	3	0	4	
Pond	0	**5**	2	3	
DF	0	2	**15**	2	
Rip/Dec	3	4	2	**1**	
					***68.35**

Topographic Features

	Sage	Pond	DF	Rip/Dec	
Sage	**27**	9	2	2	
Pond	1	**7**	2	0	
DF	0	5	**14**	0	
Rip/Dec	2	0	0	**8**	
					***70.89**

Spectral and Topographic Features

	Sage	Pond	DF	Rip/Dec	
Sage	**33**	6	0	1	
Pond	1	**7**	1	1	
DF	1	4	**14**	0	
Rip/Dec	1	1	1	**7**	
					***77.22**

Table 3. Individual error matrix kappa analysis results for spectral, topographic, and both spectral and topographic features combined in the ANN and CART models.

ANN

Matrix	Kappa	Variance	Z Stat
Spectral	0.610	0.005	9.000
Topographic	0.590	0.006	7.900
Spectral and Topographic	0.710	0.004	10.700

CART

Matrix	Kappa	Variance	Z Stat
Spectral	0.530	0.005	7.716
Topographic	0.586	0.005	8.311
Spectral and Topographic	0.664	0.004	9.932

Table 4. Pairwise comparison of the ANN and CART model at the 95% confidence level. Between both models, the topographic inputs were the only simulations that performed differently

Pairwise comparison ANN vs CART

Matrix	Z Stat	P value
Spectral	0.81	0.6
Topographic	0.04	0.03
Spectral and Topographic	0.50	0.4

Table 5. Comparison of User's and Producer's accuracy given both ANN and CART with varying inputs to models

a. Spectral

	Producer's Accuracy		User's Accuracy	
Class	ANN	CART	ANN	CART
Sage	97.50	91.67	82.98	82.50
Ponderosa	70.00	35.71	50.00	50.00
Douglas Fir	73.68	78.95	77.78	78.95
Riparian/Deciduous	0.00	10.00	NaN	10.00

b. Topography

	Producer's Accuracy		User's Accuracy	
Class	ANN	CART	ANN	CART
Sage	90.00	90.00	76.60	67.50
Ponderosa	20.00	33.33	50.00	70.00
Douglas Fir	84.21	77.78	72.73	73.68
Riparian/Deciduous	50.00	80.00	83.33	80.00

c. Spectral and Topography

	Producer's Accuracy		User's Accuracy	
Class	ANN	CART	ANN	CART
Sage	97.50	91.67	81.25	82.50
Ponderosa	60.00	38.89	75.00	70.00
Douglas Fir	84.21	87.50	84.21	73.68
Riparian/Deciduous	40.00	77.78	100.00	70.00

Table 6. The number of pixels classified by the ANN and CART with varying inputs of training. Total number of pixels is 76,176.

	Topo Tree	Topo ANN	Landsat Tree	Landsat ANN	Both Tree	Both ANN
Sage	17698	27444	42079	52129	30324	44402
Pond	866	6104	3024	10905	11189	5902
Dfir	28331	19352	29586	13055	11027	17684
Rip/Dec	29281	23276	1487	87	23636	8188

Table 7. Percent class for DCEW and surrounding areas with each model and varying inputs

	Sage	Pond	Dfir	Rip/Dec
Topo ANN	36.03	8.01	25.40	30.56
Topo CART	23.23	1.14	37.19	38.44
Landsat ANN	68.43	14.32	17.14	0.11
Landsat CART	55.24	3.97	38.84	1.95
Both ANN	58.29	7.75	23.21	10.75
Both CART	39.81	14.69	14.48	31.03

Table 8. Total percent cover of bare ground, grass, forb, shrub, detritus, and rock for all samples of sagebrush steppe in DCEW. (Confidence level 0.05)

Group	Average	STD	CI (0.05)
BA	47.89	10.63	3.29
GR	17.72	14.86	4.60
FB	13.03	7.43	2.30
SH	15.99	13.18	4.09
DT	4.15	4.45	1.38
R	1.21	2.71	0.84

Table 9. Percent cover of bare ground, grass, forb, shrub, detritus, and rock with corresponding confidence intervals at the 95% level for aspect in DCEW. *Significant difference between North and South slopes at the 95% confidence level.

	% BA	BA ± CI	% GR	GR ± CI	% FB	FB ± CI	% SH	SH ± CI	% DT	DT ± CI	% R	R ± CI
North (n=6)	35.03	8.79	*14.58	7.33	17.05	3.90	10.21	10.13	20.36	4.77	11.75	0.22
East (n=9)	49.24	5.42	19.92	9.82	12.98	1.52	12.89	7.74	3.45	2.43	1.52	1.61
South (n=19)	49.84	4.85	*11.67	5.97	14.80	4.32	18.60	6.89	3.68	2.05	1.41	1.53
West (n=6)	45.42	10.37	18.80	12.18	10.24	4.79	18.17	4.88	6.15	3.13	1.22	1.62

Table 10. Average Diameter at Breast Height, frequency, density, and relative density of mature and juvenile Douglas fir and ponderosa pine with respect to aspect in DCEW. (Confidence interval at 95% level)

		North (n=4)	East (n=6)	South (n=7)	West (n=11)
Average DBH	DF	110.96 ± 20.85	126.62 ± 53.17	81.04 ±26.59	54.47 ± 25.90
	PP	116 ± 135.24	93.99 ± 52.10	63.70 ± 21.59	70.19 ± 23.62
Frequency Mature	DF	100.00	83.33	100.00	100.00
	PP	50.00	50.00	71.43	54.55
Density Mature (30 and 100 m^2)	DF	30.50 and 101.67	15.17 and 50.57	16.00 and 53.33	15.18 and 50.6
	PP	0.50 and 1.67	6.75 and 22.50	11.43 and 38.10	11.18 and 37.27
Relative Density Mature	DF	98.79	69.20	58.33	57.59
	PP	1.21	30.80	41.67	42.41
Frequency Juvenile	DF	50.00	50.00	71.43	72.73
	PP	0.00	33.33	42.86	36.36
Density Juvenile (30 and 100 m^2)	DF	0.88 and 2.93	13.17 and 43.90	2.00 and 6.67	12.09 and 40.30
	PP	0.00	0.75 and 2.50	1.29 and 4.30	2.14 and 7.13
Relative Density Juvenile	DF	100.00	94.61	60.87	84.98
	PP	0.00	5.39	39.13	15.02

Table 11. Overall closed canopy for all Douglas fir or ponderosa pine plots.

	% Closed Canopy	Confidence Interval (95%)
Douglas fir	90.4445125	3.051976
Ponderosa pine	89.5205556	1.809123

Table 12. Percent closed canopy for dominant conifer species of Douglas fir and ponderosa pine in a 30 m^2 sampling point with respect to aspect.

		% Closed Canopy	Confidence Interval (95%)
North	DF	90.71475	8.307208
	PP	N/A	N/A
East	DF	88.68458	12.8012
	PP	88.34333	0.797367
South	DF	89.72188	7.100128
	PP	88.21875	1.967029
West	DF	91.69422	3.479969
	PP	91.99958	4.129071

Table 13. Species list of vegetation found on riparian streaches in DCEW

Common Name	Latin name
Water Birch	*Betula occidentalis*
Mountain Maple	*Acer glabrum*
Mountain Alder	*Alnus incana spp.*
Hackberry	*Celtis sp.*
Cascara buckthorn	*Frangula purshiana*
Lewis' Mockorange	*Philadelphus Lewisii*
Bittercherry	*Prunis emarginata*
Hawthorn	*Crataegus douglasii*
Willow	*Salix sp.*
Cottonwood	*Populus sp.*
Rose hip	*Rosa rugosa*
Douglas fir	*Psuedotsuga menziesii*
Sagebrush	*Artemisia sp*
Snowbrush ceanothus	*Ceanothus velutinus*
Ponderosa pine	*Pinus ponderosa*

APPENDIX B

Figures

Figures

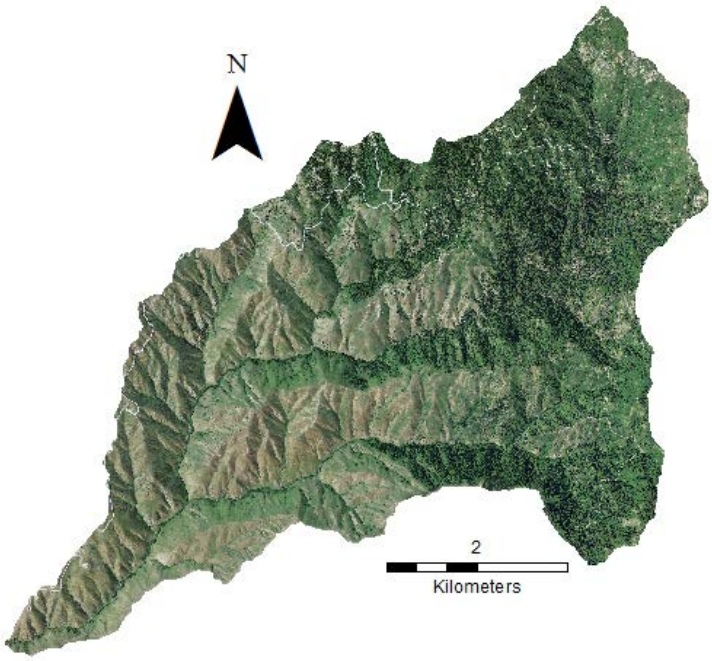

Figure 1. Aerial image of Dry Creek Experimental Watershed

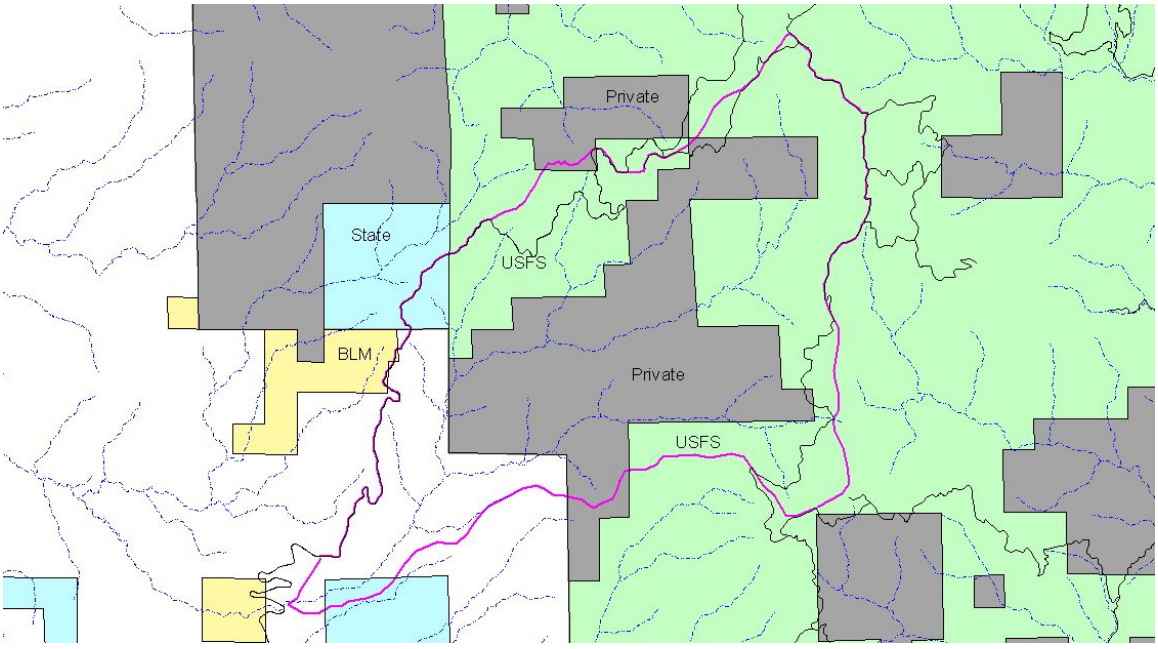

Figure 2. Distribution of land ownership for DCEW, provided by Ray Ecklund from United States Forest Service in 2013 (USFS)

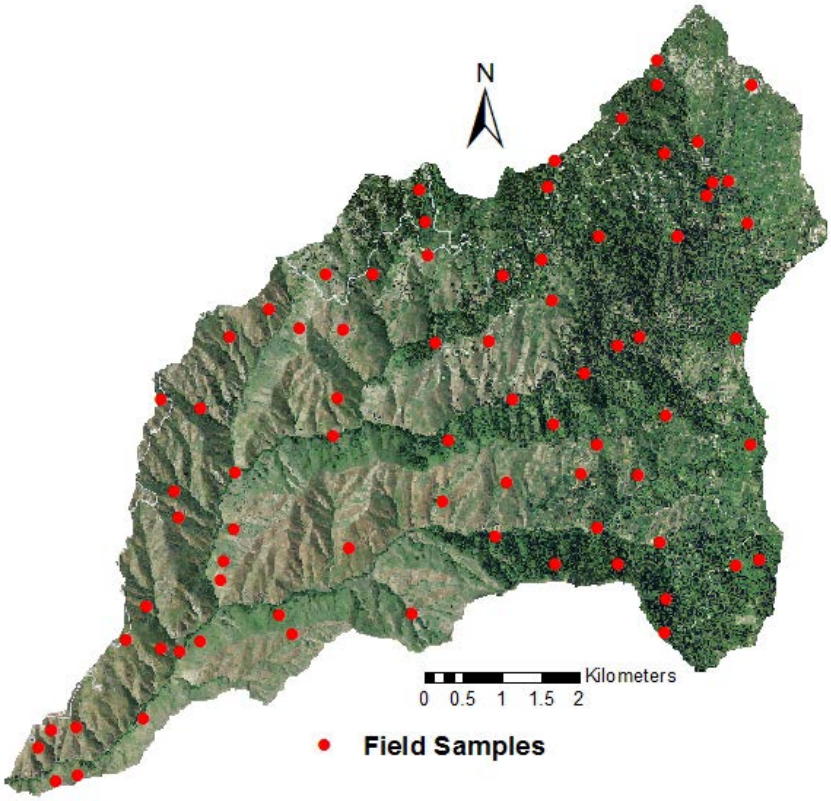

Figure 3. DCEW macro-plots locations for the 2011 and 2012 field seasons.

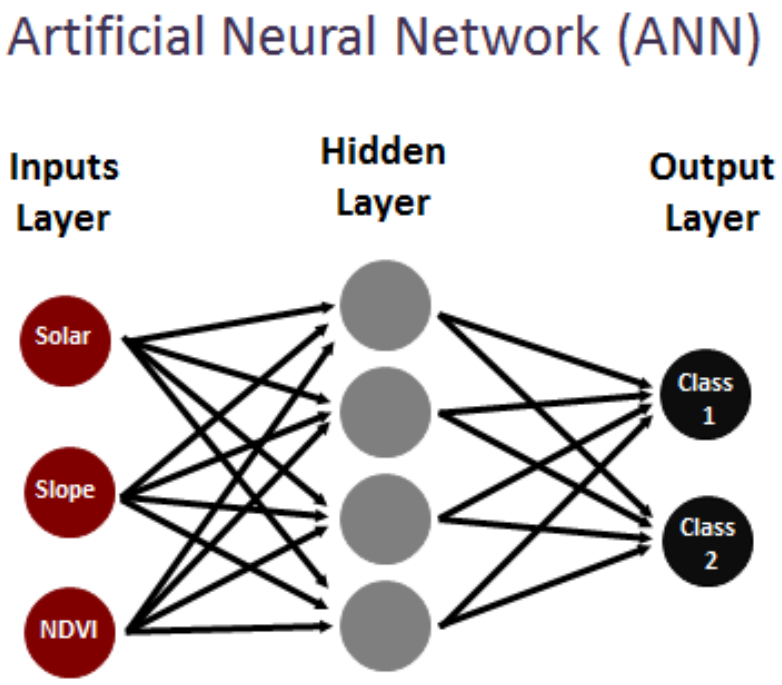

Figure 4. **An example of the artificial neural network architecture, which includes an input layer, hidden layer and output layer.**

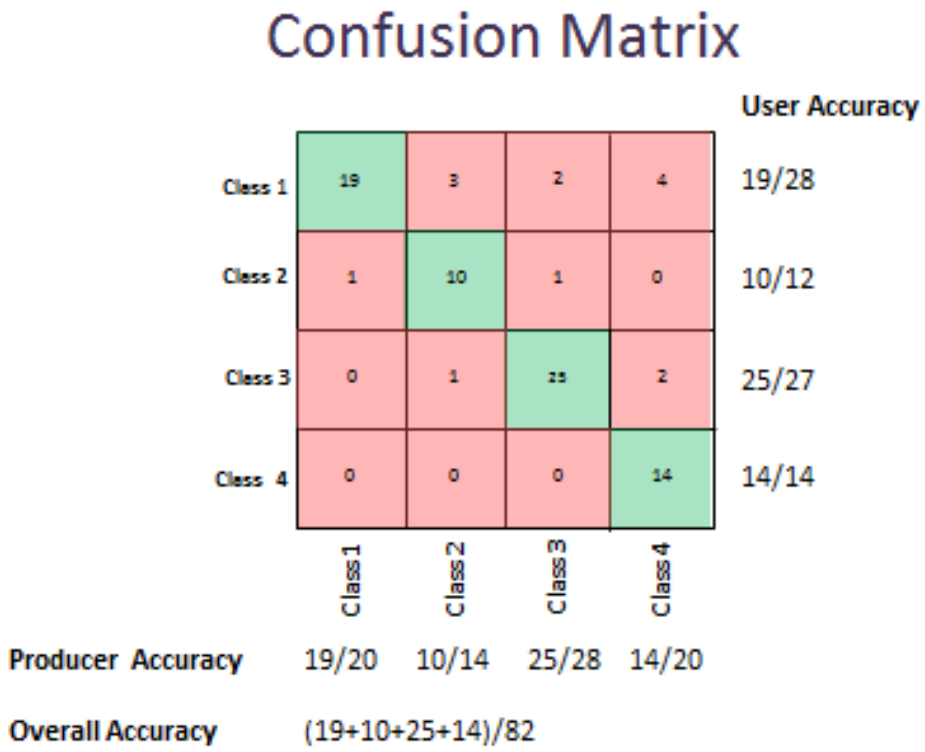

Figure 5. **An example of a confusion matrix, which includes 4 classes and the computation of the user, producer, and overall accuracies.**

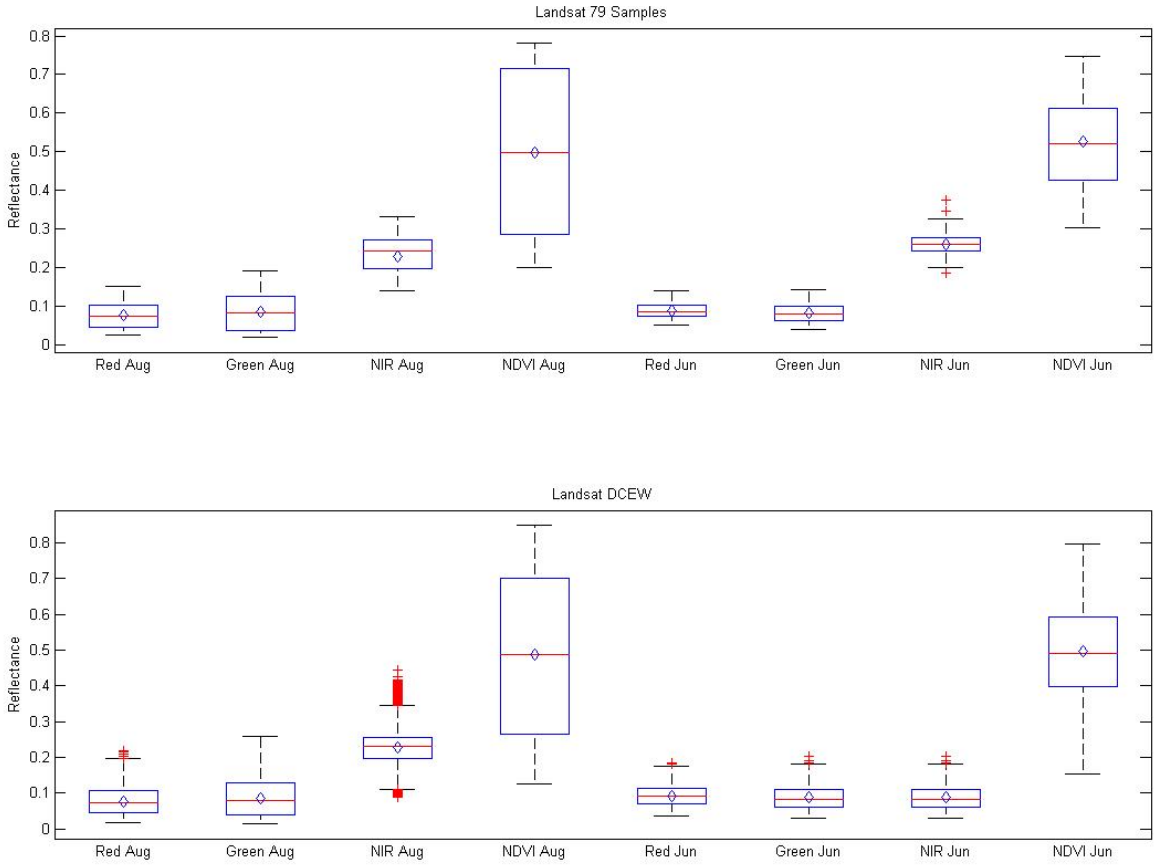

Figure 6. Distribution of remote sensing inputs using the 79 samples collected in the field (top) and all pixels used for DCEW and the surrounding area (bottom).

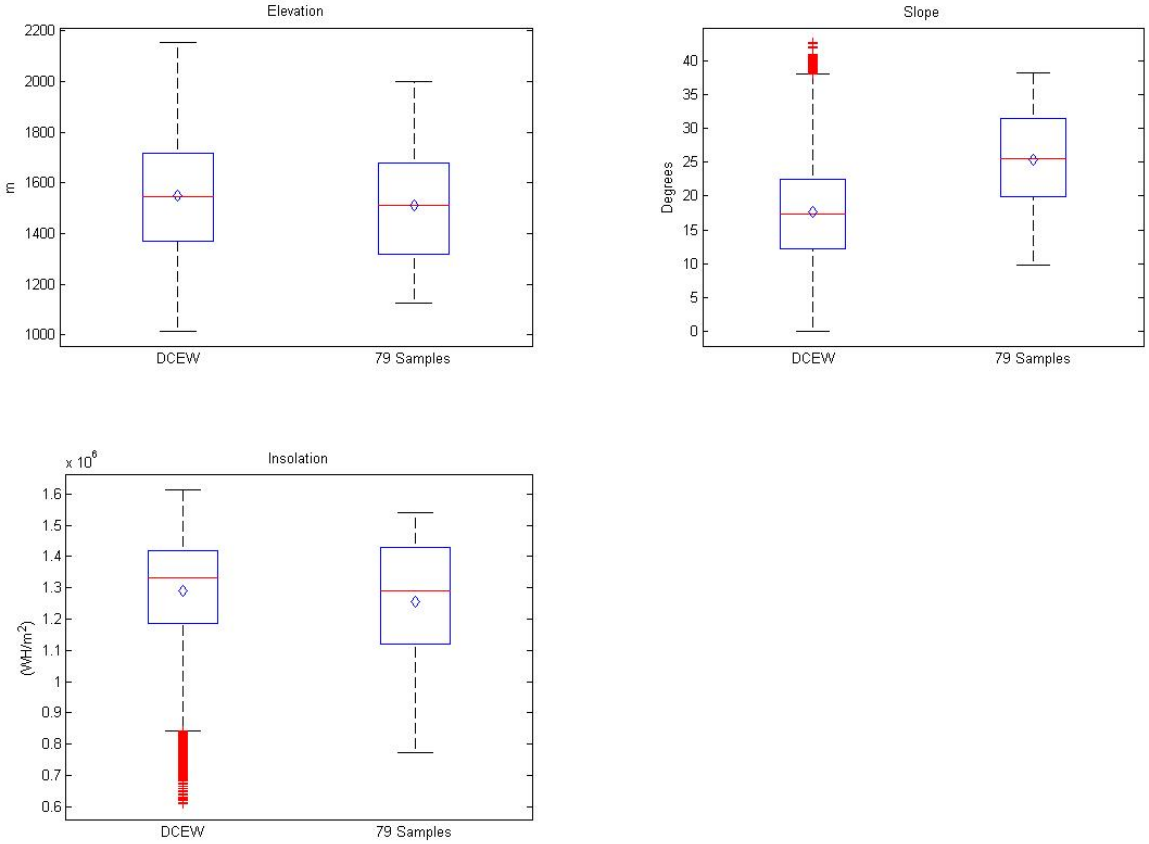

Figure 7. Distribution of topographic inputs (elevation, slope, and potential insolation) for the 79 samples collected in the field and all pixels used in DCEW and the surrounding area.

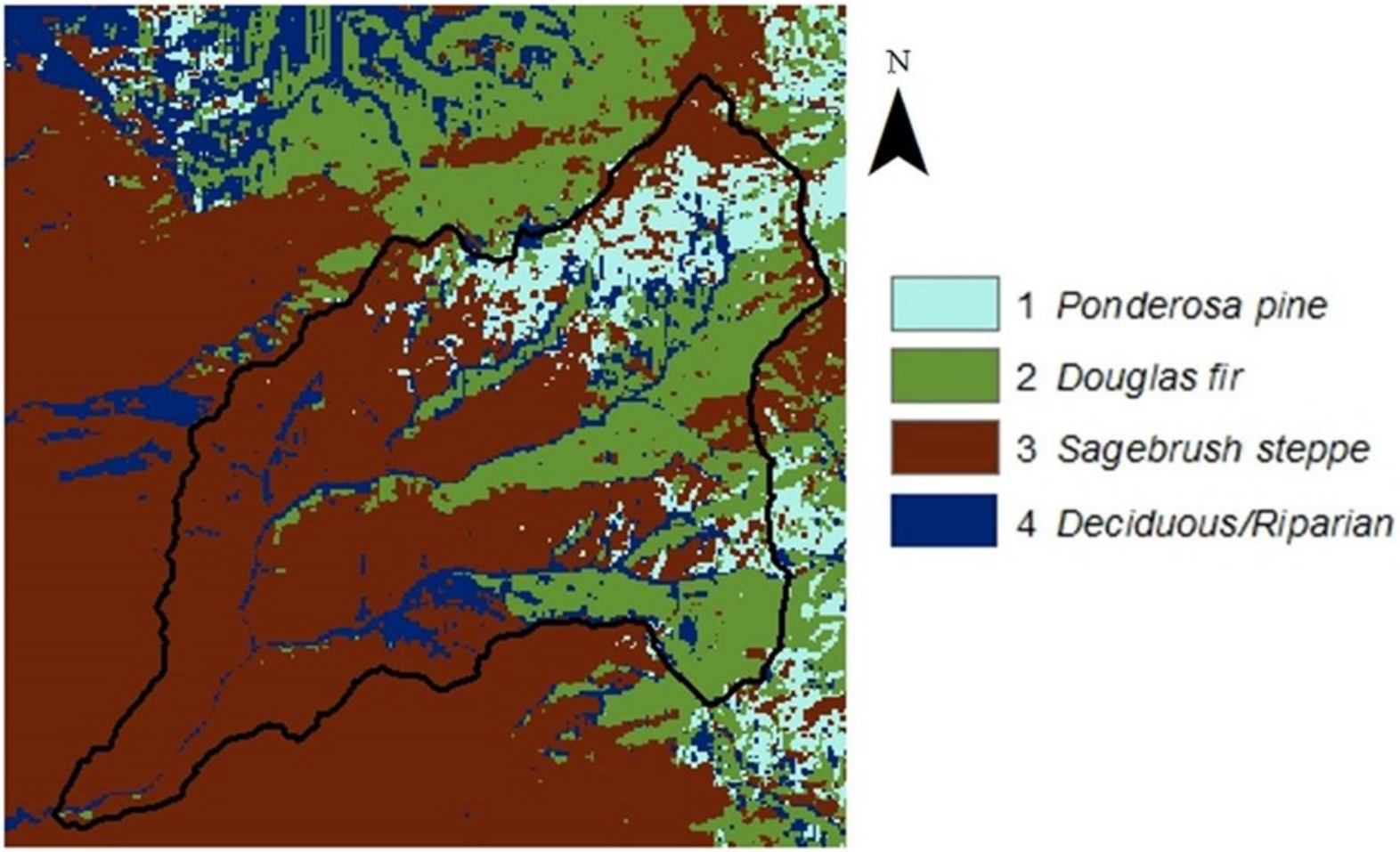

Figure 8. Output map of 4 classes (ponderosa pine, Douglas fir, sagebrush steppe, and deciduous/riparian) using the Artificial Neural Network (ANN) with 8 spectral inputs (red band, green band, near infrared band, and NDVI for June and August) and 3 topographic inputs (elevation, slope, and potential solar radiation) for DCEW and the surrounding area.

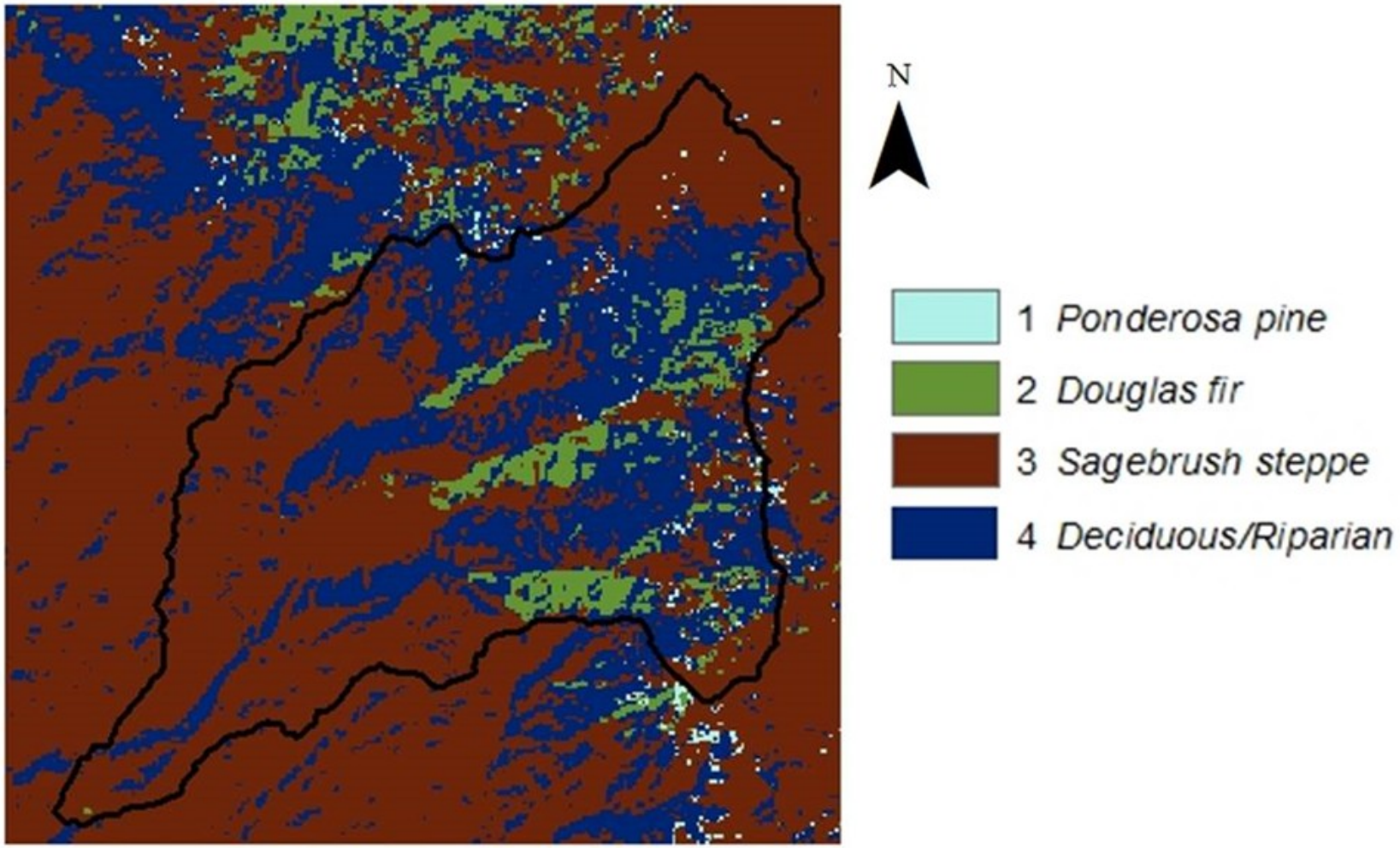

Figure 9. Output map of 4 classes (ponderosa pine, Douglas fir, sagebrush steppe, and deciduous/riparian) using the Artificial Neural Network (ANN) with 8 spectral inputs (red band, green band, near infrared band, and NDVI for June and August) for DCEW and the surrounding area.

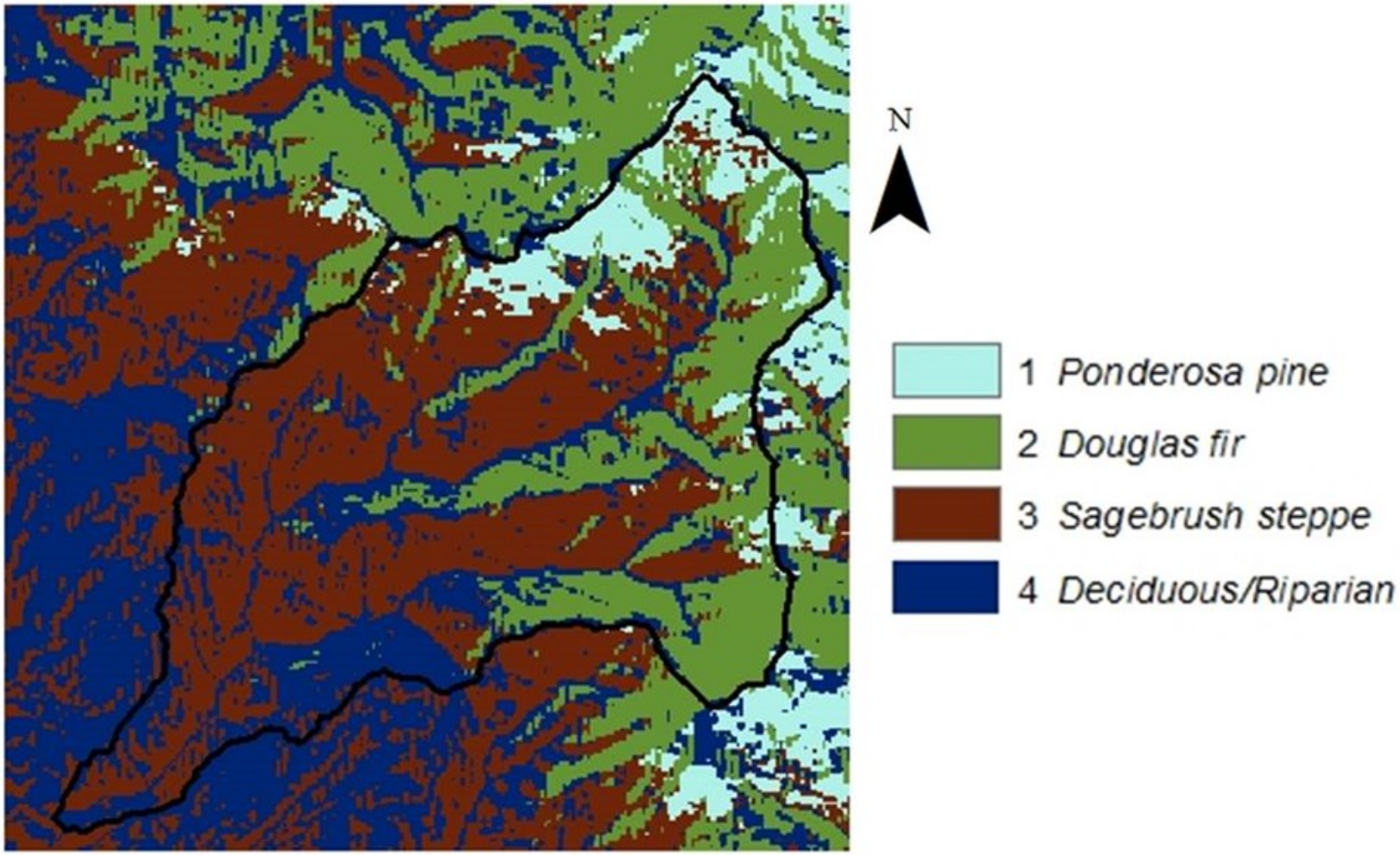

Figure 10. Output map of 4 classes (ponderosa pine, Douglas fir, sagebrush steppe, and deciduous/riparian) using the Artificial Neural Network (ANN) with 3 topographic inputs (elevation, slope, and potential solar radiation) for DCEW and the surrounding area.

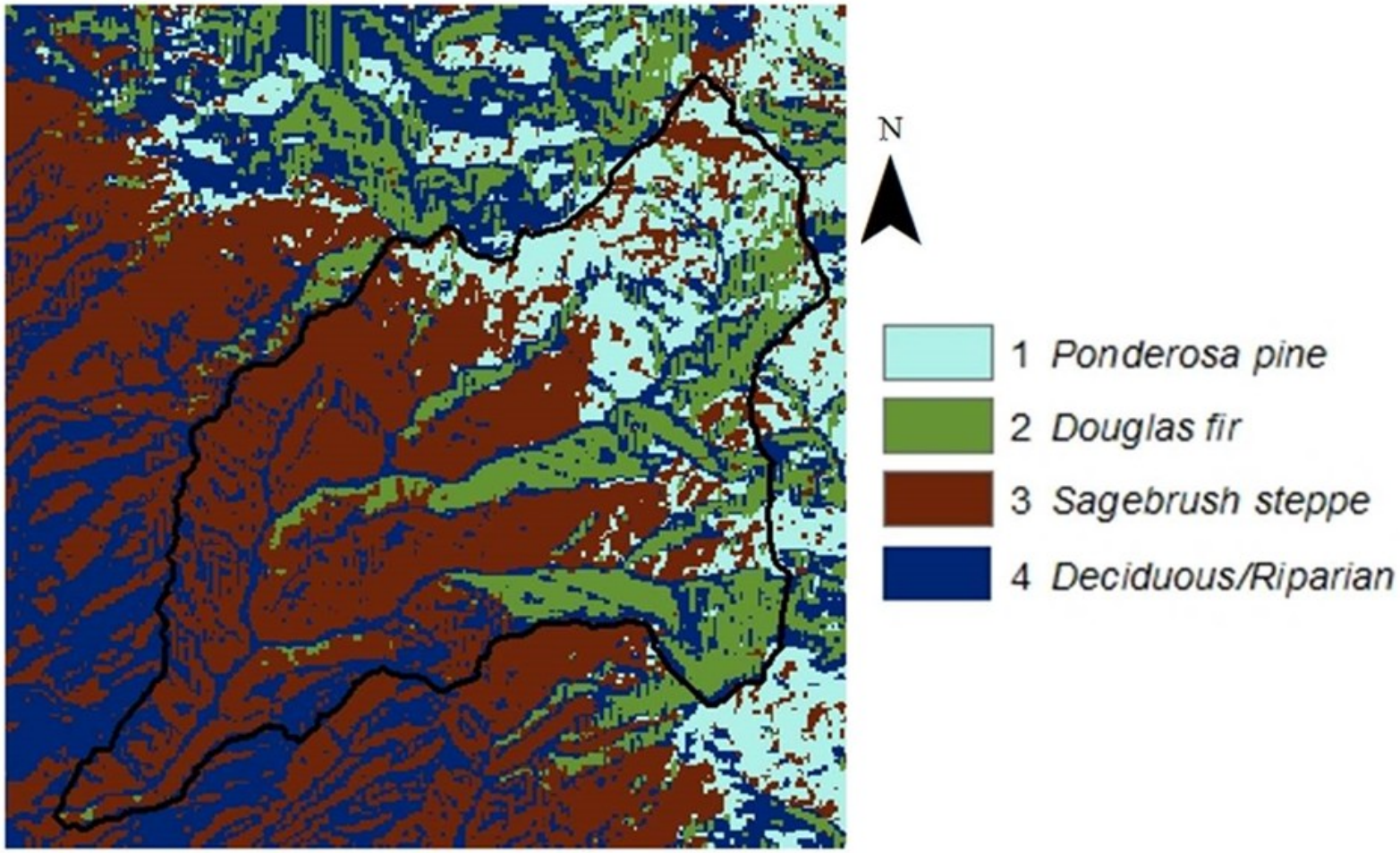

Figure 11. Output map of 4 classes (ponderosa pine, Douglas fir, sagebrush steppe, and deciduous/riparian) using the Classification and Regression Tree (CART) with 8 spectral inputs (red band, green band, near infrared band, and NDVI for June and August) and 3 topographic inputs (elevation, slope, and potential solar radiation) for DCEW and the surrounding area.

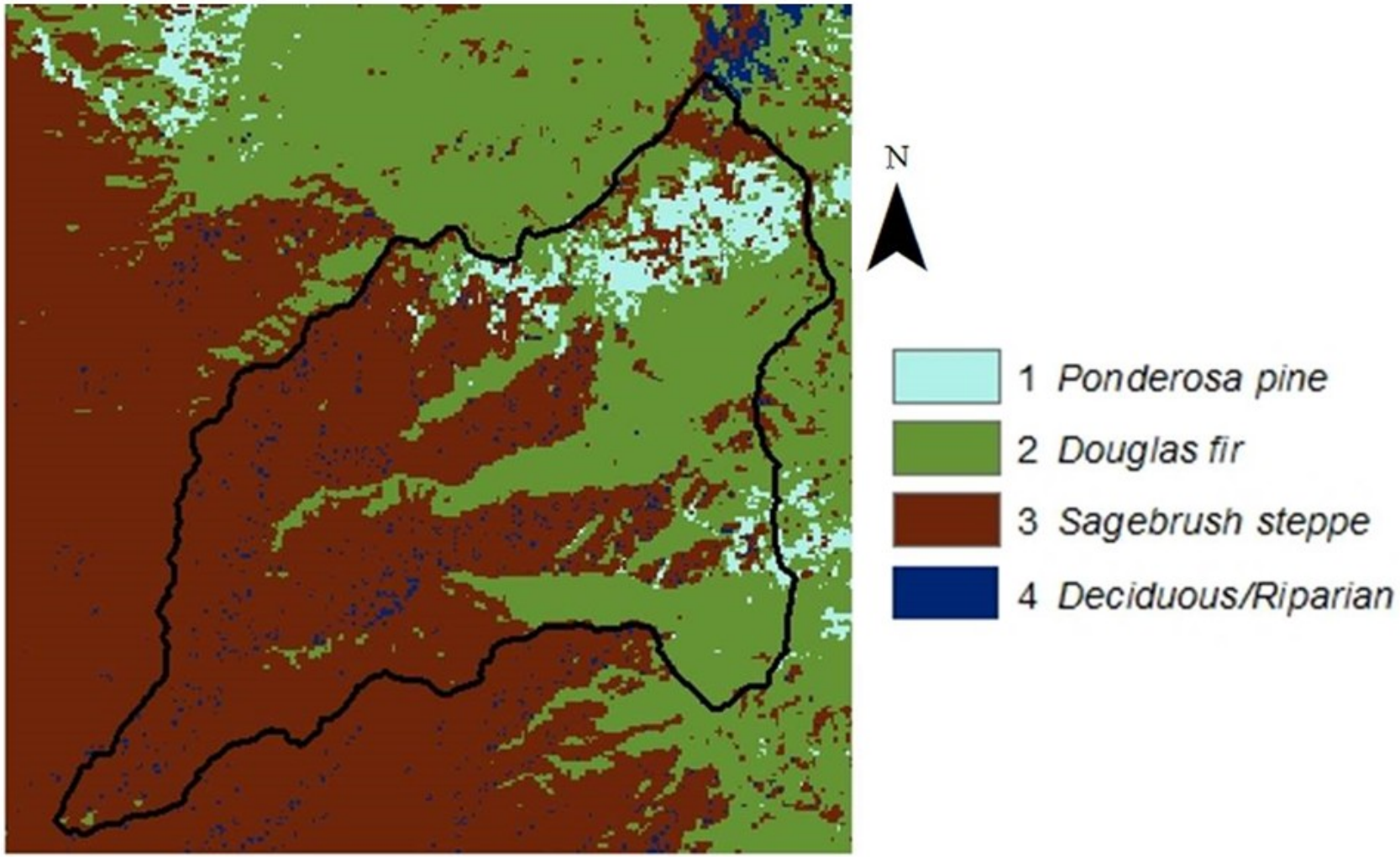

Figure 12. Output map of 4 classes (ponderosa pine, Douglas fir, sagebrush steppe, and deciduous/riparian) using the Classification and Regression Tree (CART) with 8 spectral inputs (red band, green band, near infrared band, and NDVI for June and August) for DCEW and the surrounding area.

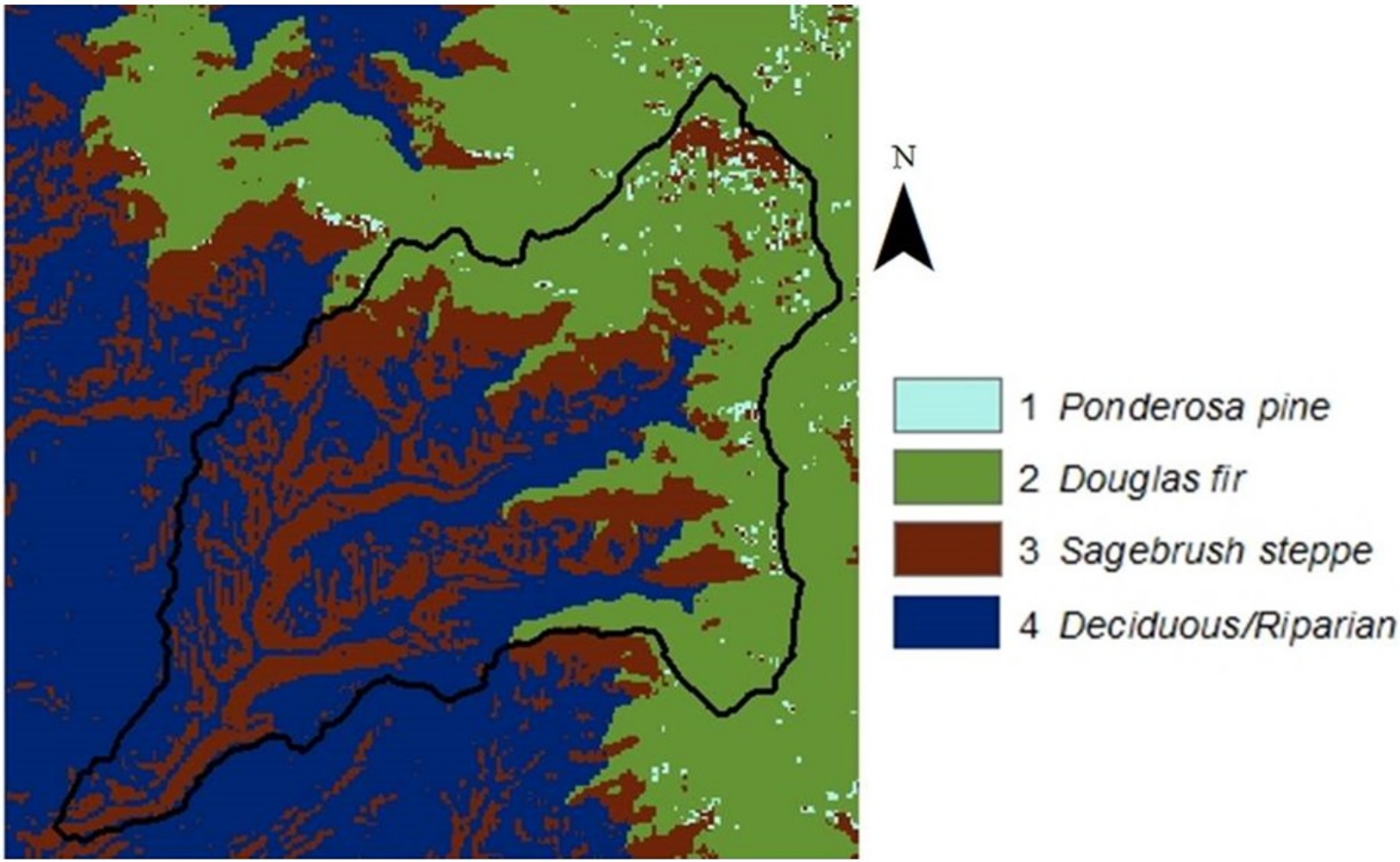

Figure 13. Output map of 4 classes (ponderosa pine, Douglas fir, sagebrush steppe, and deciduous/riparian) using the Classification and Regression Tree (CART) with 3 topographic inputs (elevation, slope, and potential solar radiation) for DCEW and the surrounding area.

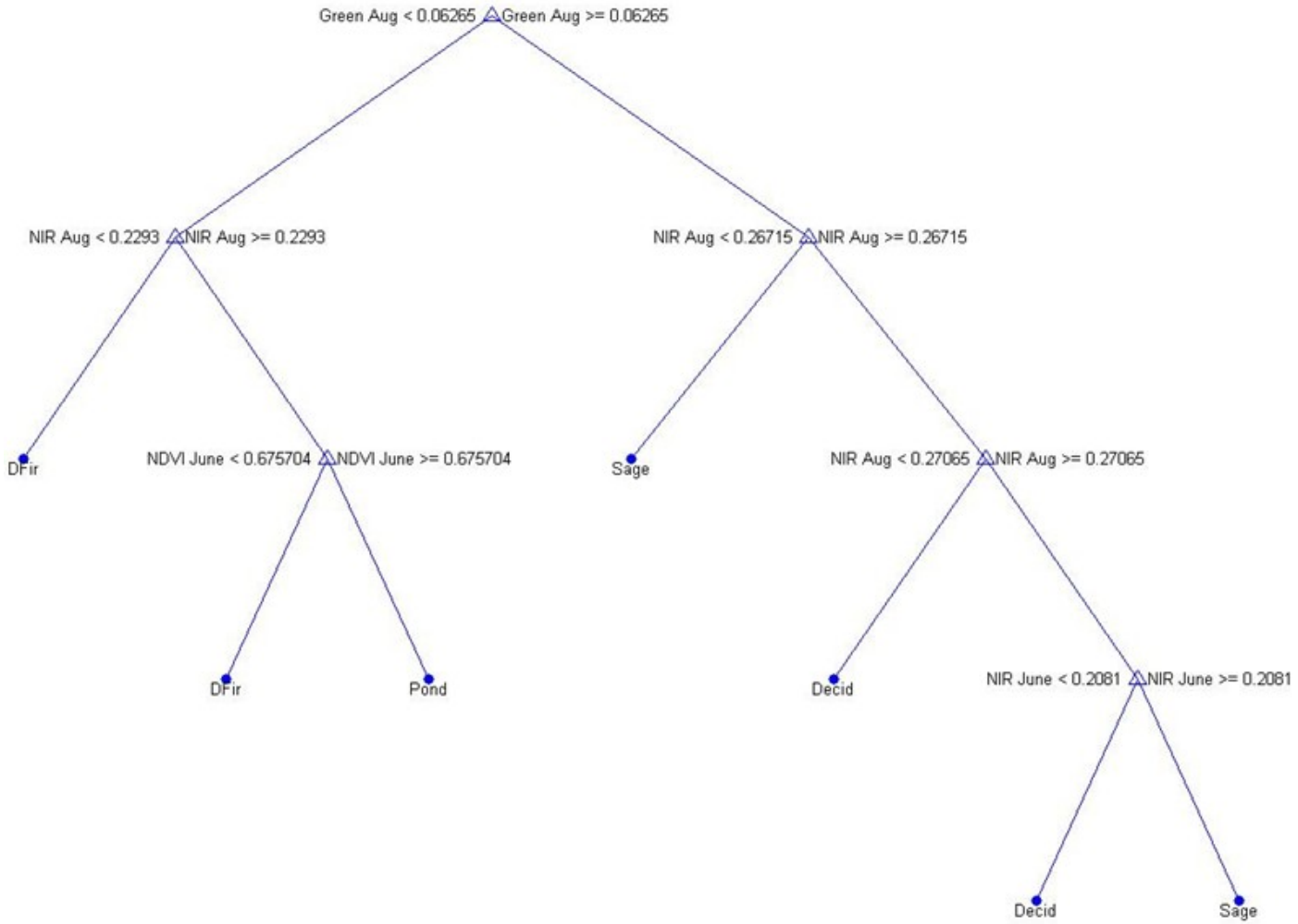

Figure 14. Classification and Regression Tree (CART) splitting using 8 spectral inputs (red band, green band, near infrared band, and NDVI for June and July) where Dfir = Douglas fir, Pond = ponderosa, Sage = sagebrush steppe, and Decid = deciduous/riparian classes

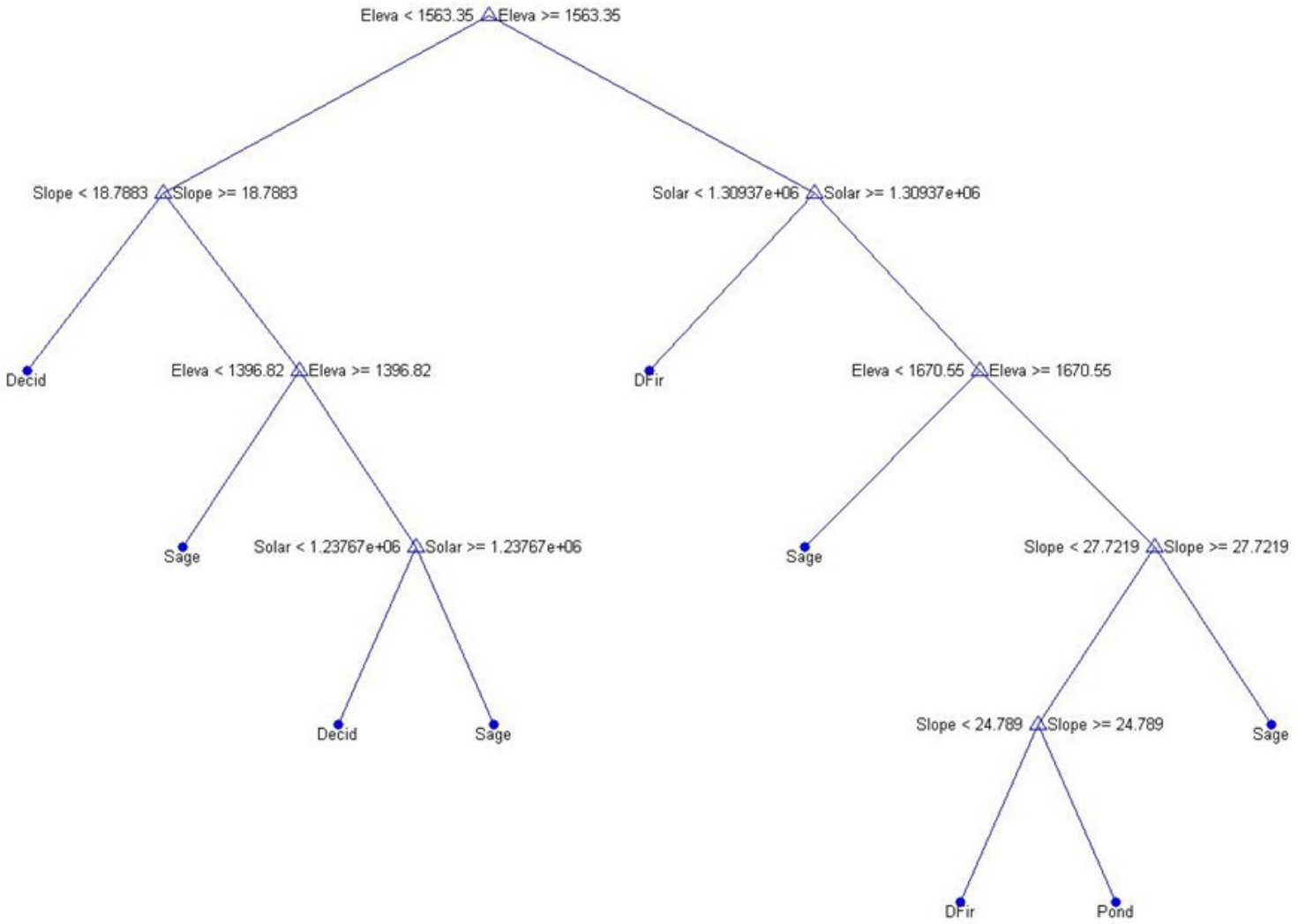

Figure 15. Classification and Regression Tree (CART) splitting using 3 topographic inputs (elevation, slope, and potential solar radiation) where Dfir = Douglas fir, Pond = ponderosa, Sage = sagebrush steppe, and Decid = deciduous/riparian classes.

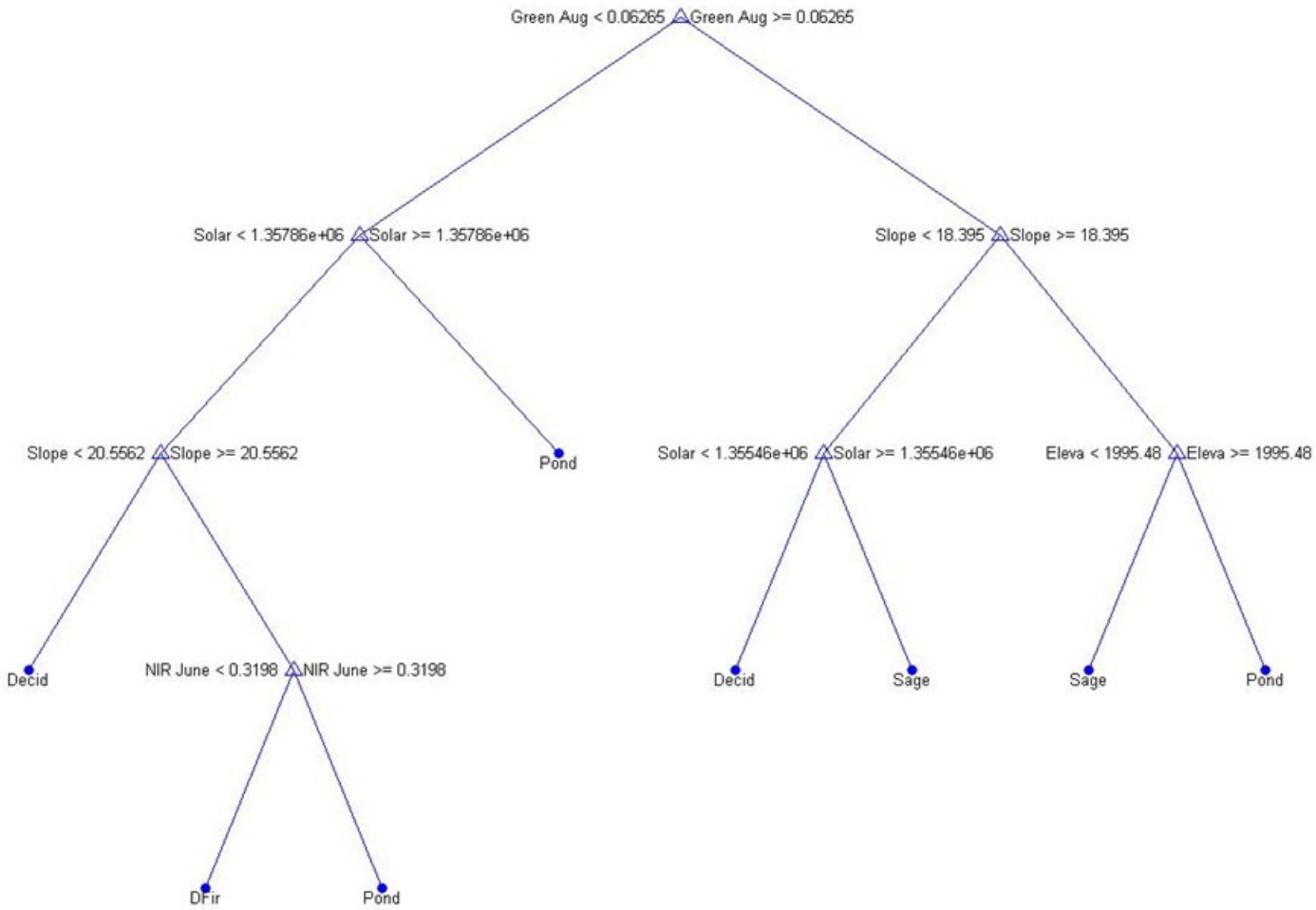

Figure 16. Classification and Regression Tree (CART) splitting using 8 spectral inputs (red band, green band, near infrared, and NDVI for June and August) and 3 topographic inputs (elevation, slope, and potential solar radiation) where Dfir = Douglas fir, Pond = ponderosa, Sage = sagebrush steppe, and Decid = deciduous/riparian classes.

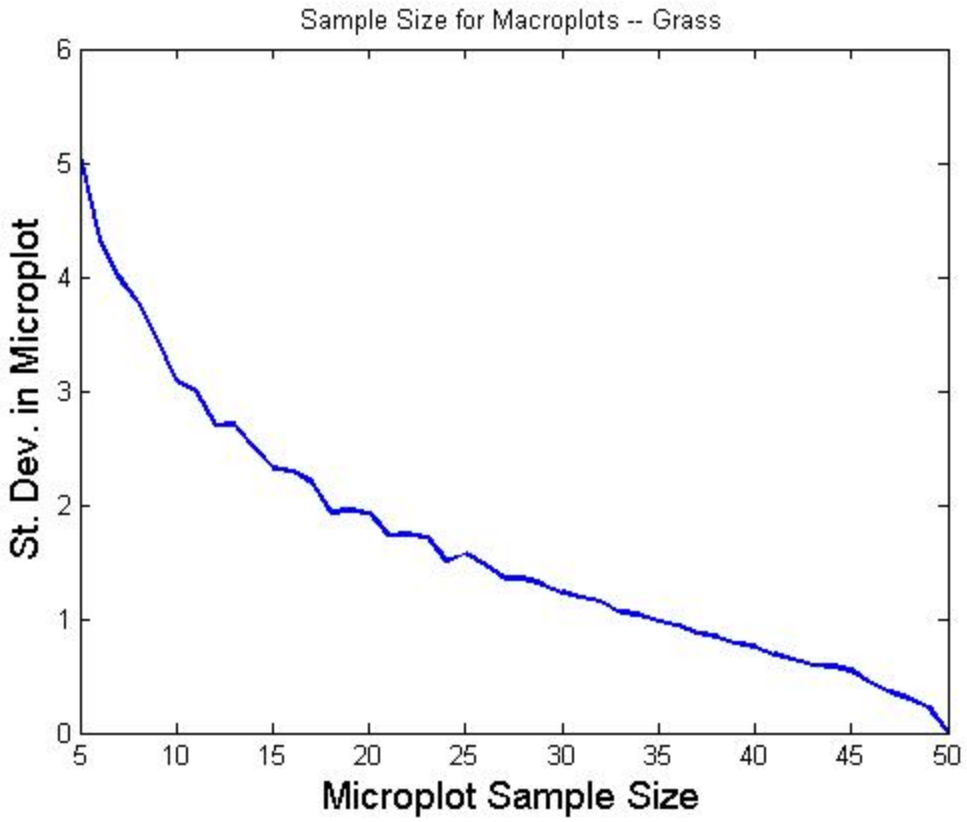

Figure 17. Standard deviation of grass vs. number of micro-plots sampled in 2011. Twenty micro-plots were determined to be the sample unit for each macro-plot in the sagebrush steppe ecotone.

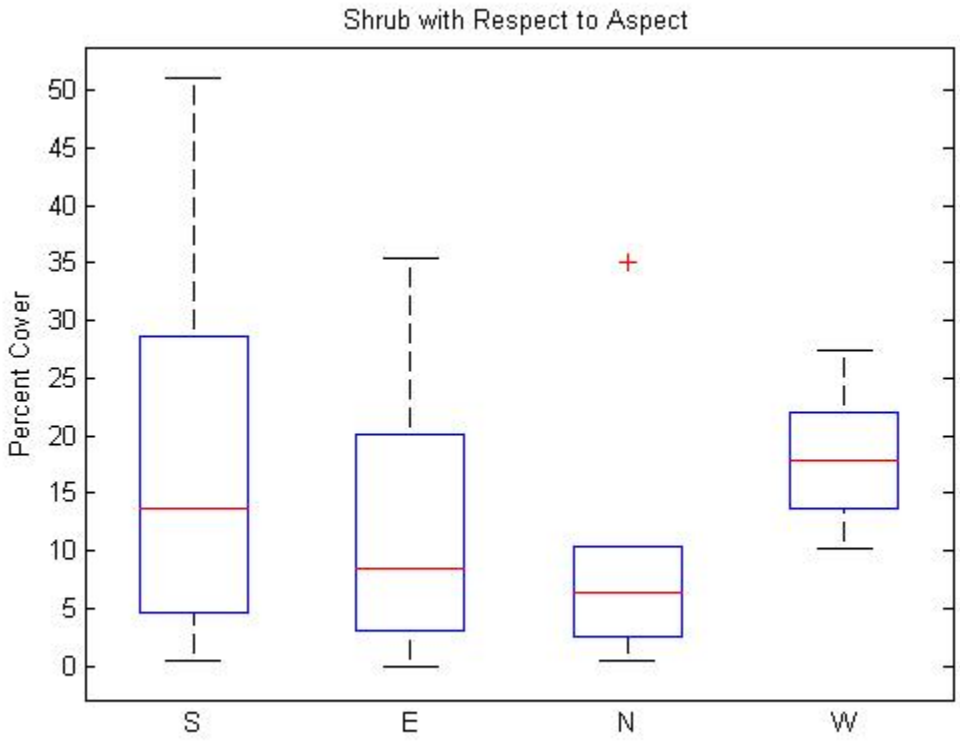

Figure 18. Distribution of shrub with respect to aspect in DCEW. (South = 19, East =9, North = 6, and West = 6)

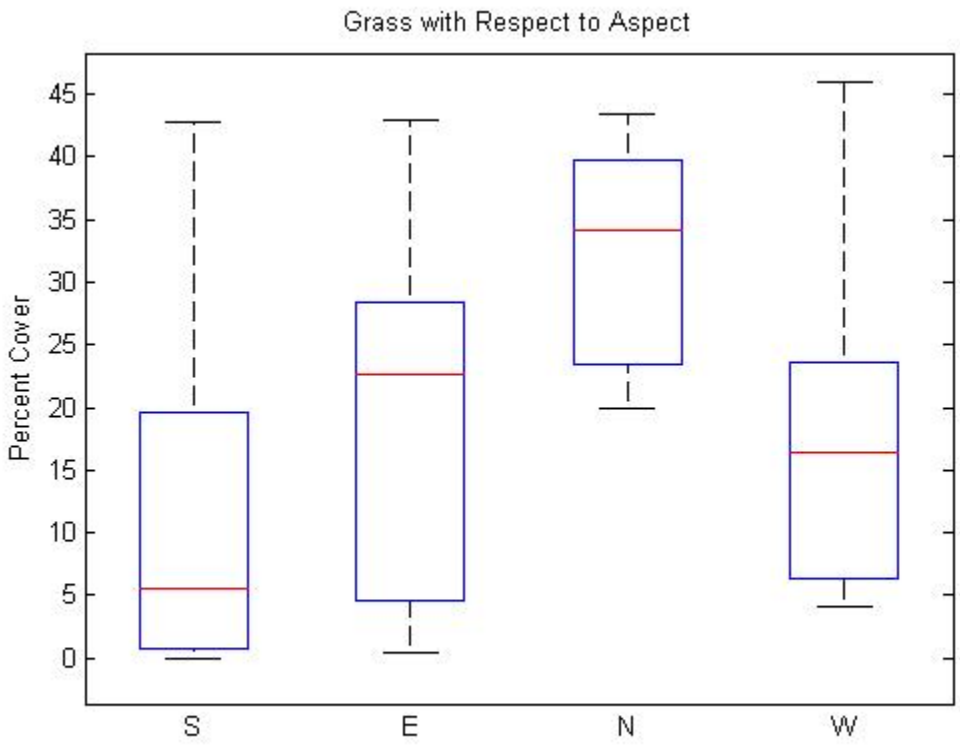

Figure 19. Distribution of grass with respect to aspect in DCEW.

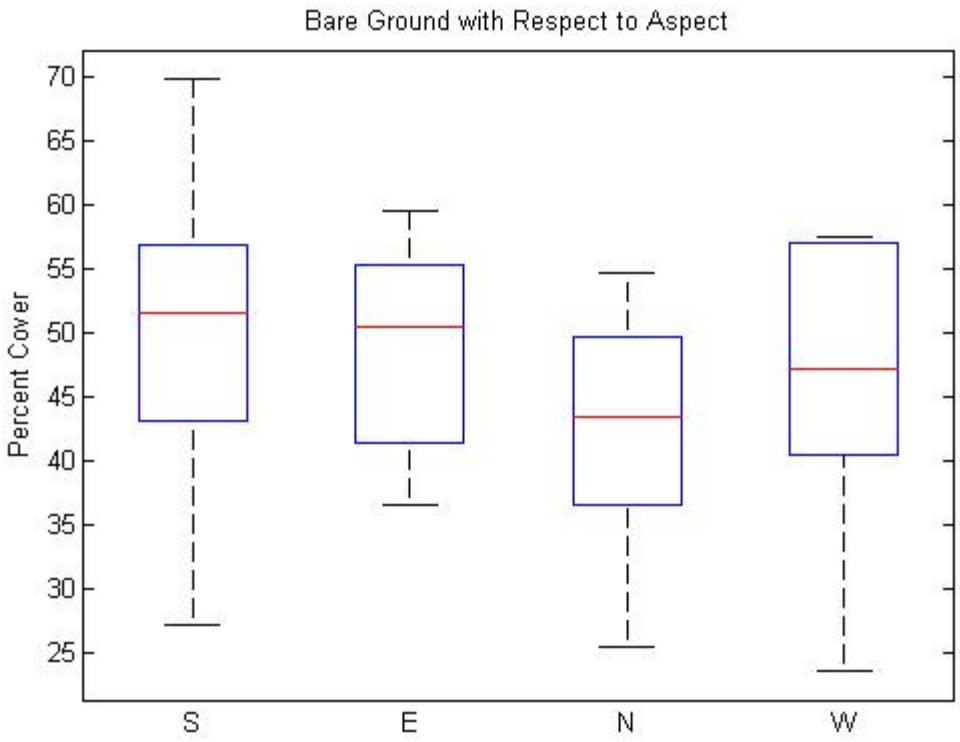

Figure 20. Distribution of bare ground with respect to aspect in DCEW.

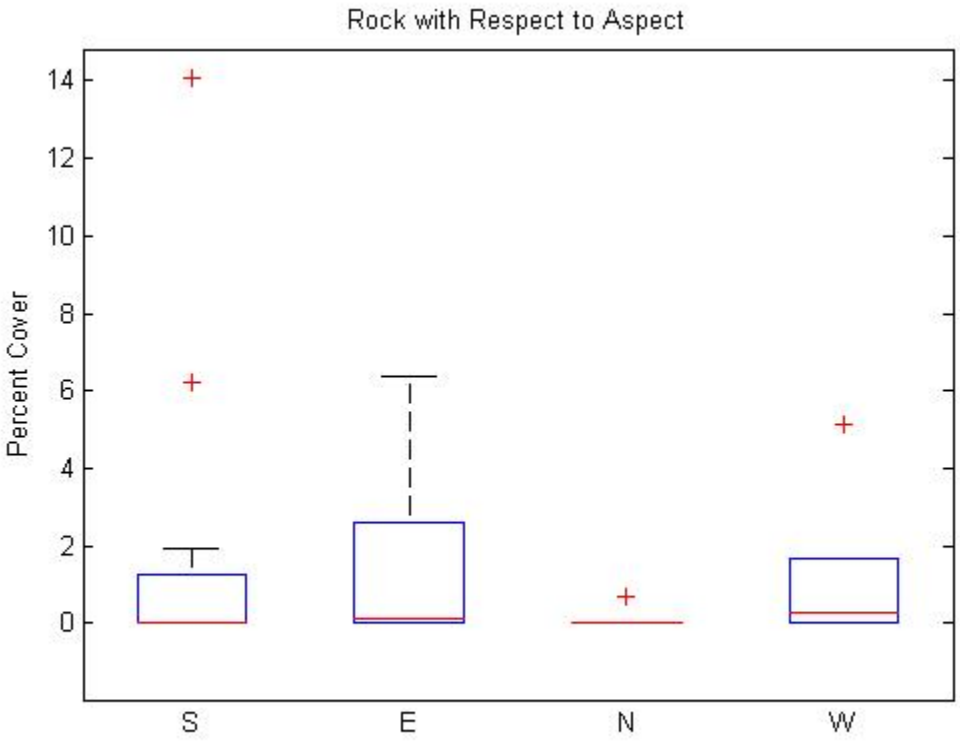

Figure 21. Distribution of rock with respect to aspect in DCEW.

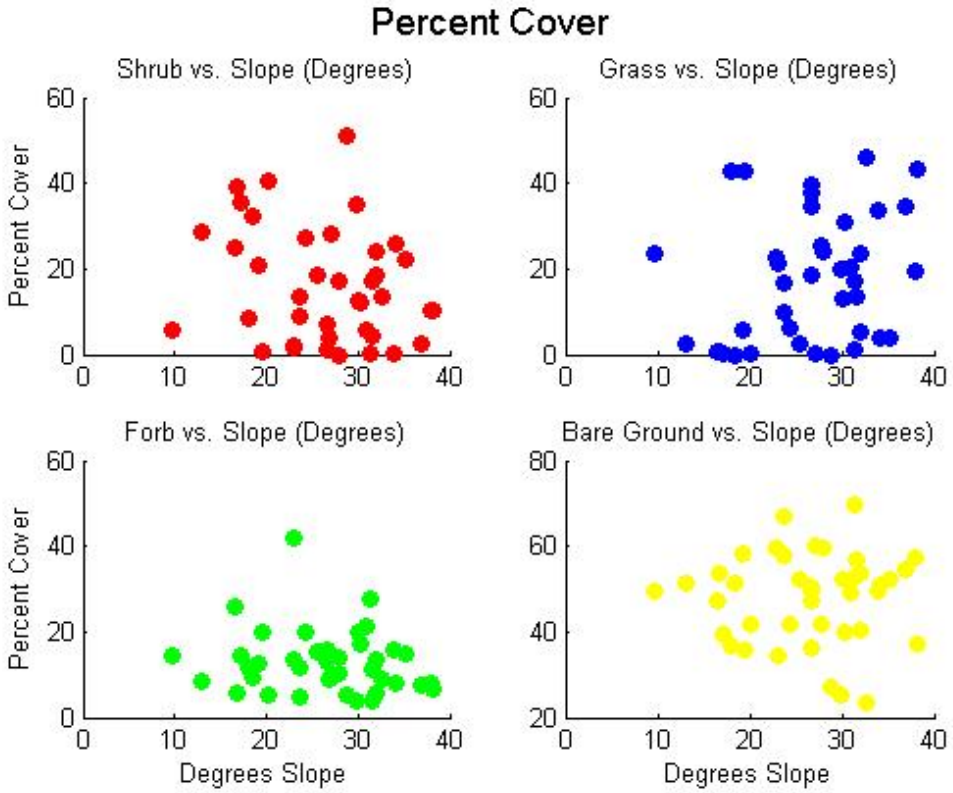

Figure 22. Scatterplot of percent cover of shrub, grass, forbs, and bare ground and slope for the sagebrush steppe ecosystem in DCEW.

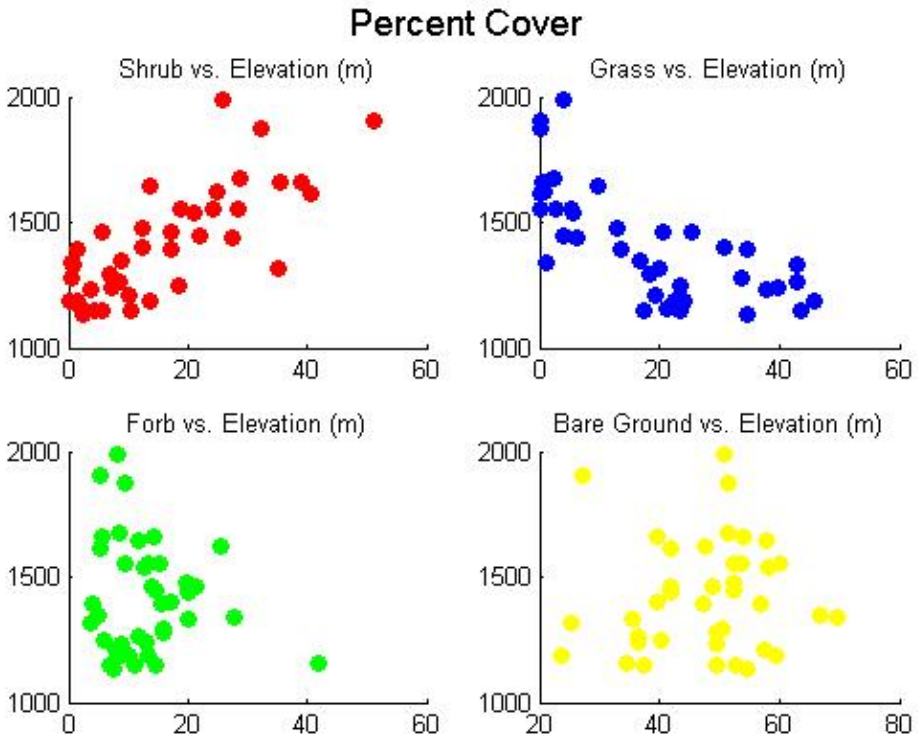

Figure 23. Scatterplot of percent cover of shrub, grass, forbs, and bare ground and elevation for the sagebrush steppe ecosystem in DCEW.

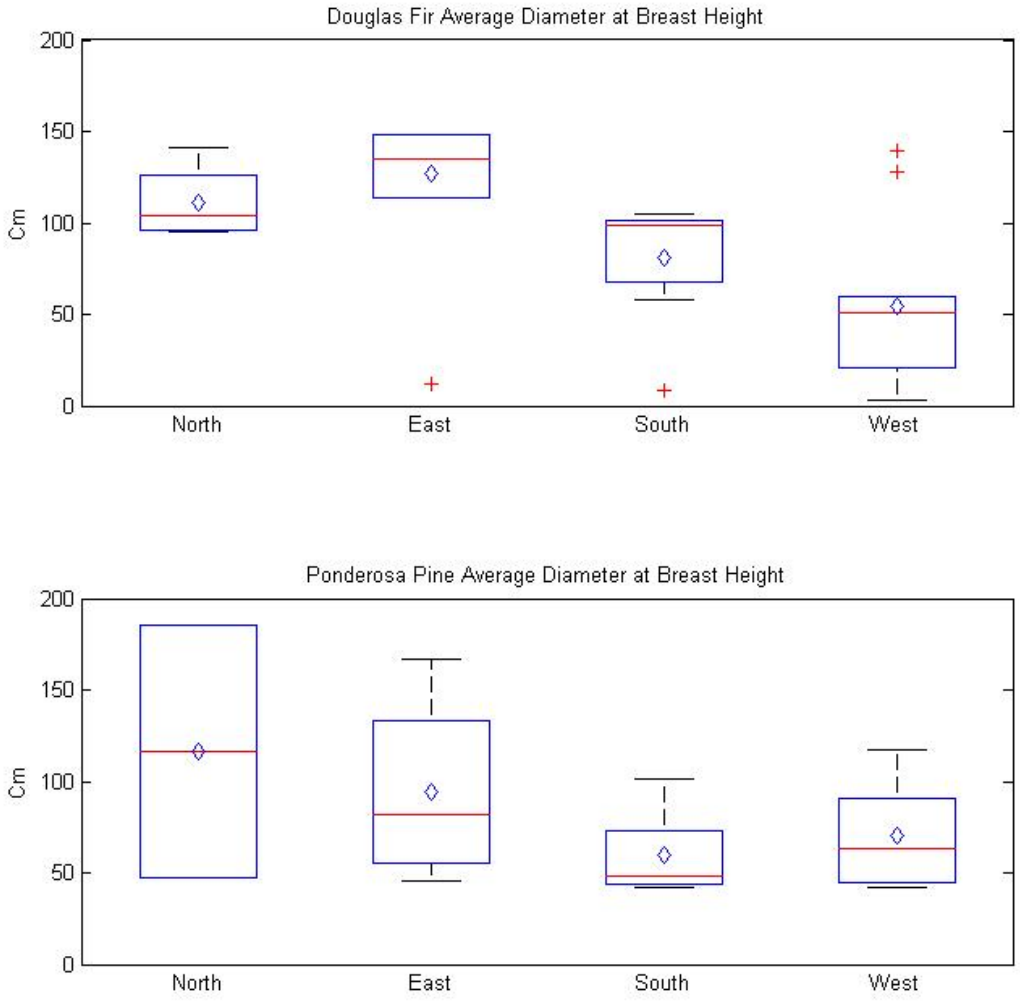

Figure 24. Distribution of Douglas fir (above) and ponderosa pine (below) Diameter at Breast Height (DBH) on North, East, South, and West aspects.

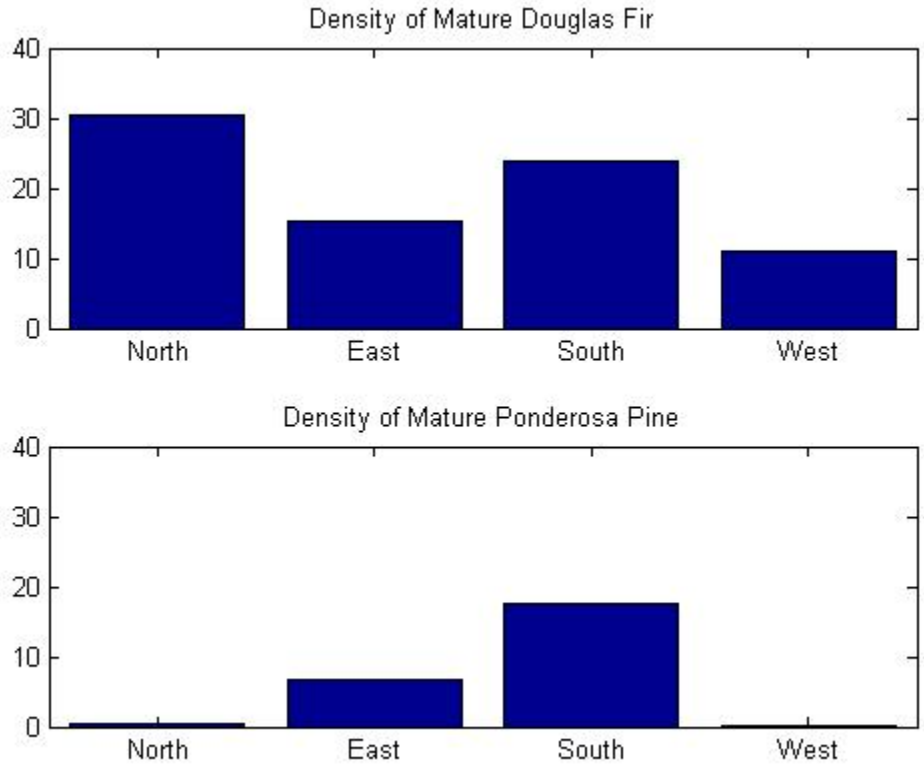

Figure 25. Density of mature Douglas fir and ponderosa pine with respect to aspect for 100 m2 macro-plot.

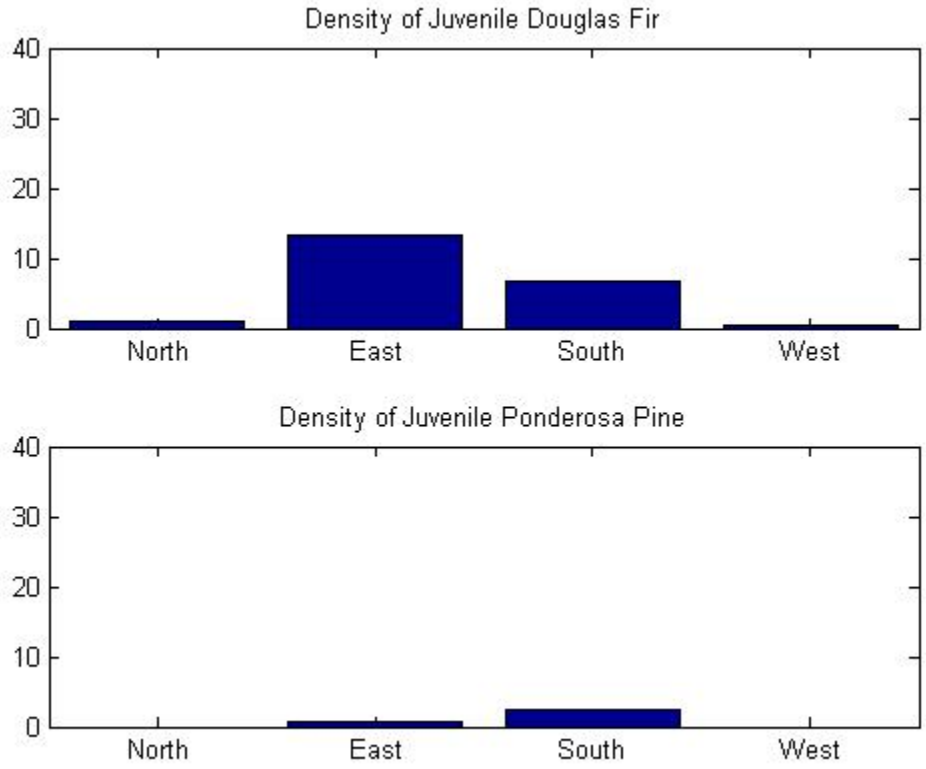

Figure 26. Density of juvenile Douglas fir and ponderosa pine with respect to aspect for 100 m2 macro-plot.

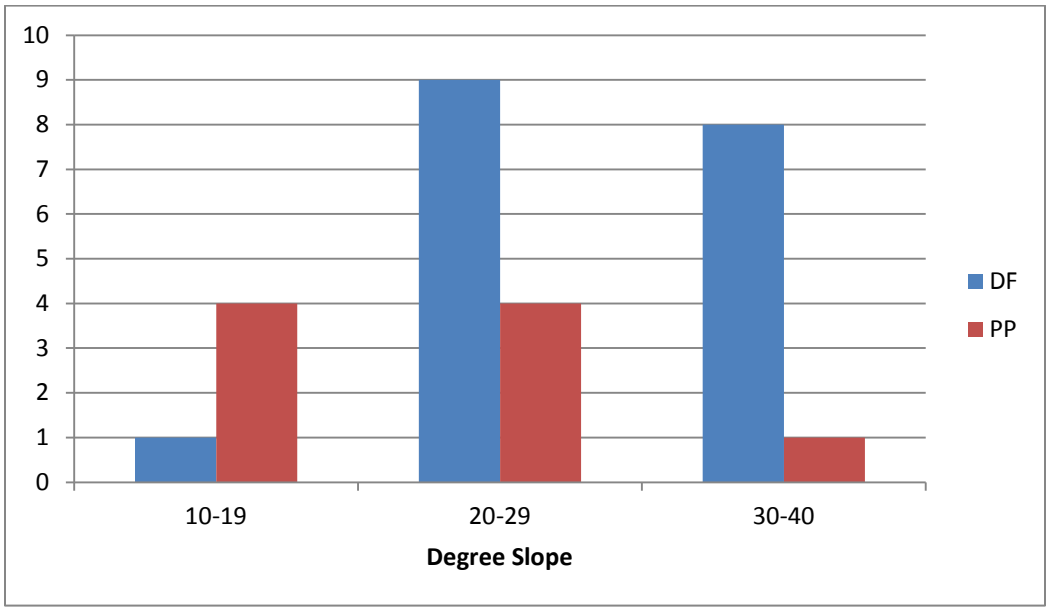

Figure 27. Histogram of the dominant classes of Douglas fir and ponderosa pine and degree slopes in DCEW.

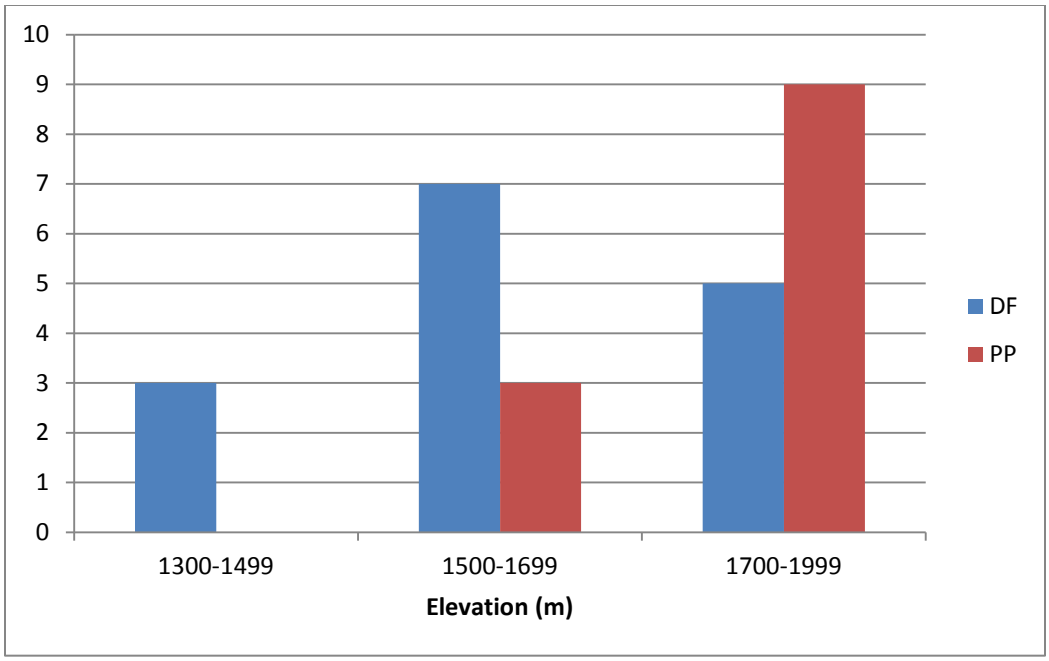

Figure 28. Histogram of the dominant classes of Douglas fir and ponderosa pine and elevation in DCEW.

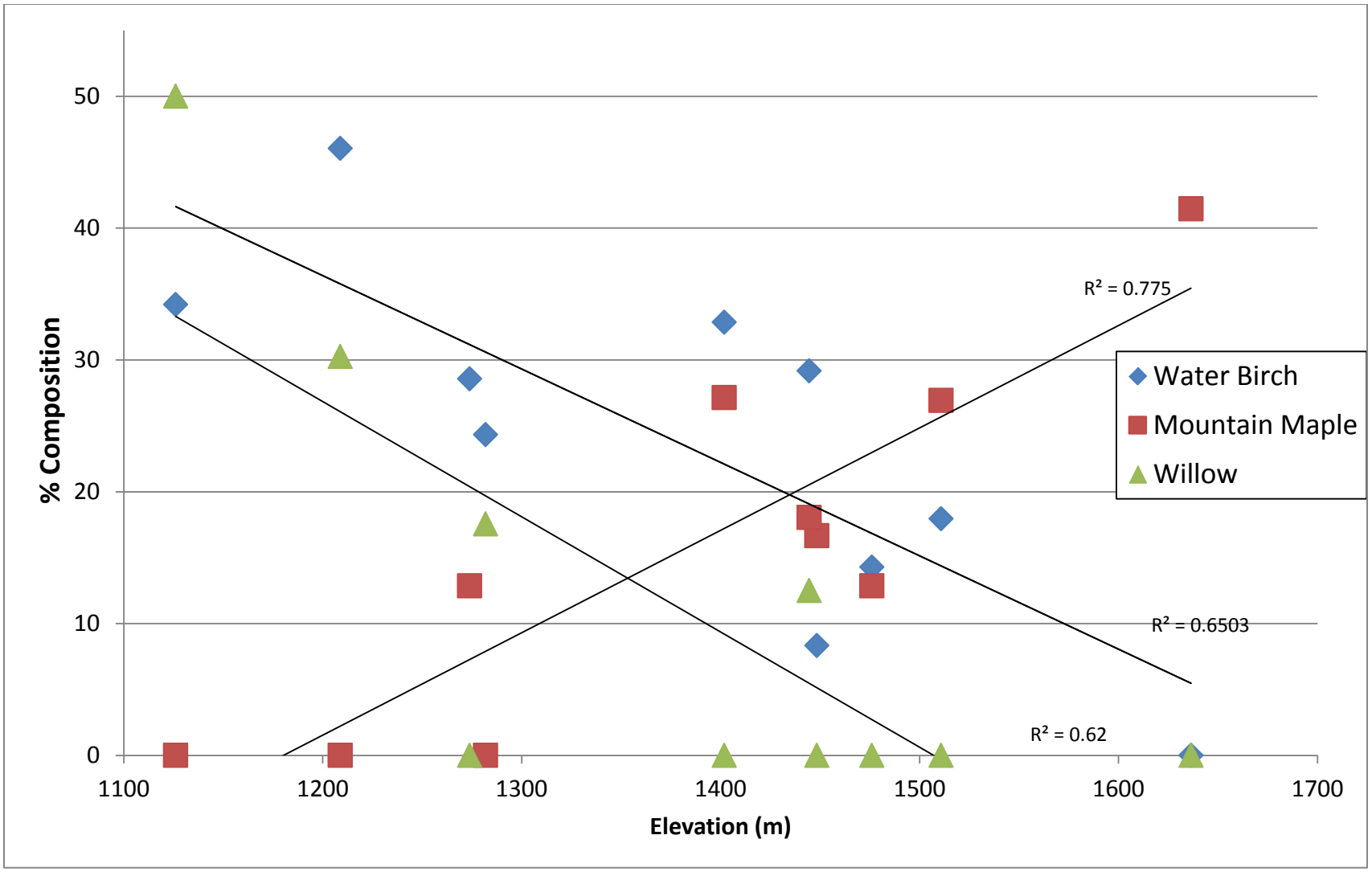

Figure 29. Riparian vegetation percent composition vs elevation

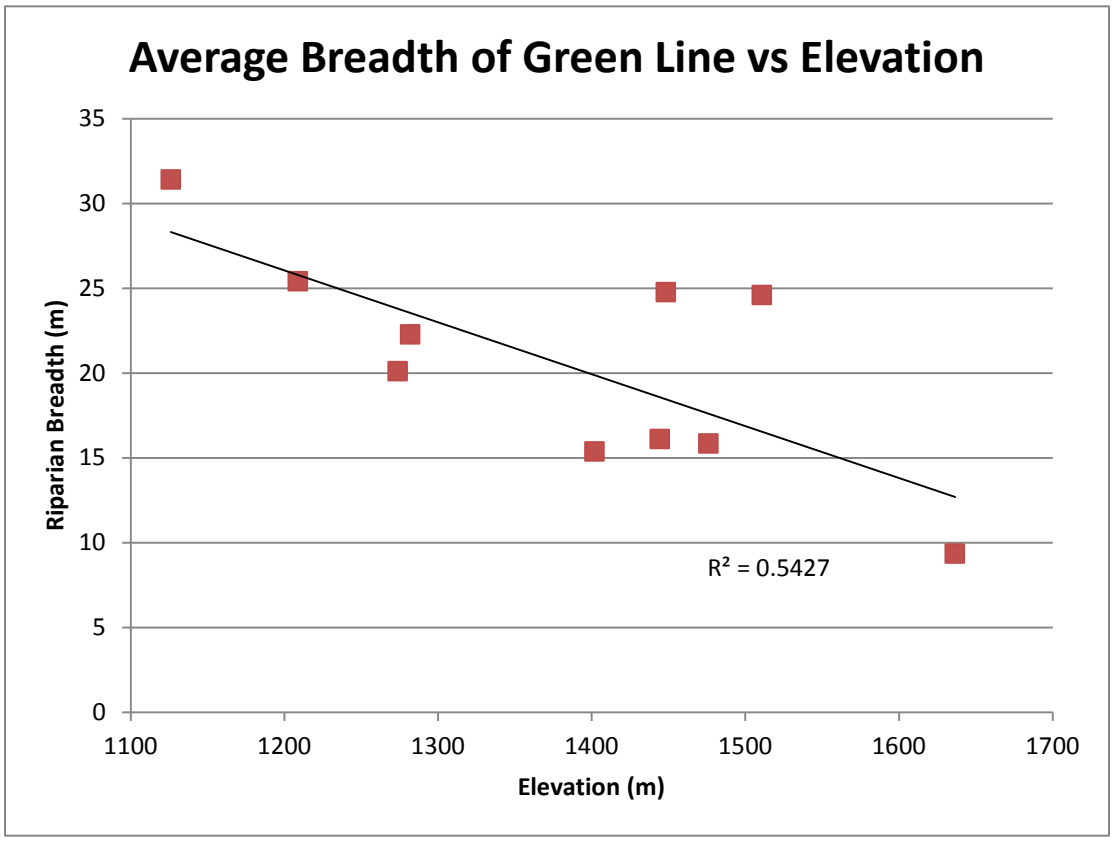

Figure 30. The average perpendicular distance of riparian vegetation measured from the center of the stream.

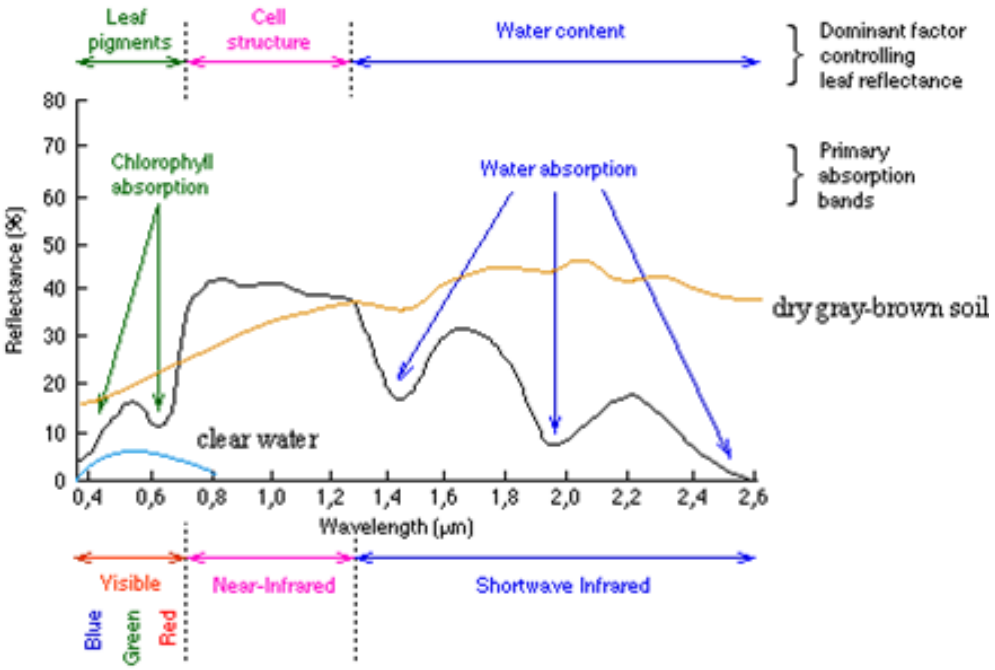

Figure 32. Wavelength characteristics for leafs

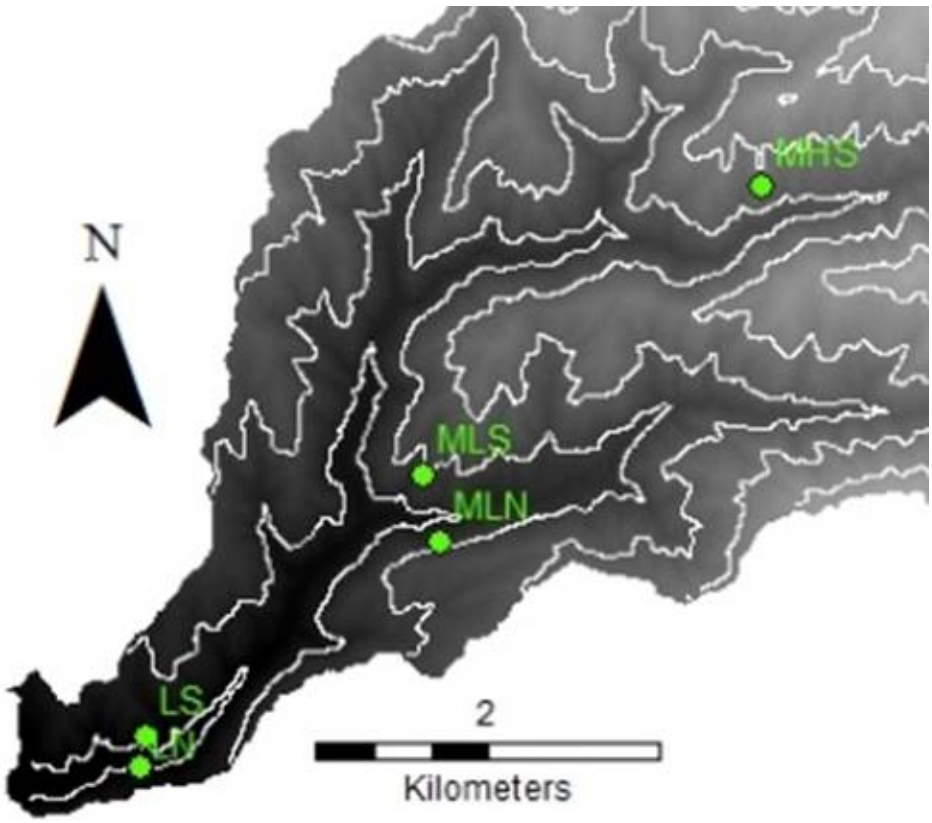

Figure 33. Location of VWC sites for DCEW. Lower South (LS), Lower North (LN), Mid-Lower South (MLS), Mid-Lower North (MLN), and Mid-High South (MHS).

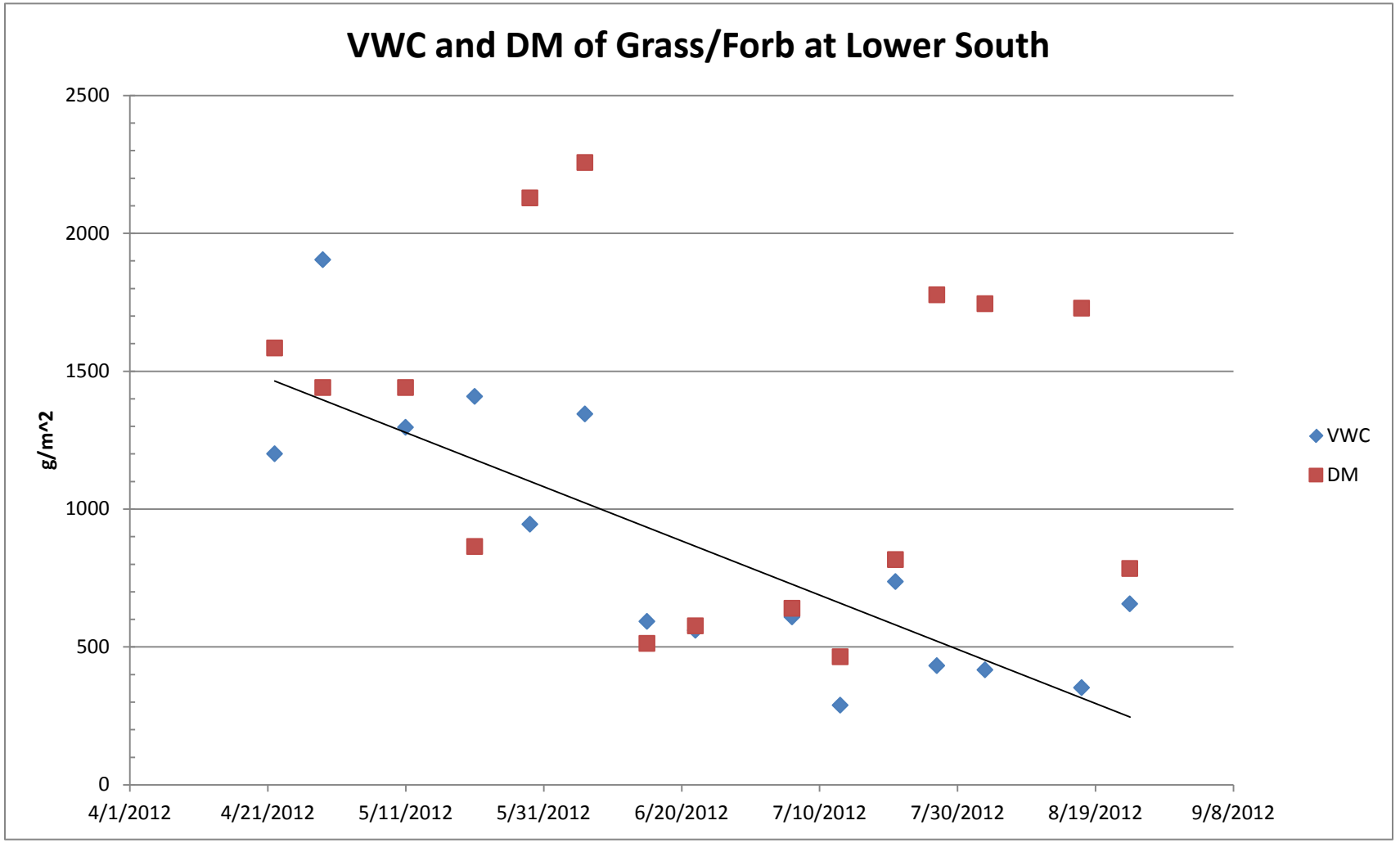

Figure 34. **Vegetation water content (VWC) and dry biomass (DM) (g/m2) with respect to time of the grass/forb samples at the Lower South location of DCEW.**

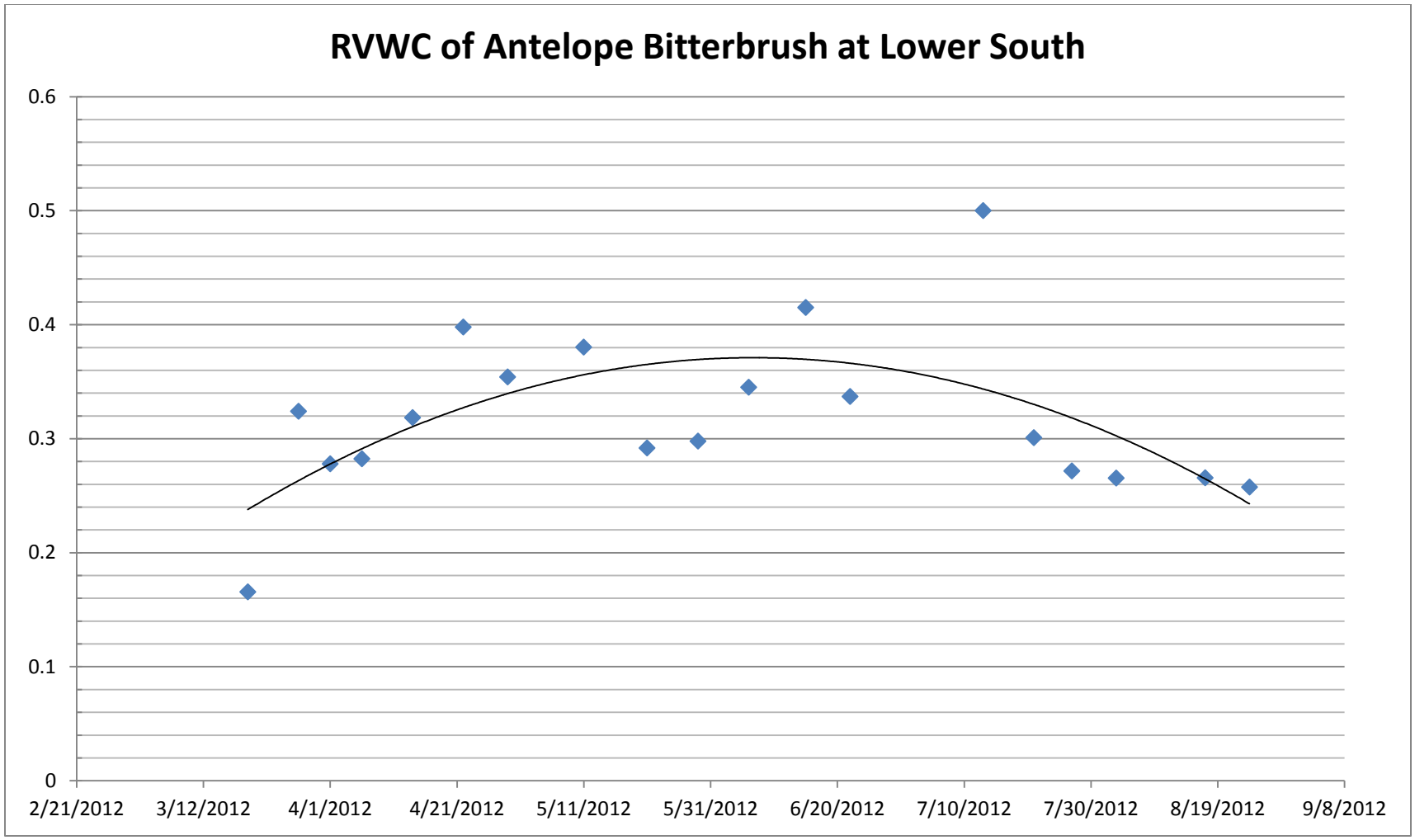

Figure 35. Relative vegetation water content (RVWC) of bitterbrush with respect to time at the Lower South location of DCEW.

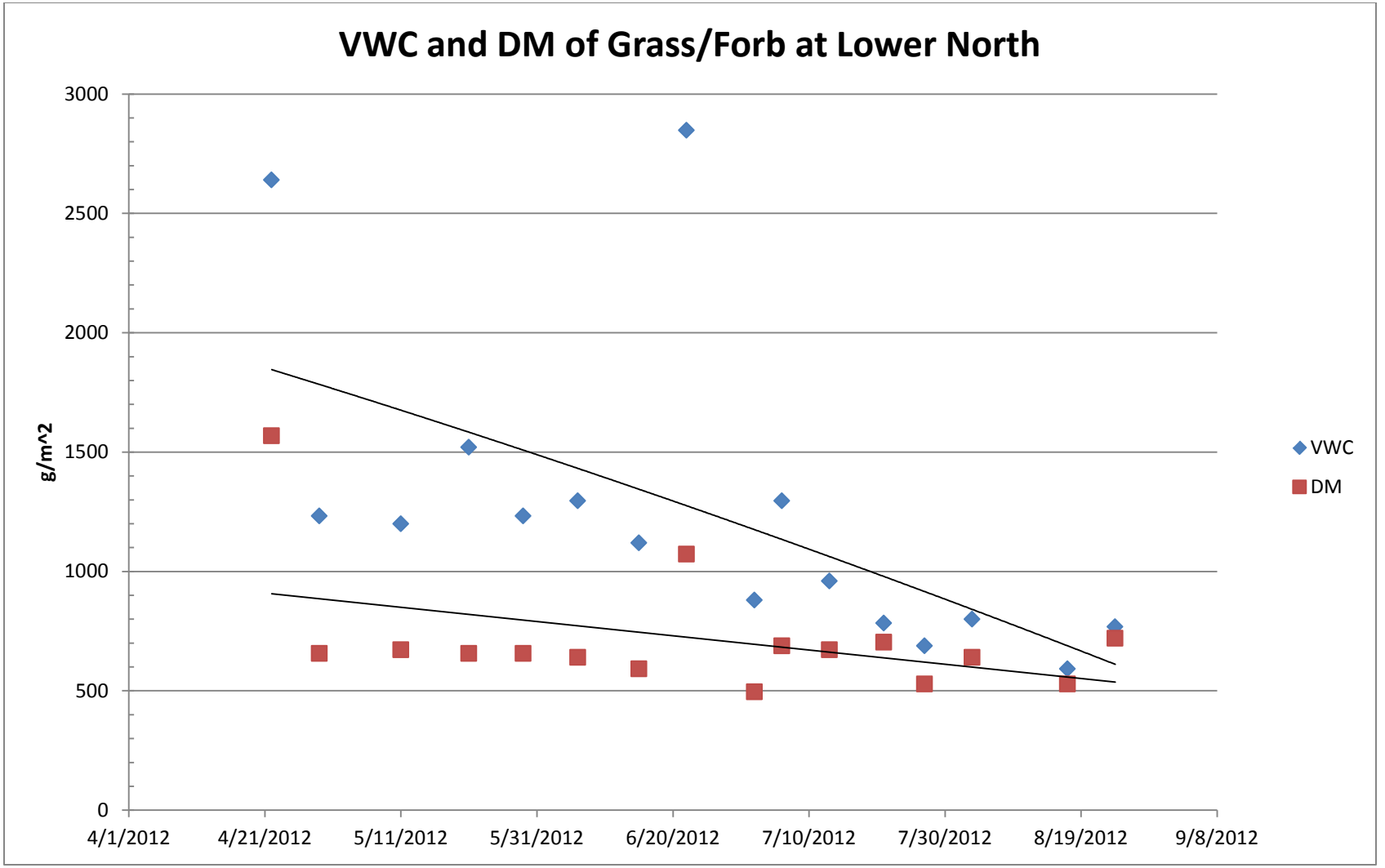

Figure 36. Vegetation water content (VWC) and dry biomass (DM) (g/m^2) with respect to time of the grass/forb samples at the Lower North location of DCEW

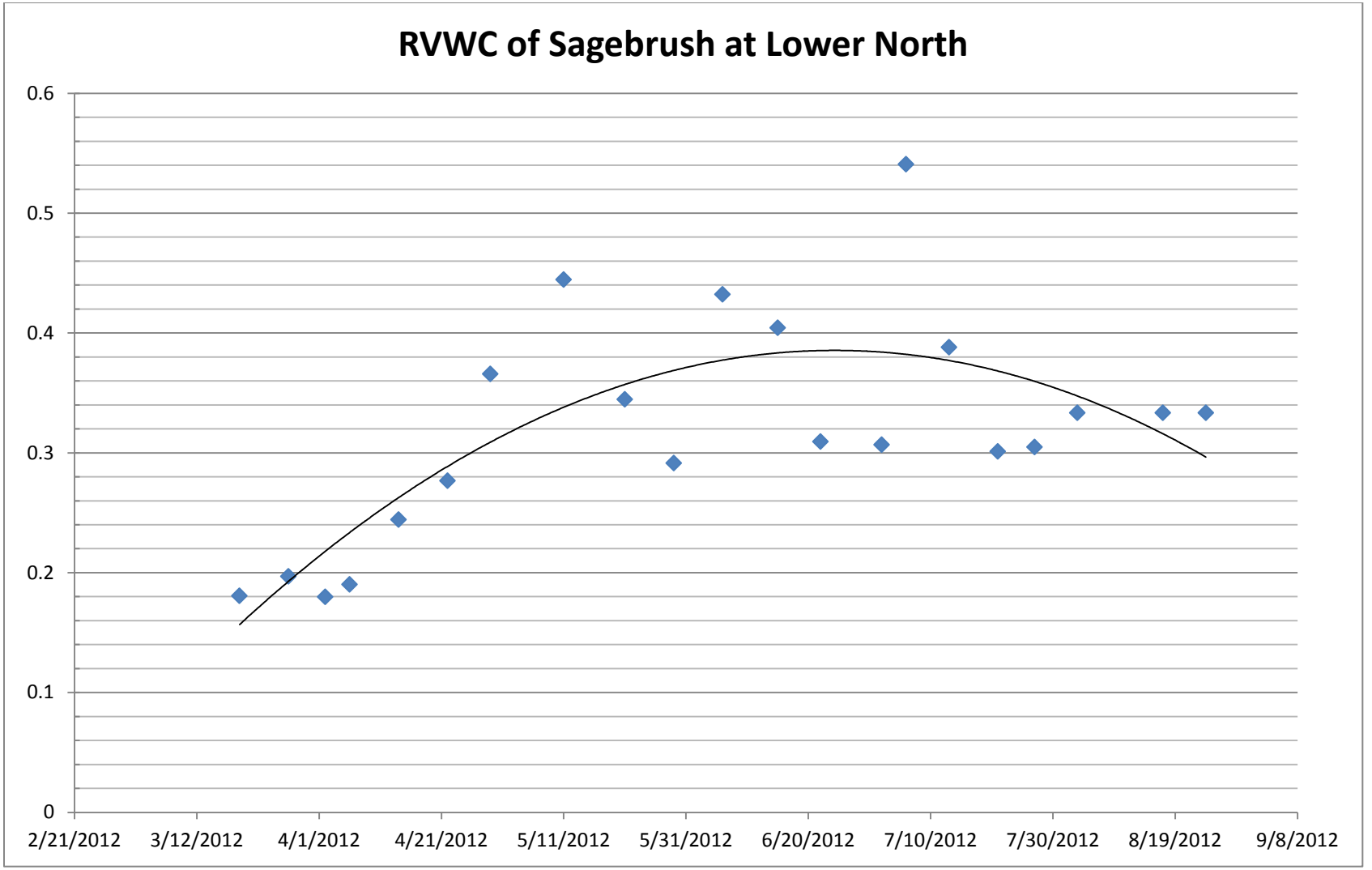

Figure 37. Relative vegetation water content of sagebrush with respect to time at the Lower North location in DCEW.

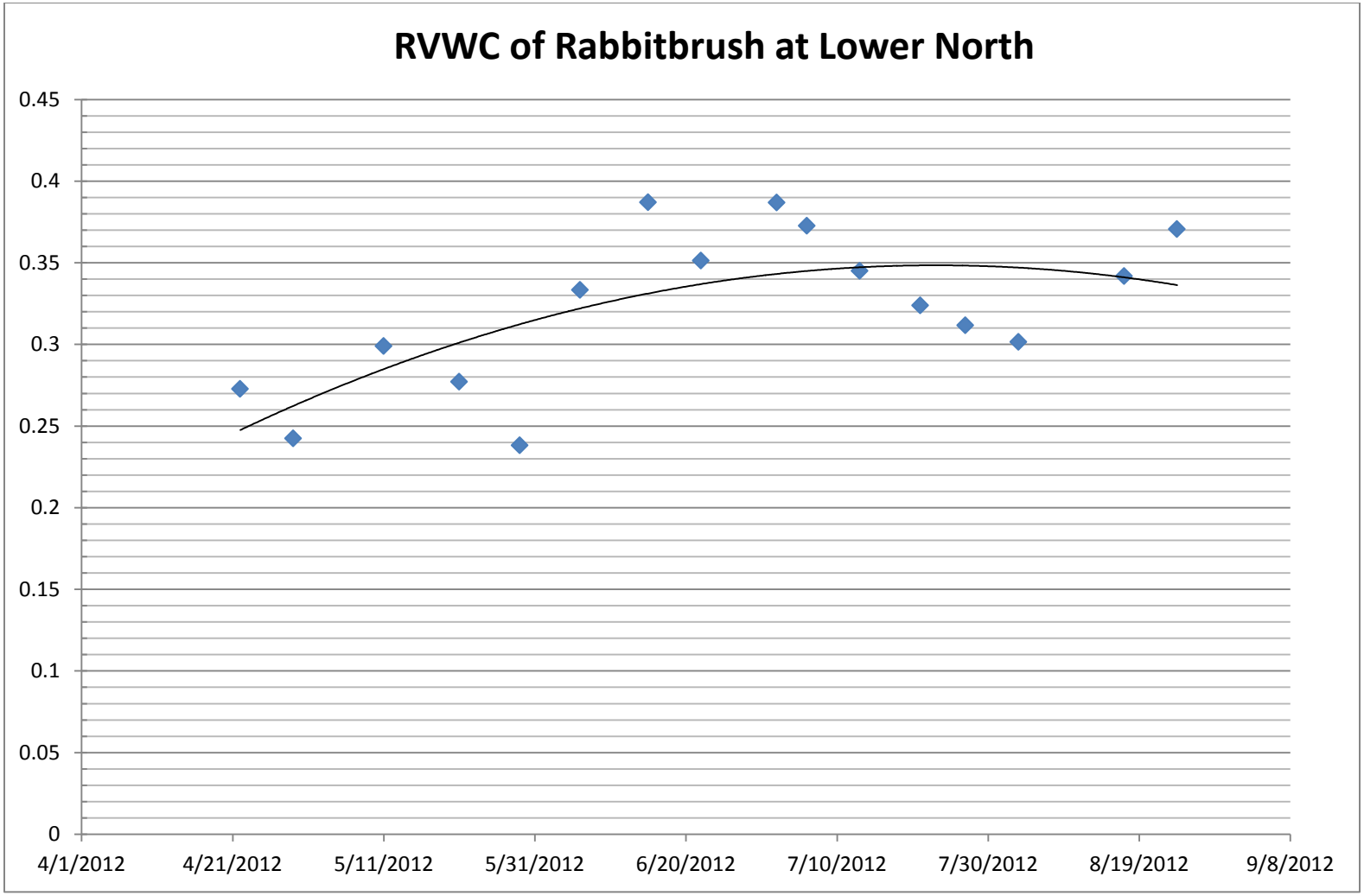

Figure 38. Relative vegetation water content of rabbitbrush with respect to time at the Lower North location

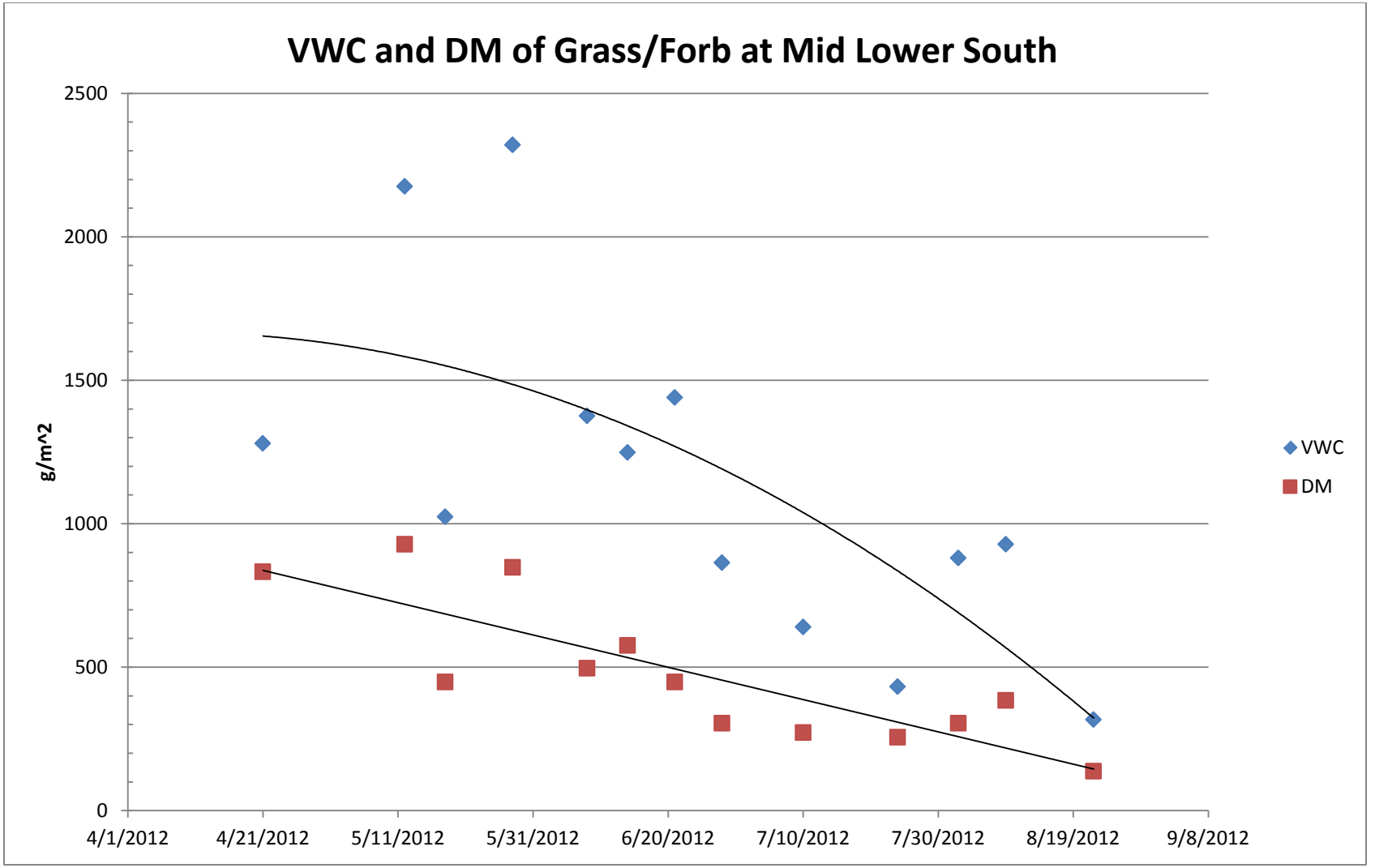

Figure 39. VWC in g/m^2 with respect to time of the grass/forb samples at the Mid-Lower South location of DCEW.

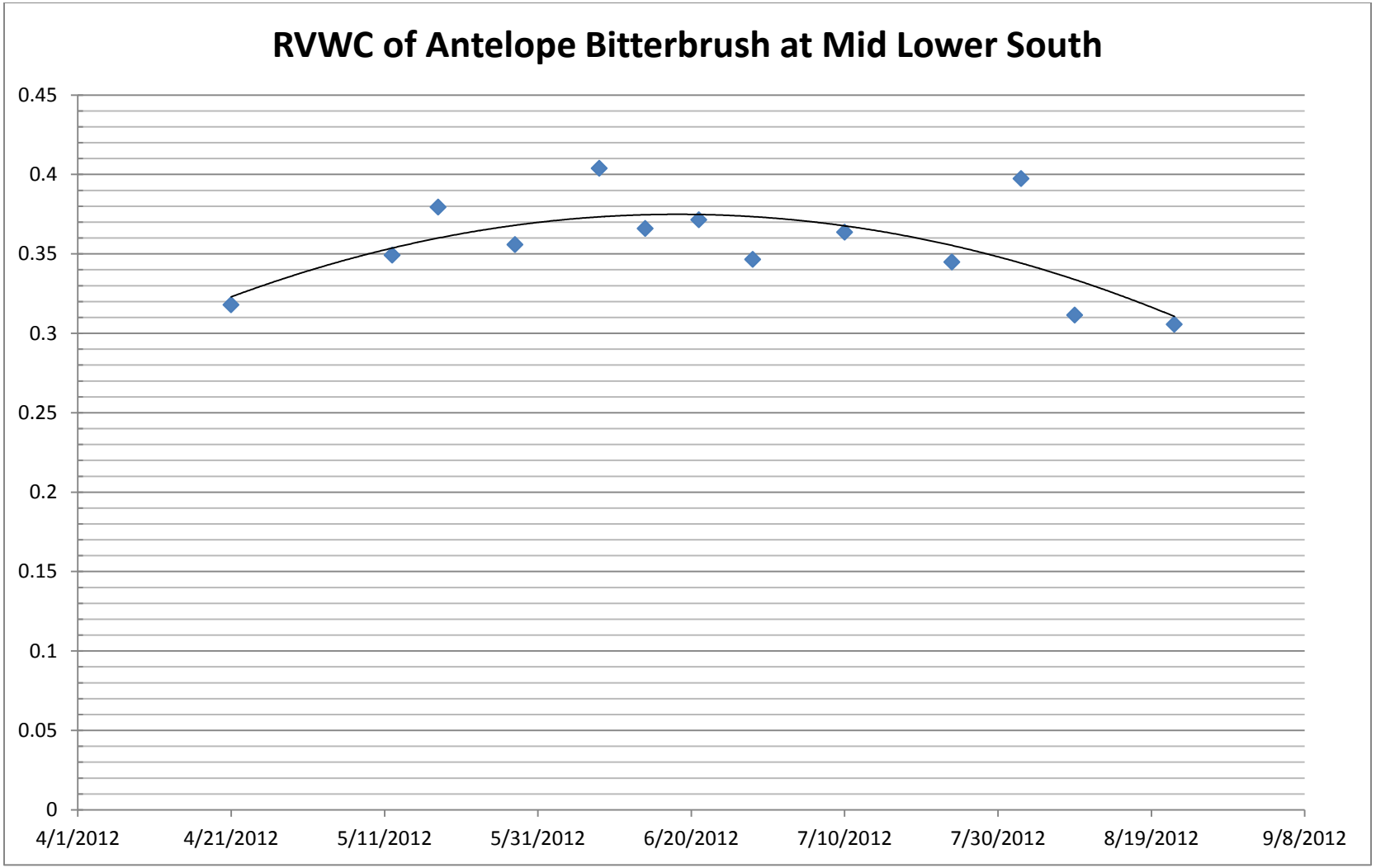

Figure 40. Relative vegetation water content of bitterbrush with respect to time at the Mid-Lower South location in DCEW.

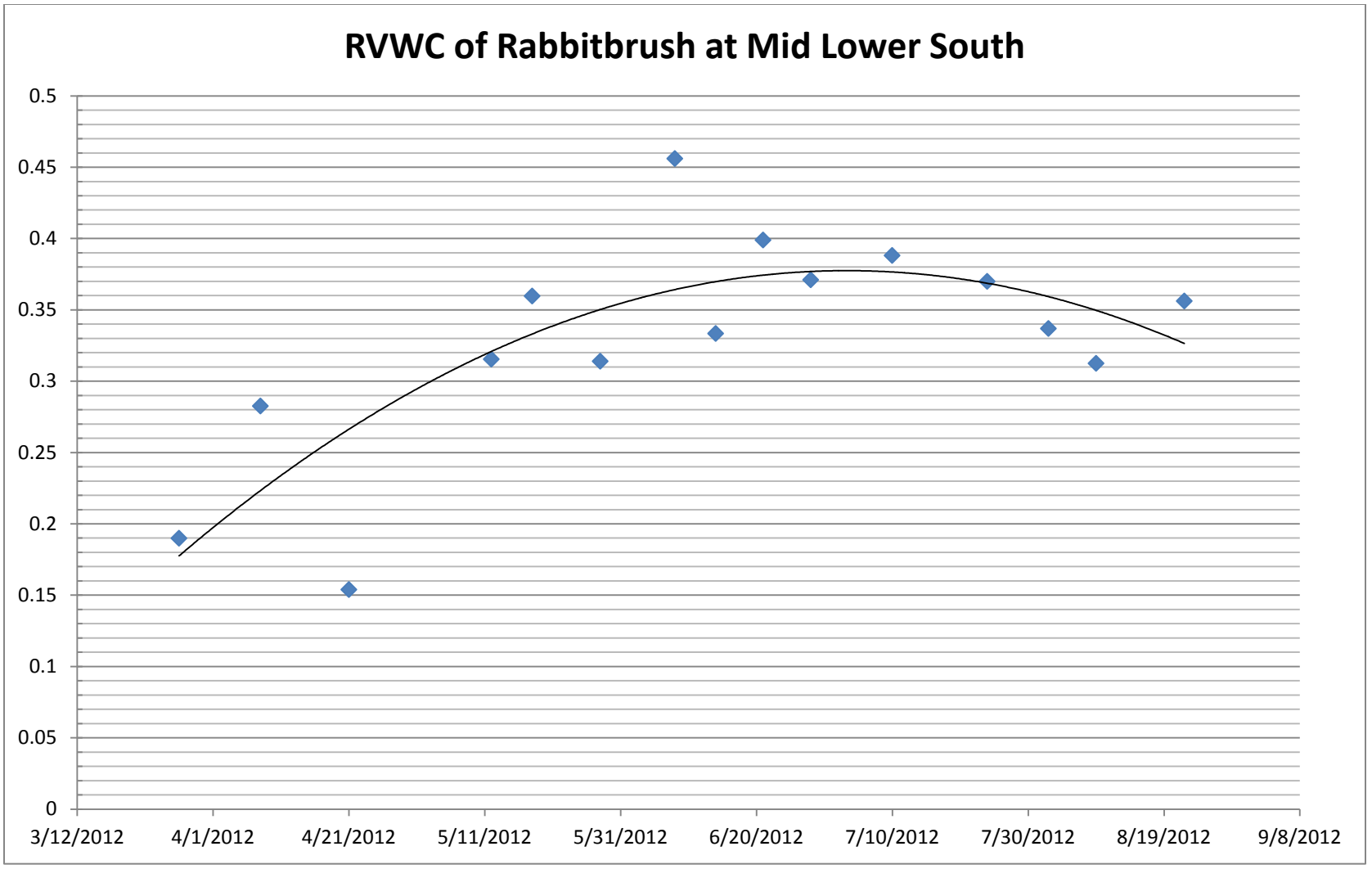

Figure 41. Relative vegetation water content of rabbitbrush with respect to time at the Mid-Lower South location in DCEW.

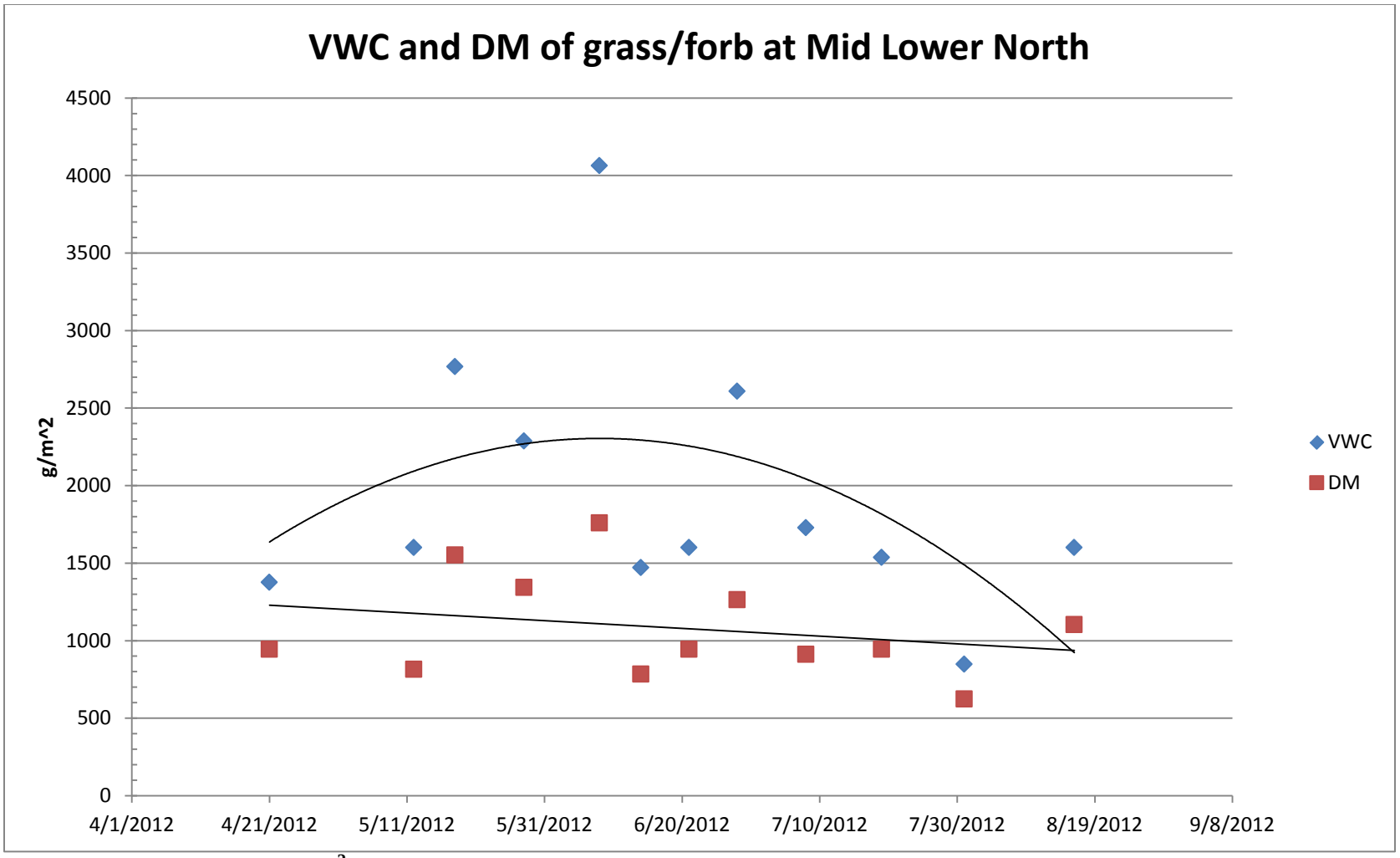

Figure 42. VWC in g/m^2 with respect to time of the grass/forb samples at the Mid-Lower North location of DCEW

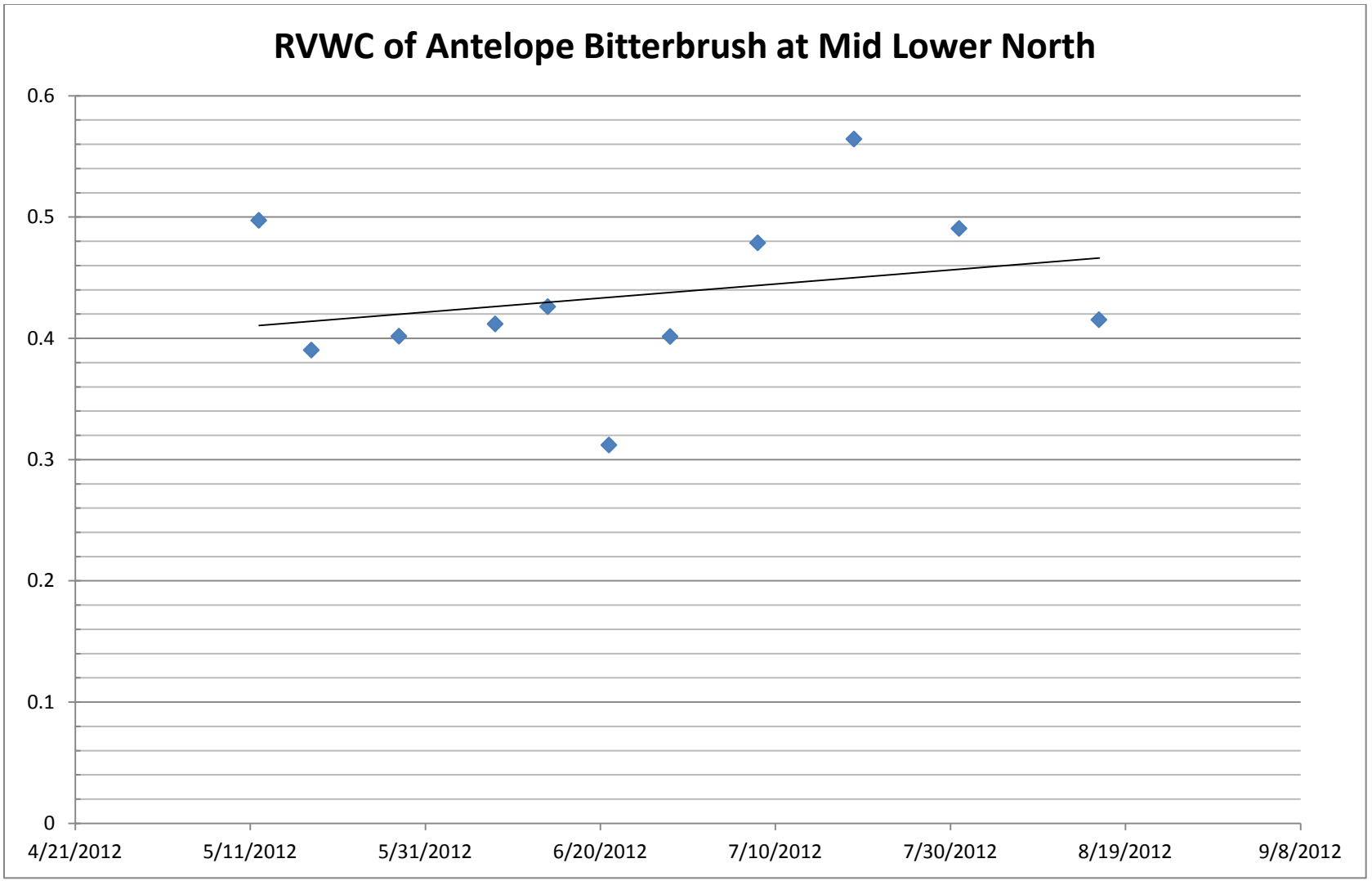

Figure 43. Relative vegetation water content of bitterbrush with respect to time at the Mid-Lower North location of DCEW.

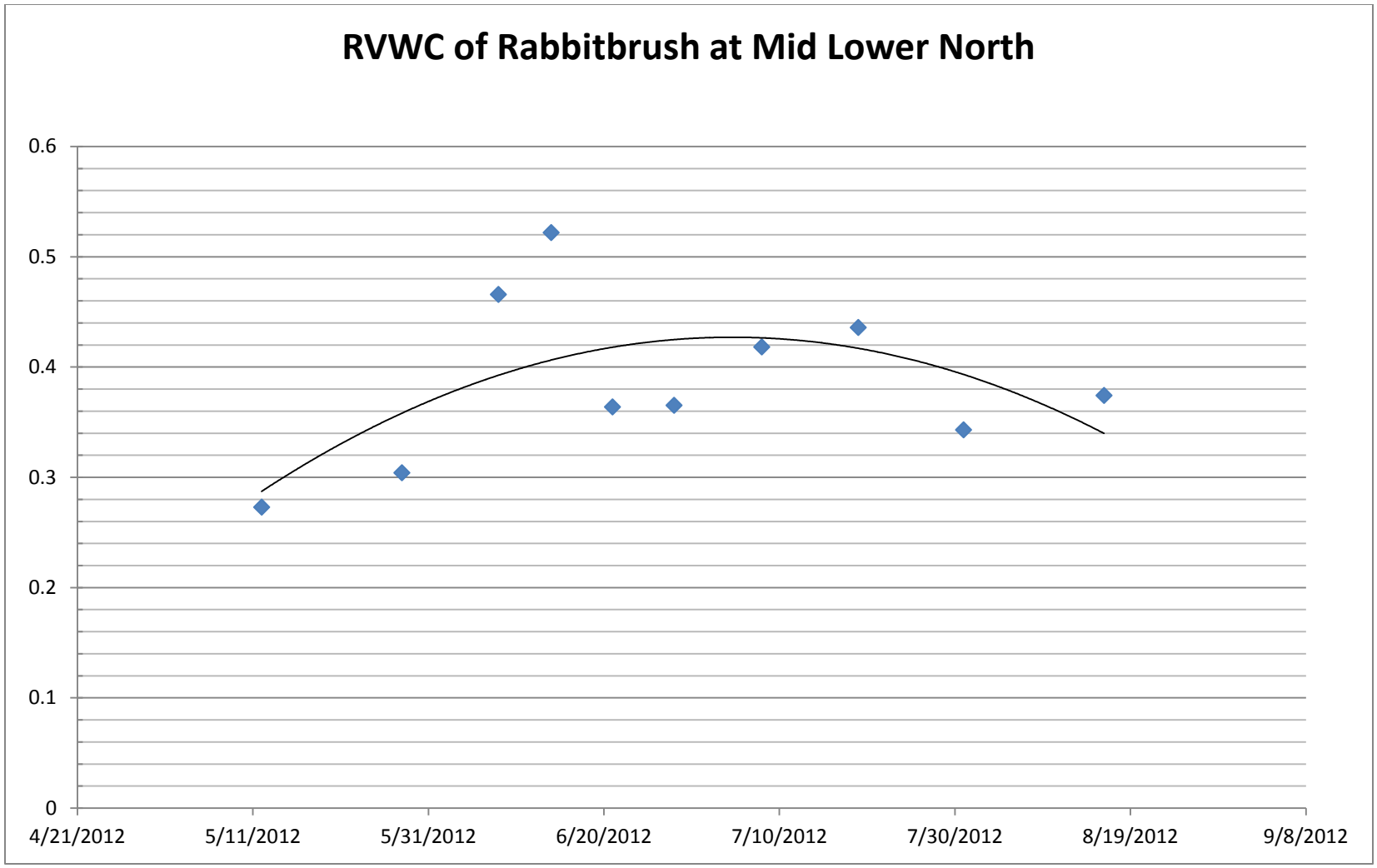

Figure 44. Relative vegetation water content of rabbitbrush with respect to time at the Mid-Lower North location of DCEW.

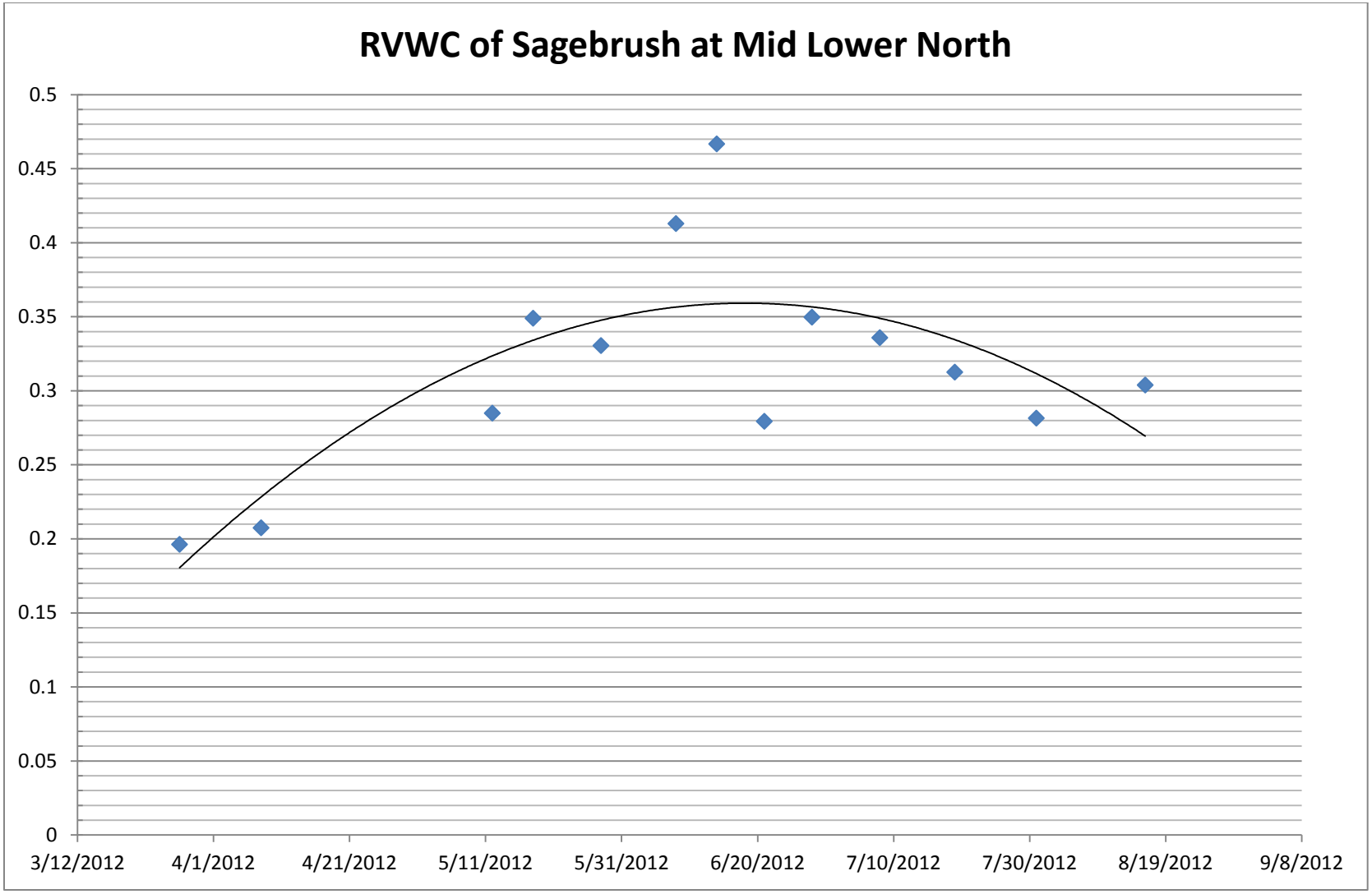

Figure 45. Relative vegetation water content of sagebrush with respect to time at the Mid-Lower North location of DCEW.

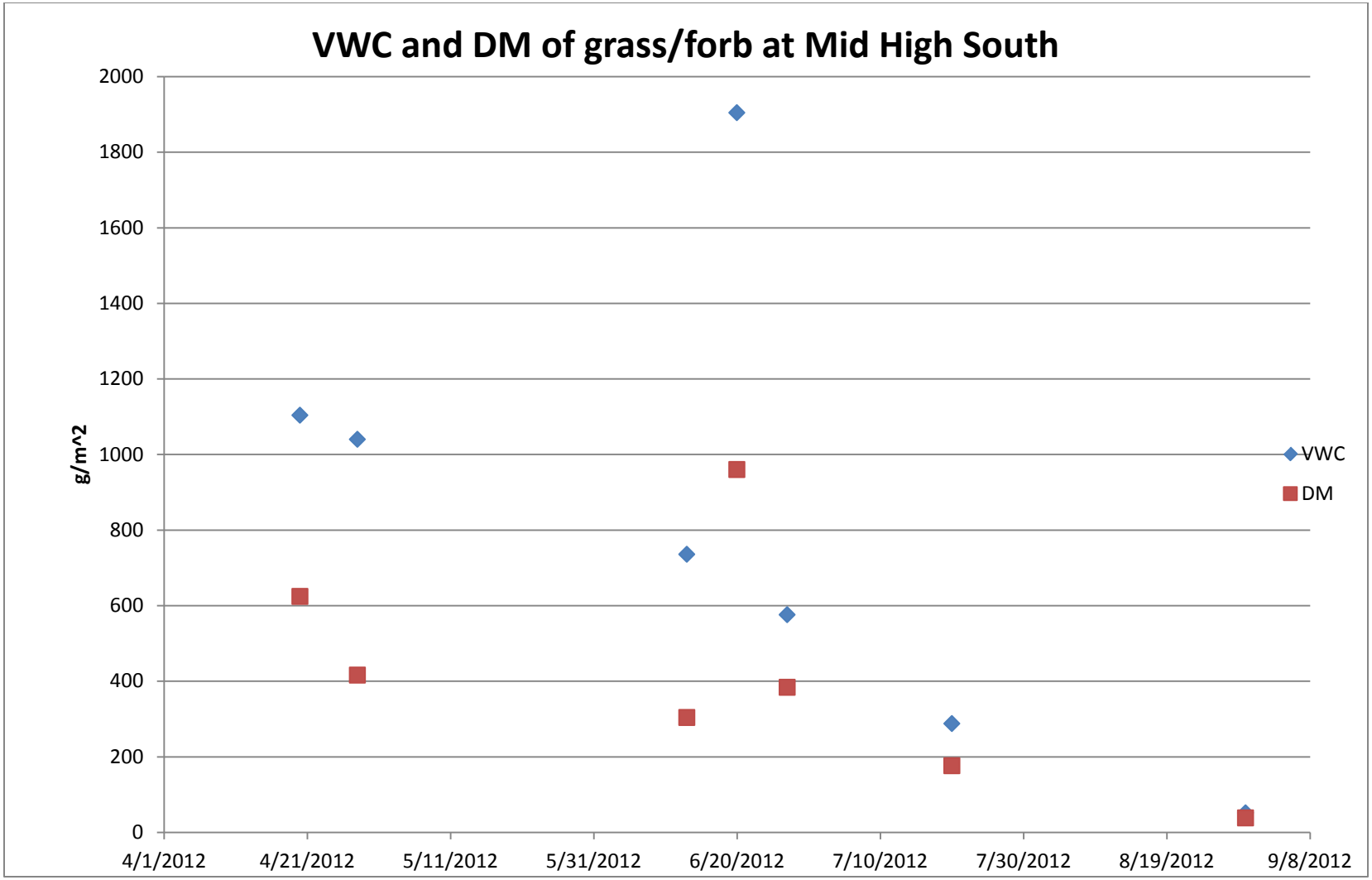

Figure 46. VWC in g/m^2 with respect to time of the grass/forb samples at the Mid-High South location of DCEW

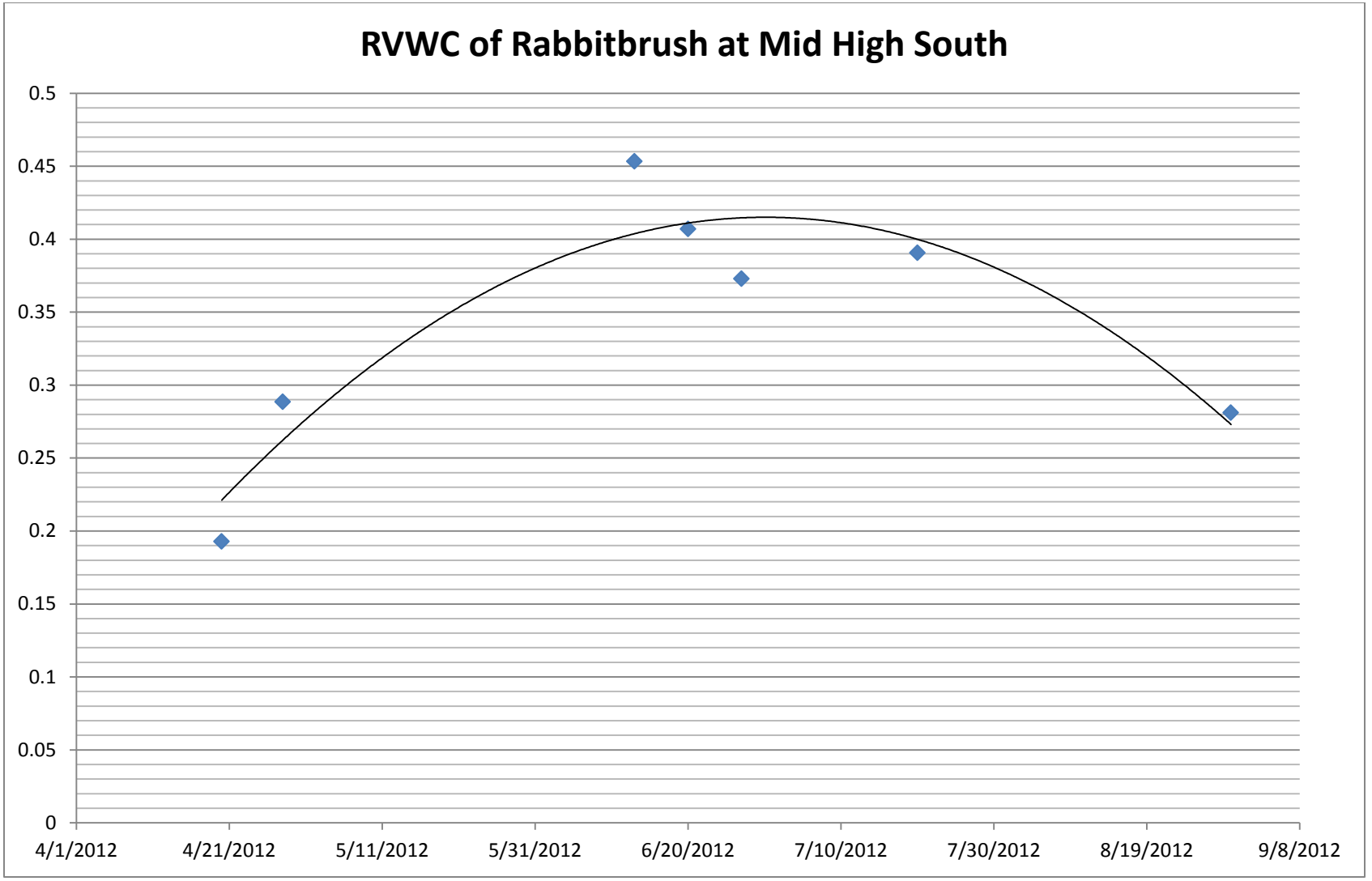

Figure 47. Relative vegetation water content of rabbitbrush with respect to time at the Mid-High South location in DCEW.

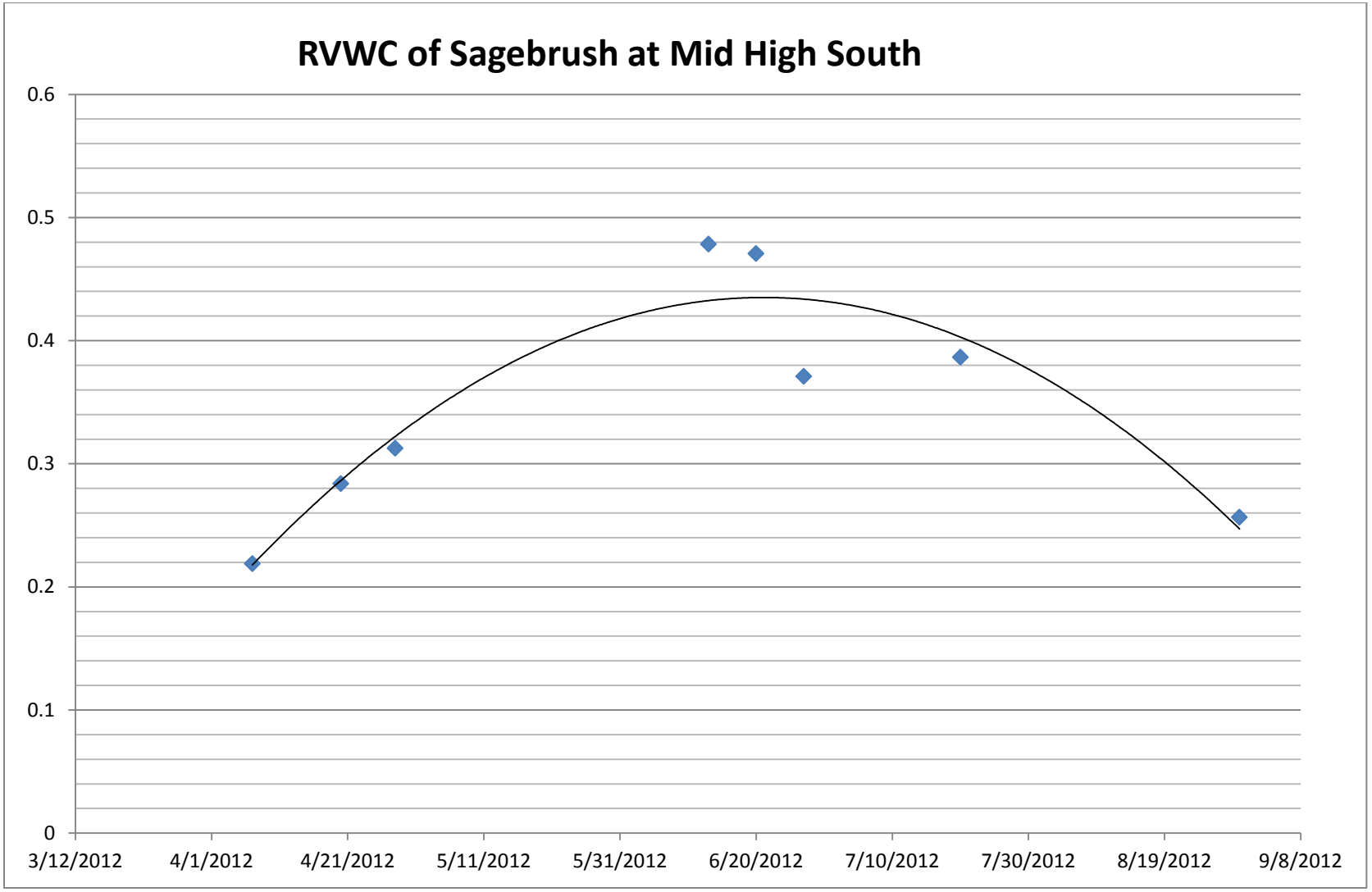

Figure 48. Relative vegetation water content of sagebrush with respect to time at the Mid-High South location in DCEW.

APPENDIX C

Pictures

Picture 1. Photograph of sagebrush steppe ecosystem of DCEW. Taken by Mel Kunkel 2010.

Picture 2. Photograph of ponderosa pine taken 2012 in DCEW.

Picture 3. Photograph of Douglas fir (http://www.bentler.us/eastern-washington/plants/trees/douglas-fir.aspx

Picture 4. Micro-plot with three 2m long transects oriented lengthwise down slope in the sagebrush ecosystem.

Picture 5. Antelope bitterbrush in bloom at the Lower South location in DCEW (May 11, 2012)

Picture 6. Rabbitbrush on Lower North site within DCEW (May 11, 2012)

Picture 7. Sagebrush on Lower North site within DCEW (May 11, 2012)

Picture 8. Grass/forb sample clipped using a 0.25 m2 quadrat.